Recent advances in phthalocyanines for chemical sensor, non-linear optics (NLO) and energy storage applications

Denisha Gounden[a], Nolwazi Nombona[b] and Werner E. van Zyl[a],*

[a]School of Chemistry and Physics, University of KwaZulu-Natal, Westville Campus, Durban 4000, South Africa
[b]Department of Chemistry, University of Pretoria, Pretoria 0028, South Africa

*Corresponding author. E-mail address: vanzylw@ukzn.ac.za (W.E. van Zyl)

Highlights

- A comprehensive review on phthalocyanines (Pc) in important applications.
- Targeting chemical sensors, non-linear optics (NLO), and energy storage technologies.
- Review focuses on recent advances (2014–2020) of phthalocyanines.
- Perspectives for huge research opportunities are highlighted.

Abstract

Phthalocyanines (Pcs) are intensely coloured, robust macrocycles that possess admirable chemical, thermal and photo- stability as a result of its extensive π-network. The Pc family has established their fundamental and technological importance in numerous applications due to structural versatility and unique properties that result from the incorporation of a variety of inorganic and organic components into its framework. The diversity of Pc structures allows for the optimisation of certain properties to obtain functional, high-performance materials. The combination of aromaticity, relatively simple synthesis and structural flexibility makes Pcs a great asset for numerous scientific and industrial advancements. This review focuses on recent advances (2014–2020) of phthalocyanines in the specific technologies of chemical sensors, non-linear optics (NLO), and energy storage applications. Many MPc complexes reported to date favour select metals and ligand derivatives which leaves huge opportunities for further exploration.

Graphical abstract

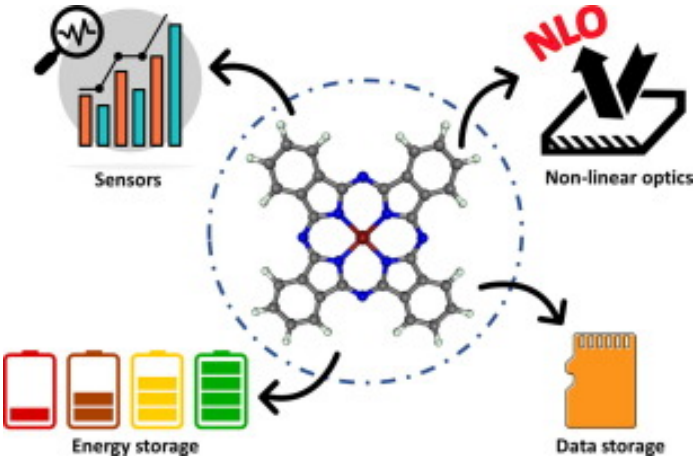

Abbreviations

A	Ampere
α-6T	α-sexithiophene
ACF	activated carbon fibres
AFM	atomic force microscopy
CNT	carbon nanotubes
ANI	Azidoaniline
CV	cyclic voltammetry
CVD	chemical vapor deposition
DBU	1,8-Diazabicyclo[5.4.0]undec-7-ene
DC	drop cast
DFT	density functional theory
DMSO	dimethyl sulfoxide
DPSV	differential pulse stripping voltammetry
EC	electrochemical capacitors
EDLC	electric double layer capacitor
EIS	electrochemical impedance spectroscopy
ESA	excited saturable absorption
FET	field effect transistor
GCE	glassy carbon electrode
GO	graphene oxide
HEMIM	1-(2-Hydroxyethyl)-3-methylimidazolium
HOMO	highest occupied molecular orbital
HM	heavy metals
IDE	interdigitated electrode
ITO	indium tin oxide
LB	Langmuir-Blodgett
LMCT	ligand to metal charge transfer
LOD	limit of detection
LRR	linear response range
LSS	charge transfer state
LUMO	lowest unoccupied molecular orbital
MLCT	metal to ligand charge transfer
MPc	metallo-phthalocyanines
MWCNT	multiwalled carbon nanotube
NBO	natural bond order
nm	nanometer
OL	optical limiter
OTFT	organic thin film transistor
Pc	Phthalocyanines
PDT	photodynamic therapy
PET	photo-induced electron transfer
ppb	parts per billion
ppm	parts per million
QCM	quartz crystal microbalance
QLS	quasi-Langmuir-Shäfer
RSA	reverse saturable absorption

SEI	solid electrode interphase
SEM	scanning electron microscopy
SMX	sulfamethoxazole
SQD	semiconductor quantum dot
SWCNT	single wall carbon nanotube
SWV	sweeping wave voltammetry
TEM	transmission electron microscope
TIRE	total internal reflection ellipsometry
VC	vacuum deposit
VOC	volatile organic compound
WHO	world health organization
WORM	write only read many
XPS	X-ray photoelectron spectroscopy
XRD	X-ray diffraction

Keywords: Phthalocyanines; Chemical sensor; Non-linear optics; Energy storage

1. Introduction

Phthalocyanines (Pcs) as a class of compounds have found widespread use in fundamental research and increasingly more in diverse and important industrial and technological areas. Different synthesis routes to phthalocyanines and insight into their structure have been well established [1], [2], [3], [4], [5], [6]. Over the past 3 decades, an increasingly strong correlation between Pc properties and their applications became apparent [2], [7]. The optical and photosensitization properties [8], [9], [10], [11] as well as the dye and pigment qualities [12] have always been on the forefront of Pc investigations. Once the fundamentals of synthesis and properties became understood, its outstanding electronic properties could be exploited, and emerging applications started to be investigated that led to its use as materials and devices [13]. This led to the use of Pcs in dye-sensitized solar cells (DSSC) that was recently comprehensively reviewed [14]. Recently, Pcs found applications in biological systems, in particular photodynamic therapy (PDT) [15], nanobiotechnology and theranostics [16]. The most recent reviews on Pcs were published in 2010 [5], [17], while its application in DSSC and perovskite solar cells were reviewed in 2019 [14], [18]. We felt an updated review of Pcs in the area of emerging applications not yet covered would be desirable. These areas include the use of Pcs in chemical sensor technology, non-linear optics (NLO), and energy storage applications. The review only focuses on recent advances in these areas from 2014 to the present, in some areas such as data storage devices it appears significant studies were performed prior to 2014 only to be rejuvenated recently.

1.1. Phthalocyanine classification

Phthalocyanines are macrocyclic, consisting of a planar conjugated system with 18 π-electrons and four isoindole subunits attached *via* meso positioned nitrogen atoms [19]. The Pc ring is a flexible structure, allowing functionalization of varying substituents at the non-peripheral (*ortho*-, α) positions {(1, 4), (8, 11), (15, 18) or (22, 25)} and peripheral (*meta*-, β) positions {(2, 3), (9, 10), (16, 17) or (23, 14)} on the ring (Fig. 1). Several metals ions can be inserted into the central cavity of the Pc structure to form a metallated Pc (MPc) with some metals allowing for axial ligation but in a metal-free Pc (H_2Pc), the molecular centre consists

of two hydrogen atoms. The choice and placement of the substituents on the Pc ring as well as the selected metal ion can influence and modulate the physiochemical properties of Pcs.

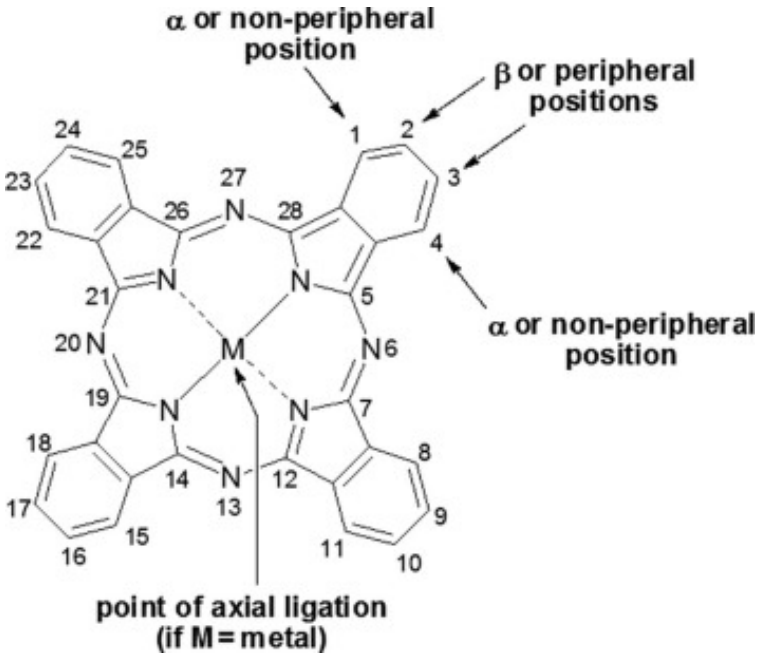

Fig. 1. Phthalocyanine structure with possible substitutions at non-peripheral (α) and peripheral (β) positions.

Unsubstituted Pcs are insoluble in many organic solvents. This is largely due to the hydrophobic nature and planarity of the Pcs that results in aggregation [6]. Solubility can be improved by attaching substituents on the Pc ring [8]. Substituents may be classified into electron-donating or electron withdrawing substituents, the former consists of amino, alkoxy or alkyl groups and the latter of sulfonyl, carboxyl or fluoro groups [20]. Substituted Pcs are usually synthesized using phthalonitrile precursors that contain the desired substituent. Phthalocyanines can be tetra- or octa- substituted as shown Fig. 2.

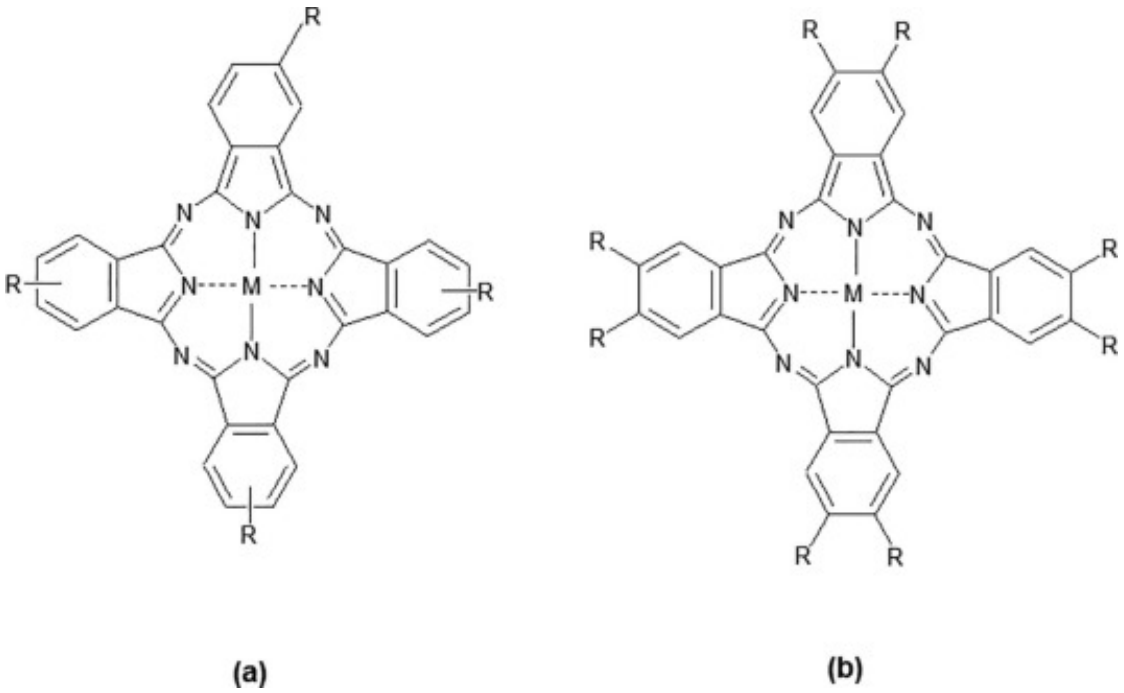

Fig. 2. (a) Tetra and (b) octa substituted Pcs. "R" represents any substituent besides hydrogen.

A brief overview of MPc properties and their adaptability towards a wide range of applications through fine-tuning of their chemical structures are outlined in Section 1.2.

1.2. Phthalocyanine properties

1.2.1. Electronic and conductive properties

The ground state electronic absorption can be understood by energy level diagrams referred to as Goutermans four-orbital model (Fig. 3) [9]. This model explains the $\pi \rightarrow \pi^*$ transitions that occur from the highest occupied molecular orbital (HOMO) to the lowest unoccupied molecular orbital (LUMO) giving rise to Q and B (Soret) bands in UV–vis spectra.

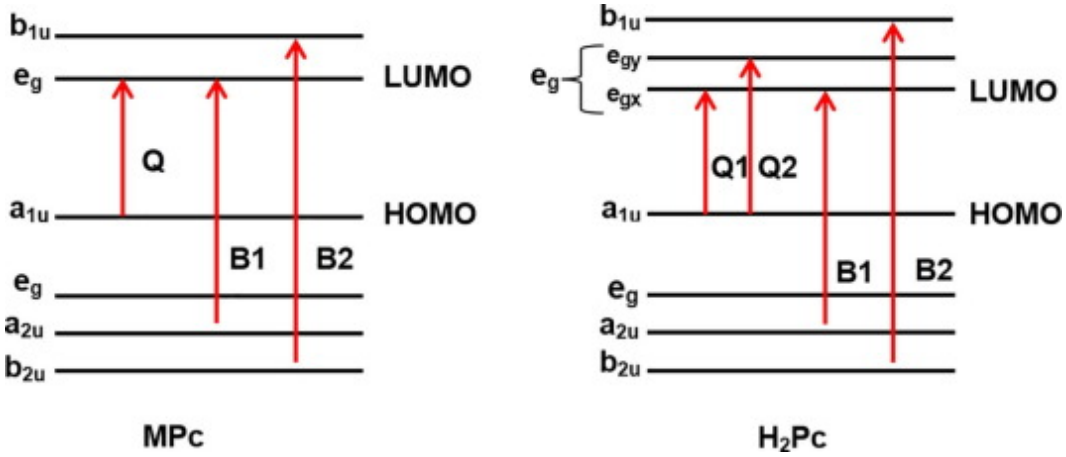

Fig. 3. Goutermans four-orbital model showing electron transitions and the origin of Q and B bands for metallated (MPc) and metal-free (H_2Pc) phthalocyanines.

The Q band corresponds to the electron transition from the a_1u orbital to the e_g orbital whereas the B band results from electron transitions from the a_{2u} orbital to the e_g orbital. Metallophthalocyanines have a degenerate e_g orbital and have a single Q band. The incorporation of a metal to the central Pc cavity forms a thermodynamically stable delocalized dianion with higher symmetry [13]. Metal-free Pcs (H_2Pc) have a non-degenerate e_g orbital (e_{gx} and e_{gy}) that result in a lower symmetry leading to the splitting of the x- and y-polarized components of the Q band [4]. Electron-donating and withdrawing substituents positioned at either the non-peripheral (α) or peripheral (β) positions have different effects on the electronic and optical properties of Pcs. Electron-donating substituents causes an increase in the electron density of the Pcs resulting in the reduction of the HOMO-LUMO gap, and spectrally leads to a Q band shift towards absorption in the red region [4]. Certain metals such as Pb and Ti can also cause the Q band to shift towards the red region [21].

The electrons associated within the conjugated system are not localized on a specific atom but are instead delocalized within the entire Pc molecule. These electrons are responsible for the semi-conducting behavior of Pcs. The planar nature of Pcs contributes to molecular stacking and creates a pathway for electron movement between Pc molecules. The conduction mechanism within Pcs originate from excitons (i.e. electron-hole pair) "hopping" or band to band transitions between Pc molecules. Pcs are classed as p-type semiconductors and their notable thermal stability allows for the sublimation of pure Pc thin films without decomposition [22]. In addition to photovoltaic devices, thin film MPcs displaying conductive properties are used as gas sensors [13] and for optical recording materials [19]. Sublimed MPcs from the metals Cu(II), Zn(II) and Ni(II) exhibit conductivities in the range 10^{-5} to 10^{-10} S cm^{-1} corresponding to (weak) semiconductors [23]. The low conductivity is due to weak intermolecular interactions due to intermolecular spacings of

0.34 nm between adjacent Pc molecules within the crystal structure. As a result, narrow energy bands are formed and the movement of generated charge carriers (i.e. electrons and holes) are driven by the electric field of an applied voltage by jumping through the potential field of the π electron-rich aromatic network [19]. The integration of Pcs in photovoltaic technologies is widely acknowledged for their strong absorption properties between the visible region up to the near infrared region and amenability towards structural modification allowing for bandgap energy and HOMO-LUMO energy levels to be tuned and designed into ideal photosensitizers or hole transport materials [14], [18].

As a p-type semiconductor, Pcs are responsive towards chemical dopants. For example, when exposed to oxygen (in air), O_2 diffuses into the lattice of the MPc and removes an electron, thereby increasing the number of positive charge carriers (i.e. holes) in the MPc [13]. In turn, this increases the conductivity of the Pc, and is represented in the equation below:$MPc + O_2 \leftrightharpoons MPc^+ + O^{2-}$

Another important solid-state property of MPcs is photoconductivity, which is increased electrical conductivity when exposed to visible light [24]. Photoconductivity is measured by the difference in conductivity when Pc films are exposed to the dark and under irradiation, i.e. upon photon absorption and electrons are excited from the HOMO (valence band) to the LUMO (conduction band) and increases the number of charge carriers present in the film and consequently increases the conductivity [25]. Photoconductivity of MPcs is an important parameter for applications in electronic and photoelectronic devices such as laser printers, liquid crystal displays, etc [19].

1.2.2. Photophysical properties

The Jablonski diagram shown in Fig. 4 is used to explain the photophysical processes that occur when Pcs absorb light of appropriate wavelengths.

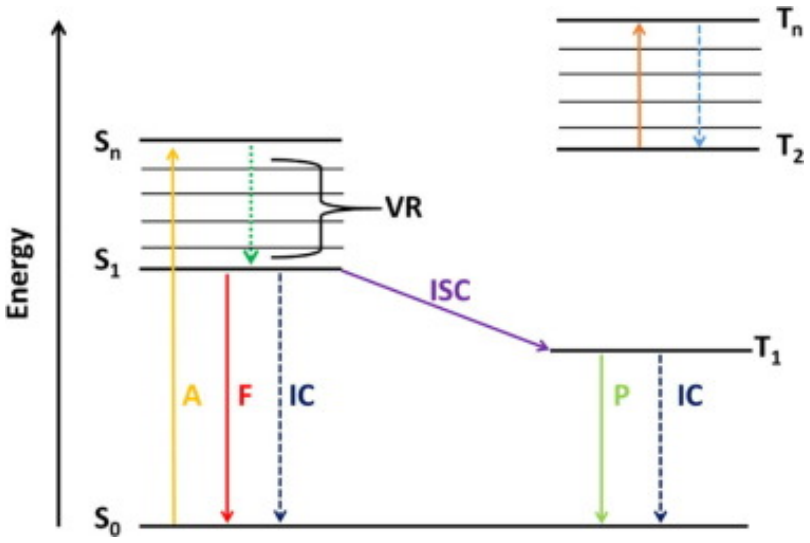

Fig. 4. Jablonski diagram displaying transition of a molecule from its lower ground state to higher excited state upon irradiation with light; (A) = absorption, (VR) = vibrational relaxation, (F) = fluorescence, (IC) = internal conversion, (ISC) = intersystem crossing, (P) = phosphorescence, S_0 = singlet ground state, S_1 = singlet excited state, T_1 = triplet excited state, T_2 = second triplet excited state. Non-radiative transitions are indicated by broken arrows and radiative transitions by straight arrows [26].

The absorption of ultraviolet or visible light (A) by Pc molecules causes excitation from a lower energy, ground state (S_0) to vibronic levels of a higher energy excited singlet state (S_1). Once the Pc molecule is excited there are numerous ways in which the energy could be dissipated. The molecule may lose some of its energy through non-radiative vibrational relaxation (VR) and relax to the lowest vibronic level of the singlet state (S_1). Vibrational relaxation occurs when energy is transferred to other vibrational modes as kinetic energy. The Pc molecule can also return to its ground state (S_0) by a radiative process referred to as fluorescence (F) or a non-radiative process called internal conversion (IC). Internal conversion occurs when vibrational energy levels overlap with electronic energy levels causing the excited electron to transition from a vibrational level in one electronic state to another vibration level in a lower electronic. Another pathway for the electron is intersystem crossing (ISC) to the excited triplet state (Tn). In this process, the electron changes spin multiplicity from the excited singlet state to the excited triplet state. In MPc molecules, ISC can be encouraged by inserting heavy metals into the Pc cavity which is an integral mechanism for optical limiting applications. The principles of optical limiting are further discussed in Section 3.1.

1.2.3. Electrocatalytic properties

The application of MPcs on modified electrodes and sensors are closely linked to its electrochemical and redox properties. Electrochemical processes that occur in MPcs may take place at the Pc ring or at the central metal ion. Metallophthalocyanine redox reactions are influenced by various factors such as i) the nature of the substituents (electron-donating/

withdrawing) functionalised on the Pc ring, ii) the oxidation states of the metal ion, iii) axial ligation and iv) the solvent used to carry out the reactions [27].

Redox reactions can occur at the central metal provided that the metal is electroactive. For this to occur the metal d-orbitals must lie between the HOMO and LUMO energy band gap of the Pc ring [27]. Metals can be grouped into redox active (metals with vacant or partially filled orbitals) and inactive metals. Fig. 5 displays energy level diagrams representing the changes observed during oxidation and reduction of the neutral Pc complexes. In its neutral form, Pcs exist as dianions (Pc^{-2}) and can be oxidised or reduced. During oxidation of the neutral Pc^{-2}, two electrons are removed from the HOMO (a_{1u}) of the Pc to form the Pc^{-1} and Pc^{0} species. The reduction process involves the addition of four electrons to the LUMO of the neutral MPc forming Pc^{-3}, Pc^{-4}, Pc^{-5}, Pc^{-6} species. The π donor–acceptor ability of MPcs act as electrocatalysts towards the oxidation and reduction of organic and inorganic substances. Metallophthalocyanines are used as chemical modifiers to reduce overpotentials of reactions occurring on electrode surfaces bringing them closer to thermodynamic equilibrium [28].

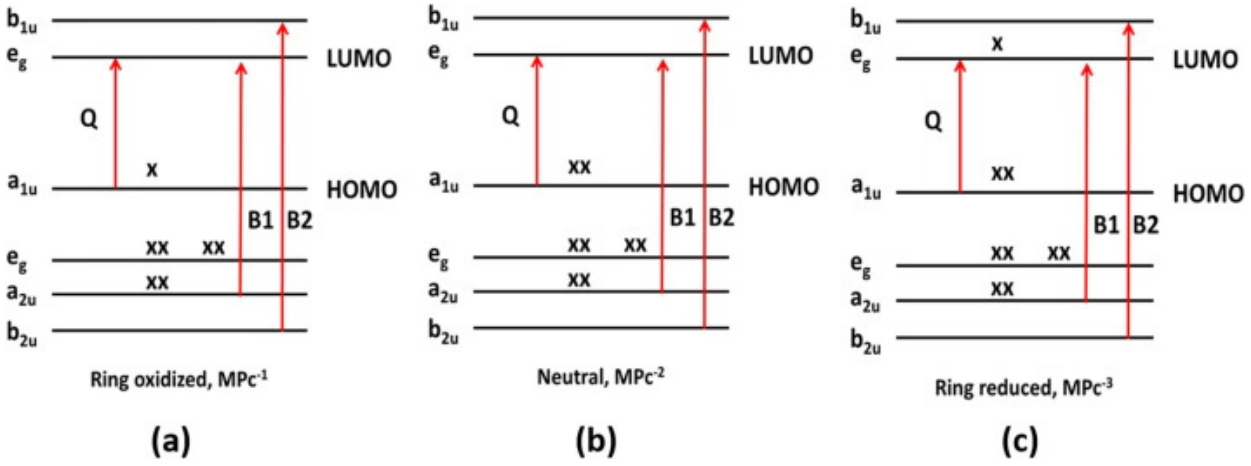

Fig. 5. Energy level diagram showing the oxidized Pc (a), the Pc dianion (b) and the reduced Pc (c). The "x" represents an electron.

2. Phthalocyanines as chemical sensors

We live in an environment with a variety of toxic substances, gases and polluted water systems. Governments are expected to monitor the nature and risk of potentially dangerous pollutants such as nitrogen oxides (NO_x), sulfur oxides (SO_x), volatile organic carbons (VOCs) and heavy metals (HMs) to ensure that the enforced control measures work effectively. The World Health Organisation (WHO) places importance and demand for real-time analysis which can be achieved from chemical sensors that convert chemical quantities into measurable electronic signals. The IUPAC defines a chemical sensor as "a device that transforms chemical information, ranging from concentration of a specific sample component to total composition analysis, into an analytically useful signal" [29]. Environmental monitoring requires robust, reliable and portable sensors for real-time, in situ detection of pollution and toxic chemicals.

Several studies document the use of Pcs as integral components of chemical sensors where different central metals and/ or the peripheral substituents were incorporated to achieve specific functionality in different media (i.e. gas and liquid) [30], [31]. The intense 18 π-

electron skeleton of Pcs encourage interactions with liquid and gaseous analytes resulting in detectable physical changes [32], [33].

2.1. Gas sensors

Interactions between Pc and gas molecules occur via reversible chemical reactions or adsorptions and irreversible chemical reactions [13], [34]. As a result of these interactions, detectable changes in mass density, optical properties and conductivity of the Pc molecules can be recorded. Electronic devices such as capacitive sensors, mass sensitive sensors, field-effect transistors (FETs), solid-state ionic sensors, quartz crystal resonators, etc. can be used to detect such physical changes.

Pcs are chemically sensitive towards reactive gases and can be oxidized or reduced by redox-active molecules such as hydrogen sulfide (H_2S) [35], [36], nitrogen oxides (NO_x) [37], [38], ozone (O_3) [39] and halogens (Br_2, Cl_2, I_2) [40], [41], [42]. These redox-based interactions can be monitored by measuring the change in the electronic conductivity of MPcs. In 2018, Sun and co-workers designed a fluoroalkoxy-H_2Pc for selective NO_2 detection [43]. The fluorinated-H_2Pcs were deposited by drop cast (DC) and vacuum deposition (VD) for comparative purposes. The performance and sensitivity of the Pc towards NO_2 was evaluated by spectroscopic and morphological characterisation. SEM, AFM and XRD indicated that DC fluoroalkoxy-H_2Pcs films formed J-aggregates whilst VD films formed H- aggregates. Fig. 6a-b show time-dependent current plots of the sensors as a function of NO_2 concentration for the DC and VD films. Both plots show a decrease in current during NO_2 exposure and an increase during recovery, suggesting an n-type response between the fluoroalkoxy-H_2Pc and the NO_2 analyte. Linear responses for both films were observed between the 0.1–1 ppm concentration range and sensitivities of 7.54% ppm for DC films and 12.05% ppm for VD films were obtained. Films were further exposed to a mixture of NO_2, NH_3 (2.5–25 ppm) and H_2S (0.25–2.5 ppm) gases but there were no observable changes in the output current, revealing the highly selective nature of the sensor. The selectiveness of the fluoroalkoxy-H_2Pcs towards NO_2 was attributed to the N-O---N–H bonding between the NO_2 gas molecules and the central cavity N–H protons of the fluoroalkoxy-H_2Pcs. Of the two deposition methods, the H-aggregated fluoroalkoxy-H_2Pcs obtained from VD provided the best sensitivity for NO_2 detection.

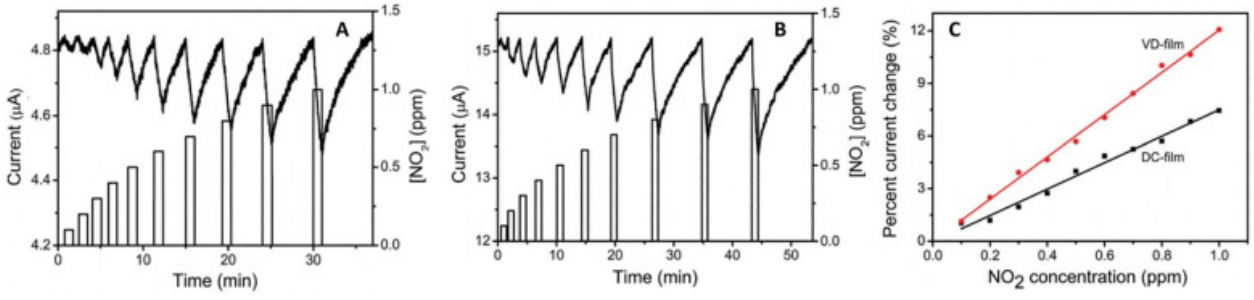

Fig. 6. (a) Time-dependent current plot of the fluro-H_2Pc sensor as a function of the NO_2 concentration for the DC film, (b) VD film and (c) the linear sensor response with NO_2 concentration of the DC film and the VD film.

Zhu et al. fabricated a novel heterogeneous active sensing layer to detect NO_2 using an organic filed effect transistor (OFET) device [44]. OFETs comprise of a three terminal system consisting of an active layer, an organic insulator as a dielectric layer and conductive metals or carbonaceous materials as electrodes [45]. Procedurally, an oxidizing gas diffuses

onto the MPc active layer and displaces other adsorbed species. A charge-transfer complex forms between the MPc and the gaseous molecules, consequently creating charge carriers (i.e. electrons and holes). The formation of charge carriers changes the conductivity of the active MPc layer which can then be measured as a response [46]. The components of the heterogeneous layers (Fig. 7) were ZnPc, p-sexiphenyl (p-6P) and α-sexithiophene (α-6T). p-sexiphenyl is a rod-shaped organic material that is able to induce growth of the organic semiconductor layer [47] whilst α-6T forms a stable phase at low deposition rates and larger layer spacing diffraction at high deposition rates [48].

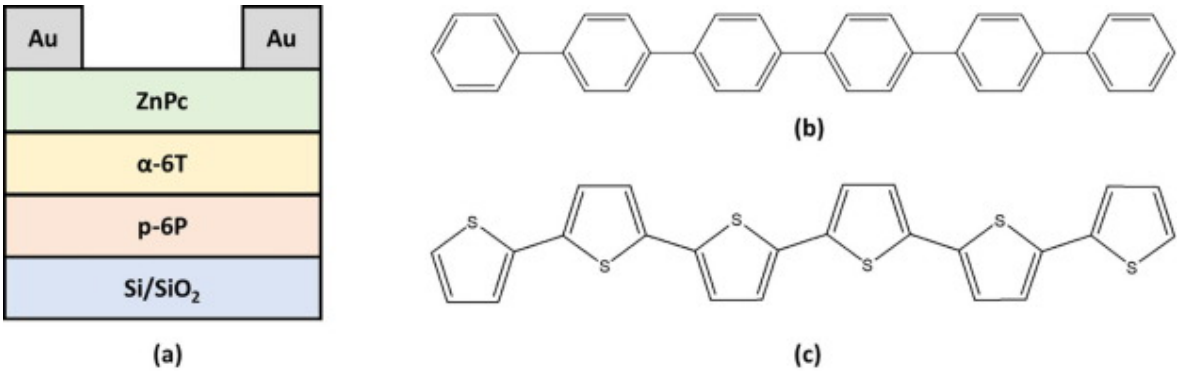

Fig. 7. (a) Structure of fabricated sensor with ultrathin heterogeneous interface of the p-6P/α-6T layer and molecular structure of (b) p-6P and (c) α-6T materials.

Four sensor compositions, p-6P/ZnPc, p-6P/α-6T, p-6P/α-6T/ZnPc, and single ZnPc layers were prepared as ultrathin heterogeneous interface layers using vacuum evaporation. The performance of the p-6P/α-6T/ZnPc gas sensor was significantly enhanced in comparison to the other sensor compositions. Apart from displaying a gas response of 157% to 500 ppb NO_2 gas, sensitivity of 570% ppm^{-1} and a LOD of 0.5 ppm, the OFET results also indicated that the saturation current of the p-6P/α-6T/ZnPc composition was 1.136 A, which was 4 times, 126 times and 95 times larger than that of of *p*-6P/ZnPc, *p*-6P/α-6T, and single ZnPc compositions, respectively. This performance was attributed to combined contributions from each component in the heterogeneous composition of the sensing layer and the ultrathin morphology. The granular morphology of the combined 6P/α-6T/ZnPc layers allowed for the efficient diffusion and infiltration of the NO_2 gas molecules. The NO_2 molecules interacted first with the ZnPc and thereafter diffused into ZnPc particle gaps to reach the interface between the ZnPc and α-6T layers. During this process, two types of electron exchanges are proposed to occur between the NO_2 analytes and the interfacial layers, i) electron exchange between the NO_2 and ZnPc which involves NO_2 molecules extracting electrons from the ZnPc, producing numerous holes in the ZnPc material, and ii) electron exchange between the NO_2 and α-6T which involves NO_2 molecules extracting electrons from α-6T, also producing holes in the α-6T material.

The holes produced during these electron exchanges accumulate between the insulating SiO_2 layer and p-6P layer that eventually creates and expands the conductive channel for larger current responses. The 6P/α-6T/ZnPc layers created a synergistic relationship that is capable of sensitive NO_2 adsorption.

Kumar et al. fabricated chemiresistors with a heterojunction active adsorption layer made from randomly assembled networks of ZnO nanowires and CoPcs (ZnO/CoPc) for H_2S detection [49]. Whilst optimising the thickness of the CoPc layer (i.e. 25 nm), it was

discovered that a thickness >15 nm caused the heterojunction films to exhibit a change from an n-type to p-type conduction as the thicker CoPc layers appeared to provide uniform coverage over the ZnO. The modification of the n-type ZnO nanowires with the optimised 25 nm layer of CoPc displayed the best response, sensitivity and recovery towards H_2S. It is important to note that pure ZnO and pure CoPc films displayed kinetically slower responses. Confirmed by detailed X-ray photoelectron spectrsocopy (XPS), these results were based upon the direct interaction between the H_2S and CoPc. The H_2S molecules can interct with the CoPc in two process, namely i) Direct interaction of the H_2S with sites free from adsorbed O_2 molecules, and ii) the competitive displacement of chemisorbed O_2 by H_2S from the CoPc surface and is understood by the following chemical equation:

$$H_2S + 3O^{2-} \rightarrow H_2O + SO_2 + 6e\text{-}$$

H_2S is referred to as a reducing gas and an electron donor when interacting with the CoPc, whilst the CoPc is considered a p-type semiconductor that contains hole charge carriers. The adsorbed H_2S molecules would then inject electrons into the CoPc, promoting the combination of electrons and holes resulting in measurable changes to the charge and carrier density. Work function measurements also supported the formation of a p-n junction and charge transfer between the ZnO to the CoPc.

Using a quartz crystal microbalance (QCM), Harbeck et al. have conducted a series of studies that utilises metal-free and MPcs functionalised with alkoxy, fluoro alkyl and tosylamino moieties to determine their detection potential towards VOCs. Collectively, their studies indicated that unlike other MPcs sensor studies that reported interactions between the central metal ion and analyte, active sorption sites for the VOCs stem from the C–H groups on the Pc skeleton and are essential for H-bonding with VOC π-systems as summarized below [50], [51]:

- MPcs functionalised with electronegative fluoro groups were excellent candidates for detecting polar VOCs as they displayed high π-π interactions with polar compounds.
- Branched alkoxy Pcs displayed an unexpected affinity towards hydrocarbon compounds due to strong van der Waals interactions taking place between the alkyl moieties and the non-polar analytes.
- The N–H group that exists in the core of metal-free Pcs as well as in the tosylamino functionalised Pcs are active sorption sites that can interact with the π system of polar compounds.
- H-bonding can occur between the Pc π system and the acidic proton of alcohols.
- The central metal is an active centre for the adsorption of alcohols as the metal atom (M) can form M – OH bonds.

Kumar et al. confirmed this as their studies tested the effects of the metal centre and the role of peripheral substituents on Pcs towards toluene using QCM [52], [53]. They reported that Co, Cu, Fe, and Zn metal centres did not significantly improve sensitivity towards toluene. Toluene was found to display strong interactions between the electron cloud of the Pc ring as well as C–H bonds between the peripheral substituents containing *tert*-butyl and fluorinated groups. There are several other sensor studies that detail the incorporation of MPcs into the active sensing layer for the detection of common VOCs such as chloroform[54], ethanol [55] and acetone [56].

Gas sensing capacities have been improved by forming composites that include nanomaterials. A synergistic relationship was shown by Wang et al. who sought to enhance NH_3 detection by fabricating nanocomposites of amino-functionalised CoPc and reduced graphene oxide (GO) nanoparticles [57]. Three α-substituted CoPcs were used in the study: amino CoPc (amino-CoPc), ρ-aminobenzyloxy (aminobenz-CoPc) and substituent free CoPc (unsub-CoPc). The hybrid materials were prepared by mixing reduced GO with CoPcs which were drop cast onto gold IDEs. A gas sensing test system with high purity NH_3 gas mixed with air as the carrier and the response (%) was defined relative to the change in resistance of the active layer and can be observed in the equation below:

$$response(\%) = \frac{\Delta R}{R_a} x100 = \frac{R_g - R_a}{R_a} x100$$

where R_a – resistance values under initial air flow, R_g – resistance values under NH_3 gas.

Under optimised concentrations of the respective nanocomposites, the three CoPc/GO composites displayed improved selectivity, sensitivity and recovery towards NH_3 when compared to pure reduced GO. The aminobenz-CoPc/GO hybrid exhibited the best performance, reporting a response of 50 ppm, a LOD of 78 ppb and recovery time of 225 s. By comparison to pure reduced GO, the aminobenz-CoPc/GO composite displayed a 23-fold higher response to 50 ppm NH_3. Electrochemical impedance spectroscopy (EIS) and DFT studies confirmed that the superior NH_3 detection was a result of the synergistic relationship between the aminobenz-CoPc and GO. The strong adsorption of the NH_3 gas occurred at the aminobenz-CoPc whilst the high electrical conductivity was provided by the reduced GO to encourage faster charge transfers between the CoPc and GO. These results were outperformed by their more recent study that tested composites of phenoxy substituted CoPcs (p-CoPcs) and reduced GO towards NH_3 detection [58]. The best performing composite was the carboxylphenoxyl-CoPc/GO composite that showed a high response towards NH_3 of 42.4% to 100 ppm of NH_3, a lower LOD of 3.7 ppb and a reversible recovery time of 120 s. The subsequent DFT studies were performed to investigate the effects of the different p-CoPcs on NH_3 sensing. The study was modelled around possible interactions between NH_3 and the various p-CoPcs and revealed that the carboxylphenoxyl-CoPc/GO composite had the shortest bond length ($r_{Co–N}$, 2.193) compared to the other three composites. The shorter bond length led to stronger adsorption between the NH_3 and carboxylphenoxyl-CoPc. These results were further substantiated by performing adsorption energy and natural bond orbital (NBO) calculations.

Saini et al. and more recently Sharma et al. both detail the detection of Cl_2 gas using octabutoxy and fluorinated functionalised metal Pcs, respectively. Saini's work highlighted the benefits of fabricating octabutoxy CuPcs and ZnPcs with nanowire and nanobelt morphologies whilst Sharma's work fabricated composites of fluorinated CuPcs, ZnPcs and CoPcs with non-covalently attached carbon-based materials. The performance of the sensors from the respective studies are shown in Table 1.

Table 1. Linear range, sensitivities and LODs obtained from different sensors for Cl_2 gas and pesticides: fenitrothion, diazinon and eserine. ([59], [60], [61], [62], [63], [64], [65], [66], [67], [68], [69], [70].)

Sensor	Analyte	Linear range	Sensitivity	LOD	Technique	
$ZnPc(OBu)_8$) nanobelts	Cl_2	5–1500 ppb	-	5.0 ppb	static gas sensing	[
$CuPcOC_4$ nanowires	Cl_2	5–1500 ppb	-	5.0 ppb	static gas sensing	[
$F_{16}ZnPc$/MWCNTs-COOH	Cl_2	100–2000 ppb	21.28% towards 2.0 ppm Cl_2	0.06 ppb	static gas sensing	[
$F_{16}CuPc$/SWCNT	Cl_2	-	35.82% towards 2.0 ppm Cl_2	0.27 ppb	static gas sensing	[
$F_{16}CuPc$/MWCNT	Cl_2	-	23.0% towards 2.0 ppm Cl_2	0.85 ppb	static gas sensing	[
$F_{16}CoPc$/SWCNT–COOH	Cl_2	-	82% towards 2.0 ppm Cl_2	0.04 ppb	static gas sensing	[
$F_{16}ZnPc$/SWCNT–COOH	Cl_2	-	82% towards 2.0 ppm Cl_2	0.05 ppb	static gas sensing	[
MnPc/N_3-PANI/ITO	Diazinon	0.20-7.50 μmol dm^{-3}	9.15 A cm^{-2} M^{-1}	0.062 μmol dm^{-3}	SWV	[
MnPc/N_3-PANI/ITO	Eserine	0.10-5.00 μmol dm^{-3}	5.78 A cm^{-2} M^{-1}	0.088 μmol dm^{-3}	SWV	[
MnPc/N_3-PANI/ITO	Fenitrothion	0.12-15.00 μmol dm^{-3}	4.67 A cm^{-2} M^{-1}	0.049 μmol dm^{-3}	SWV	[
CoPc-M/GCE*	Diazinon	0.38-5.07 μmol dm^{-3}	1.50 A cm^{-2} M^{-1}	0.120 μmol dm^{-3}	SWV	[
CoPc/GCE	Fenitrothion	1.20-42.0 μmol dm^{-3}	0.26 A cm^{-2} M^{-1}	0.460 μmol dm^{-3}	SWV	[
MWCNT/GCE	Fenitrothion	0.01-5.0 μmol dm^{-3}	7.2 (μA/μM)	6.4 nM	CV	[
poly(2-HBZ)/GE*	Fenitrothion	0.018–3.60 μmol dm^{-3}	-	4.70 nM	CA*	[
poly-zincon/GCE	Fenitrothion	$5x10^{-3}$ - 8.6 μmol dm^{-3}	-	1.5 nmol L^{-1}	DPV	[
Nano-MIP-CPE*	Diazinon	0.10-2.00 μmol dm^{-3}	95.08 A cm^{-2} M^{-1}	7.9×10−3 μmol dm^{-3}	SWV	[

*CA: chronoamperometry.

*CoPc-M: cobalt phthalocyanine functionalised with morpholin groups.

*poly(2-HBZ)/GE: poly(2-hydroxybenzamide)-modified graphite electrode.

*Nano-MIP-CP electrode: nano-molecularly imprinted polymer-carbon paste electrode.

Cl_2 is recognised as a toxic gas with an occupational exposure limit of 500 ppb [71]. Exposure to Cl_2 gas for an average of six hours can lead to respiratory complications and sensory irritation [72]. All of the MPc-based Cl_2 gas sensors reported in Table 1 are capable of detecting Cl_2 at ambient temperatures below 500 ppb under static conditions. These sensors also proved to be selective towards Cl_2 even in the presence of other gases such as NO, NO_2 and NH_3. The proposed gas sensing mechanism are explained as follows: MPcs are often described as electron donors whereas electronegative Cl_2 molecules are electron

acceptors. It is recognized that when MPcs are exposed to ambient conditions, oxygen will adsorb and will remove electrons from the conduction of the MPc to form two charged species:

$$MPc + O_2 \rightleftharpoons MPc^+ + O_2^-$$

Once exposed to the reducing nature of Cl_2, the adsorbed O_2^- are displaced by the Cl_2 molecules, which also adsorbs to free metal coordination sites on the film, as shown in the following chemical equations:

$$2MPc + Cl_2 \rightleftharpoons 2MPc^+ + 2Cl^-$$

$$Cl_2 + 2O_2 \rightleftharpoons 2Cl^- + 2O_2$$

The Cl_2 analyte essentially removes electrons from the MPc and leaves behind a number of holes in the MPc film which results in increased film conductance. Saini's studies showed nominal differences in their output as neither the central metals nor morphology greatly influence the calculated LODs. The LODs obtained from Sharma's research were far superior and was attributed to combined, synergistic effects between the MPcs and CNTs. The MPcs molecules were found to be exohedrally attached to the surface of the CNTs through extensive π-π interactions, forming a charge transfer conjugate. Raman and XPS spectroscopic measurements were used to justify the improved charge transfer between the Cl_2 molecules and the MPc-CNT composites. Additionally, the molecular orbitals of the fluorinated MPcs are thought to be closer to the Fermi level, leading to higher ionisation potentials and better electron affinity that provided better device performance [73].

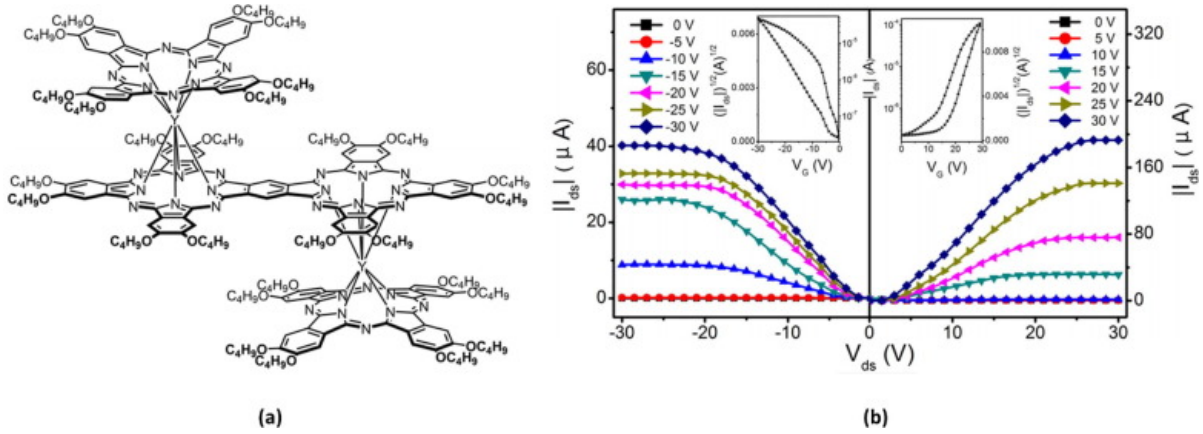

Fig. 8. (a) Molecular structure of BiYPc and (b) Output characteristics (I_{ds} versus V_{ds}) and transfer characteristics ($|I_{ds}{}^{1/2}|$ versus V_g) for the ambipolar OFET device.

Organic materials used in electronic devices generally show unipolar behaviour, i.e. they typically contain either electrons or holes as major charge carriers whereas materials that have the ability to transport both, electrons and holes are commonly referred to as "ambipolar" [74]. Ambipolar materials are extremely valuable as they can replace the need for two transistors with n- or p- type channels in a device. Often, ambipolar devices are created by blending two materials with n- and p- type characteristics, however, this is not the case with Pcs. The Pc family has a flexible electronic structure and can be tuned such that the Pcs can demonstrate n-type, p-type and even ambipolar behaviour. Studies investigating the

properties of rare earth metal Pcs in double and even triple decker configurations indicated that extending the conjugation from mononuclear to binuclear can affect changes towards the semi-conducting nature of the material, e.g. an n-type to ambipolar [75]. Lu et al. investigated this further by fabricating a binuclear Pc with yttrium (Y) metal centers in a double decker configuration (BiYPc) for the oxidization and reduction of NO_2 and NH_3 gas, respectively (Fig. 8) [76].

The BiYPc was fabricated onto OFET devices using a quasi-Langmuir Shäfer (QLS) method [77]. Previous studies revealed that device performance depended both on the energy levels of the materials and the internal structure and morphology of the materials. Therefore, the BiYPc films were subjected to UV–vis, XRD, AFM and CV analysis. The XRD diffractograms reported a diffraction peak at $2\Theta = 28.88°$ which was attributed to the π-π stacking distance between the substituents of adjacent sandwich molecules, thus confirming the effective intermolecular π-π interactions in the BiYPc film whilst AFM analyses showed grain crystallites with an average diameter of

52 nm. These nanosized particles were expected to reduce traps and minor defects located close to grain boundaries and provide a larger surface area for more active sites for gas adsorption. The HOMO-LUMO of the BiYPc films were deduced from CV. Due to the free radical nature of rare earth double decker Pcs, they possess a semi-occupied HOMO orbital [78] and a similar case was observed in this study. The HOMO and LUMO energy levels of the BiYPc were located in ranges that are required for n- and p-type organic semiconductors, suggesting the possible ambipolar semi-conducting behaviour of BiYPc. As seen in Fig. 8, the OFET devices displayed ambipolar behaviour, recording an average carrier mobility for electrons at 1 ± 0.2 cm^2 V^{-1} s^{-1} and 0.40 ± 0.1 cm^2 V^{-1} s^{-1} for holes. To test the ambipolar nature of the BiYPc in a sensor, the device was exposed to varying concentrations to an electron accepting gas, NO_2 (0.5–3 ppm) and an electron-donating gas, NH_3 (7.5–20 ppm) under N_2 conditions. A noticeable decrease in the current is observed when the device is exposed to NO_2 accompanied by an increase during the recovery, thereby confirming the n-type behaviour of the BiYPc film towards the oxidizing gas. When exposed to the reducing NH_3 gas, the current decreases as well, confirming the p-type behaviour of the BiYPc. The decreased currents when exposed to both gases established the ambipolar nature of the BiYPc. Functionalised double and triple decker rare earth metal europium Pcs have also been highlighted for their similarly induced ambipolar behaviour towards oxidising NO_2 and reducing NH_3 gas [79], [80], [81], [82], [83].

2.2. Sensors for water treatment

Electrochemical methods are a relatively simple and cost-effective approach for the detection of numerous trace heavy metals, organic pollutants and pesticides in solution as they have displayed excellent sensitivity and potential for speciation [84], [85]. For electrochemical detection, electrode surfaces require modification to selectively interact with target analytes. The molecule or material used for modification should ideally have i) at least one electroactive group, and ii) binding sites designed for the target analyte.

Functionalised M.C.s carry both an electrochemically active metal center and provide many binding sites due to their flexible framework. Macrocycles such as MPcs carrying substituents containing S, O and N moieties act as binding sites, forming stable complexes with transition metals [86]. Electrode surface modification using MPcs can be achieved by various techniques including a simple drop-casting, electrodeposition, electropolymerization,

Langmuir–Blodgett (LB) deposition, spin coating, molecular beam and vapor deposition [64], [87].

2.2.1. Heavy metals

An asymmetric alkynyl-hexynoxy derivatised cobalt (CoPc) complex was synthesized by Fomo et al. for the simultaneous electrochemical detection of, Cd^{2+}, Cu^{2+}, Hg^{2+} and Pb^{2+} ions [88]. A GCE was modified with the CoPc *via* an electro-click reaction that takes places over two steps, i) azido-aniline hydrochloride was electrochemically grafted on the bare GCE, and ii) the alkyne terminated CoPc was chemically "clicked" *via* a covalent attachment onto the grafted surface over an 18 h period. XPS measurements were used to confirm the successful modification of the GCE. Mechanistically, the heavy metal ions selectively coordinate to the electronegative N and S atoms on the Pc ring as well as the benzothiazole substituent. Using differential pulse stripping voltammetry (DPSV), the modified CoPc-GCE showed well separated, individual peaks at −0.75 V, −0.16, 0.06 V and −0.47 for Cd^{2+}, Cu^{2+}, Hg^{2+} and Pb^{2+} ions, thus exhibiting their feasibility towards simultaneous detection. Under optimized conditions, the anodic peak current was proportional to the heavy metal ion concentration over a wide linear range of 0–0.1 mM. The LODs for the sensor towards Cd(II), Cu(II), Hg(II) and Pb(II) were 347.06 nM, 327.71 nM, 81.94 nM and 55.87 nM respectively. The sensor showed the most sensitive response of 1979.48 ± 11.47 μA mM^{-1} towards Pb(II) and the least sensitive response was observed for Cd(II), 204.50 ± 1.10 47 μA mM^{-1}. The DPSV scans revealed that the addition of Cd(II) and Pb(II) shifted the peak potential of Hg(II) and Cu(II) to more negative potentials and decreased the intensity of the peak current as compared to detecting the Hg(II) and Cu(II) alone. This was attributed to the formation of intermetallic compounds during the deposition step which consequently increases the sensitivity of the sensor towards Cu(II) and Hg(II) ions [89].

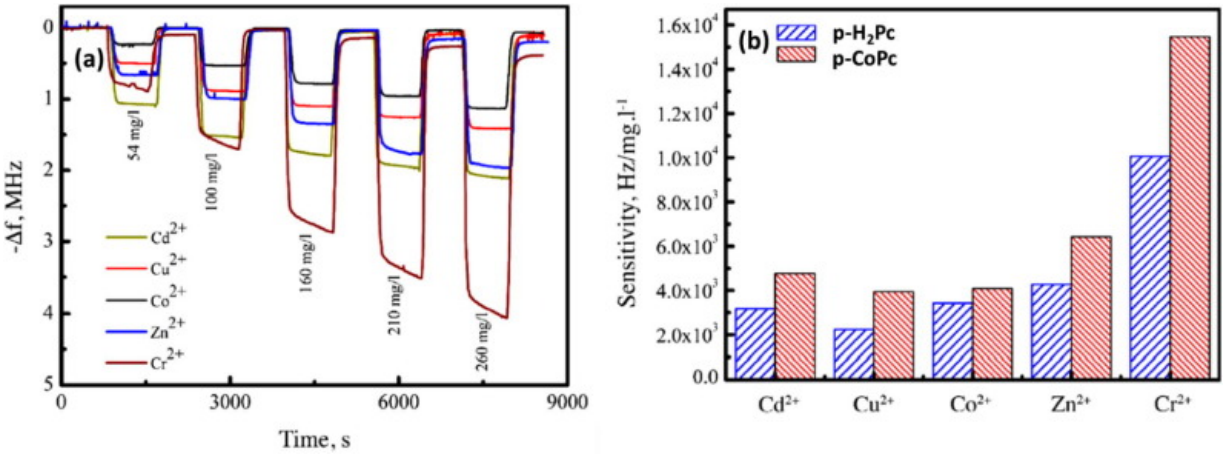

Fig. 9. Sensor signals of the p-CoPc QCM sensor during exposure to the five different analytes at indicated concentrations and (b) experimental sensitivities of p-H_2Pc and p-CoPc QCM sensors for all metal ion analytes as obtained in the liquid sensing experiments at room temperature.

Novel pyridone functionalised metal-free Pcs (p-H_2Pc) and CoPc (p-CoPc) were synthesised and used in the fabrication of a QCM sensor for the detection of Cd^{2+}, Co^{2+}, Cu^{2+}, Cr^{2+} and Zn^{2+} ions in water samples [90]. An AT-cut quartz crystal resonator was coated with the respective Pc sensing materials to investigate their response towards the five stated heavy metal ions. With increasing heavy metal ion concentrations (54–260 mg mL^{-1}), the

performance of the QCMs were determined by monitoring the frequency shift that occurred as a result of the ions in solution, see Fig. 9 for response curves of 5 analytes (QCM sensors).

These curves clearly illustrated the excellent response from the p-CoPc coated QCM sensors towards all the metal ion analytes. The study explains that the driving force behind the high responses are due to complex formation between the metal ions and the lone pairs on the N-containing pyridine groups on the Pc rings. As per Fig. 9, the trend observed for the QCM sensitivities were: $Cr^{+2} > Zn^{+2} > Cd^{+2} > Co^{+2} > Cu^{+2}$ for the p-H_2Pc QCM sensor and $Cr^{+2} > Zn^{+2} > Co^{+2} > Cd^{+2} > Cu^{+2}$ for p-CoPc QCM sensor. These results were expected as sensing properties in Pcs are known to be affected by the addition of a central metal that can enhance or reduce associated ionisation energies. Therefore, the more sensitive responses attained by the p-CoPc were attributed to a larger film surface area, as the small ionic radius of Co increased the contacting probability of the N atoms with heavy metal ions in solution and improved the detection sensitivity.

Gounden et al. demonstrated this by combining magnetic silica-coated iron oxide nanoparticles (Si-Fe_2O_3) with *tert*-butyl phenol substituted CoPcs and FePcs to electrochemically detect As, Cd, Hg and Pb ions in aqueous solutions [91]. The combination of Si-Fe_2O_3 nanoparticles with CoPc (CoPc/Si-Fe_2O_3) or FePc (FePc/Si-Fe_2O_3) resulted in increased active surface area of the GCE as per the Randles-Sevcik equation. Differential pulse anodic stripping voltammetry (DPASV) was used to evaluate both composites towards the four HMs under optimised conditions. The FePc/Si-Fe_2O_3 composite showed the lowest detection limits (S/N = 3) of 3.66, 11.56, 2.28, 4.54 μg L^{-1} for As, Cd, Hg and Pb respectively. A linear working range of 10–100 μg L^{-1} was obtained for As^{3+}, $Hg^{2+,}$ and Pb^{2+} ions while it was between 20 and 100 μg L^{-1} for Cd^{2+} ions. Reproducible signals were also obtained by both composites during the simultaneous detection of all four HMs for ten consecutive scans.

2.2.2. Organic pollutants

Biological entities such as enzymes, antibodies, and peptides are commonly incorporated into electrochemical sensors to function as molecular recognition elements for detection of organic pesticides in the environment but apart from their excellent selectivity, biological components typically display poor stability which limits their potential in sensing devices. Akyüz et al. were able to overcome such challenges by synthetically mimicking the function of biological elements using terminal alkyne substituted manganese phthalocyanine (MnPc) to detect fenitrothion, diazinon, and eserine pesticides, Fig. 10 [64].

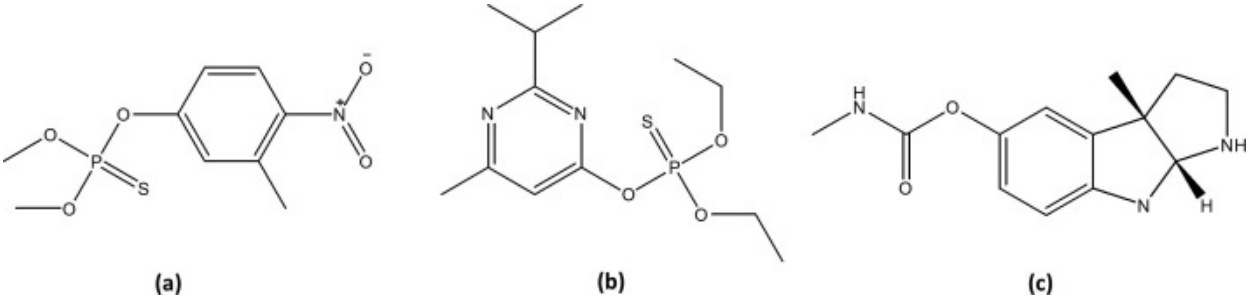

Fig. 10. Molecular structures of (a) fenitrothion, (b) diazinon and (c) serine.

The LB depositing technique was used to create ultrathin MnPc films (10 layers) on the electrode surface (i.e. ITO). The MnPc/ITO was immersed in a solution of 4-azidoaniline (N_3-ANI) to initiate a self-click reaction between the azide group of the N_3-ANI and terminal alkyne groups of MnPc. The newly formed MnPc/N_3-ANI/ITO electrode was further modified by converting the aniline groups into polyaniline via electropolymerization to form MnPc/N_3-PANI/ITO. The three target pesticides were added to a pH 7 phosphate buffer and analysed with SWV. When using the unmodified ITO electrode, fenitrothion displayed a redox peak at −0.5 V whereas the modified MnPc/N_3-PANI/ITO electrode displayed a decrease in the peak at −0.5 V and an increase in a newly formed peak at −0.8 V. The observation of the new peak indicated selectivity of the modified electrode towards fenitrothion. However, no new peaks were observed in the presence of both diazinon and eserine and indicated non-selectivity towards said pesticides. Table 1 provides a comparison of LODs and sensitivity obtained from different sensor studies towards fenitrothion. When compared to other modified Pc electrodes, the MnPc/N_3-PANI/ITO electrode displayed the best LOD of 0.062 μmol dm^{-3}.

In another electrochemical detection study for fenitrothion, Canevari et al. modified a GCE with a hybrid material consisting of silica coated MWCNTs and ruthenium Pc (SiO_2/MWCNTs/RuPc) [92]. The synthesis of the RuPc was unique in that an *in-situ* approach was used. This process involved dispersing SiO_2-MWCNTs into a Ru acetate solution. This solution was heated to dryness to incorporate the Ru onto the SiO_2/MWCNTs *via* silanol group interactions. The SiO_2/MWCNTs/Ru material was then heated with a phthalonitrile to form the RuPc on the SiO_2/MWCNTs. Shifts in the Q and B bands obtained from UV–vis spectroscopy confirmed the formation of the hybrid material. The electrocatalytic response of the SiO_2/MWCNTs/RuPc/GCE towards fenitrothion was compared to a bare GCE and SiO_2/MWCNTs/GCE (Fig. 11a). The DPV of SiO_2/MWCNTs/RuPc/GCE displayed the highest current response in the presence of 1.66×10^{-5} mol L^{-1} fenitrothion confirming that the presence of the RuPc improves electron transfer processes and provides better sensitivity (0.0822 μA μM^{-1} mm^{-2}) and LOD (0.45 ppm). The SiO_2/MWCNTs/RuPc/GCE also appeared to be robust during interreference studies with other organophosphorus pesticides (Fig. 11b).

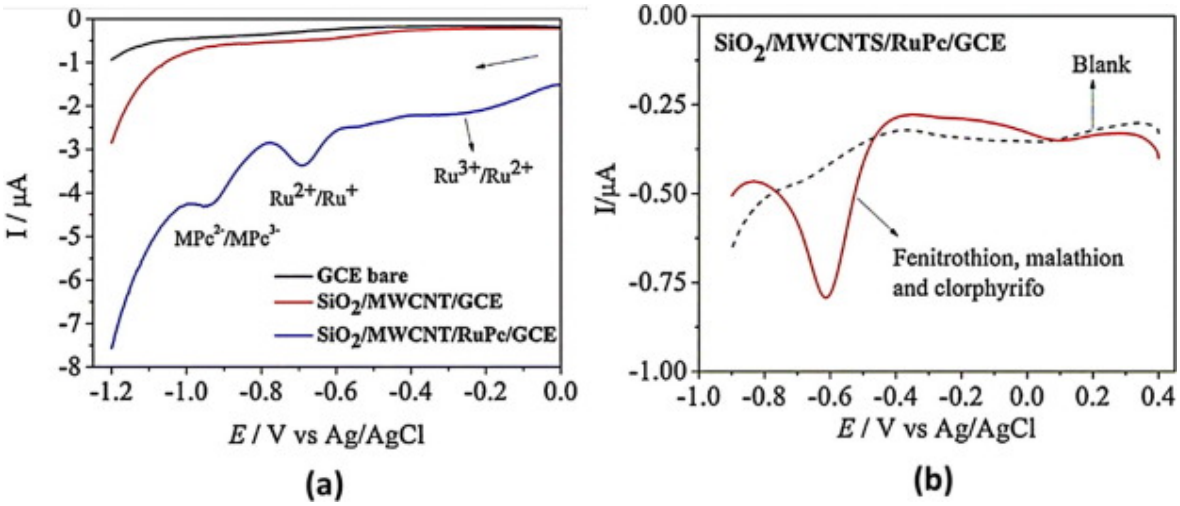

Fig. 11. (a) DPV of the GCE, SiO_2/MWCNT/GCE and SiO_2/MWCNTs/RuPc/GCE in 0.1 M acetate buffer (pH 4.5; potential range of 0 V to −1.2 V, scan rate 20 mV s^{-1}) and (b) Interference study of fenitrothion determination in the presence of chlorpyrifos and malathion pesticides in acetate buffer pH 4.5.

Phenols and phenol derivatives are classed as organic pollutants released into the environment as a direct result of industrial applications. The manufacture of drugs, dyes, detergents, plastics, fungicides and pesticides are all sources of toxic phenolic compounds that readily contaminate water systems. These environmental pollutants have always been a cause for concern due to their persistent behaviour and ease of diffusion in aqueous media [93]. To remediate this, studies toward designing a range of polyalkoxy and fluorinated substituted MPcs as the active layer of a QCM based sensor to detect a range of phenolic compounds in liquid [94]. The respective MPcs were airbrushed onto the QCM transducers and their response towards increasing concentrations of bisphenol A, phenol, pentachlorophenol and other common organic solvents such as chloroform, chlorobenzene, and tetrachloroethylene were measured. QCM measurements indicated that the selectivity of the sensor was influenced by the type of substituent on the MPc whereas sensitivity was mainly influenced by the central metal. The novelty of the study was that two octa-substituted CuPcs, namely 2,3,9,10,16,17,23,24-octakis-[2-(2-ethoxyethoxy)ethoxy] phthalocyaninato copper(II) (CuPc1) and 2,3,9,10,16,17,23,24-octakis(2,2,3,3-tetrafluoropropoxy) phthalocyaninato copper(II) (CuPc2) displayed excellent results towards a first time reported analyte, pentachlorophenol (Fig. 12). These two CuPcs exhibited strong sorption properties for pentachlorophenol achieving sensitivities as high as 200 Hz mg^{-1} L^{-1}. The selectivity obtained was also noteworthy as the sorption of the common organic solvents were at least 30 times lower in comparison.

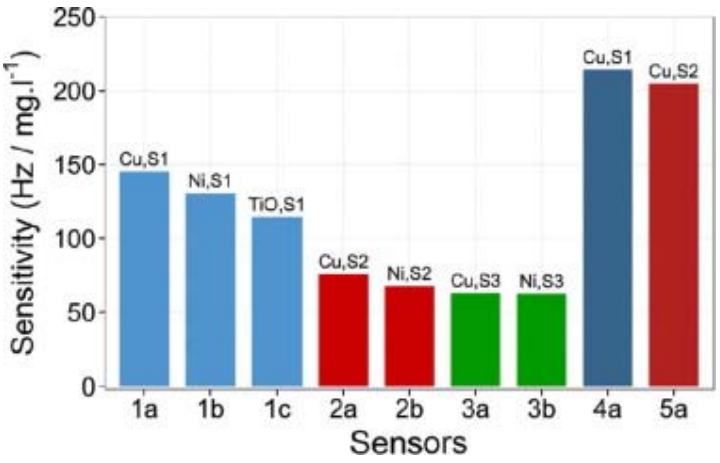

Fig. 12. Comparison of pentachlorophenol sensitivities (Hz/mg L^{-1}) for MPcs coated QCM sensors.

Pentachlorophenol was also an analyte of interest for Banimuslem et al. as they synthesized a hybrid active layer comprising of acidified SWCNTs and a tetra-hexadecylthio ($R = -S(CH_2)_{15}CH_3$) substituted CuPc complex for optical detection using total internal reflection ellipsometry (TIRE) [95]. TIRE is based on the working principle ellipsometry, a recognized analytical technique used for thin film analysis [96]. This technique can be used to obtain parameters such as layer thickness or refractive indices by modelling the experimental data around an appropriate optical model [97]. The data was fitted based on a four-layer model (consisting of an aqueous solution, gold film, organic layer, and BK7 glass), see Fig. 13.

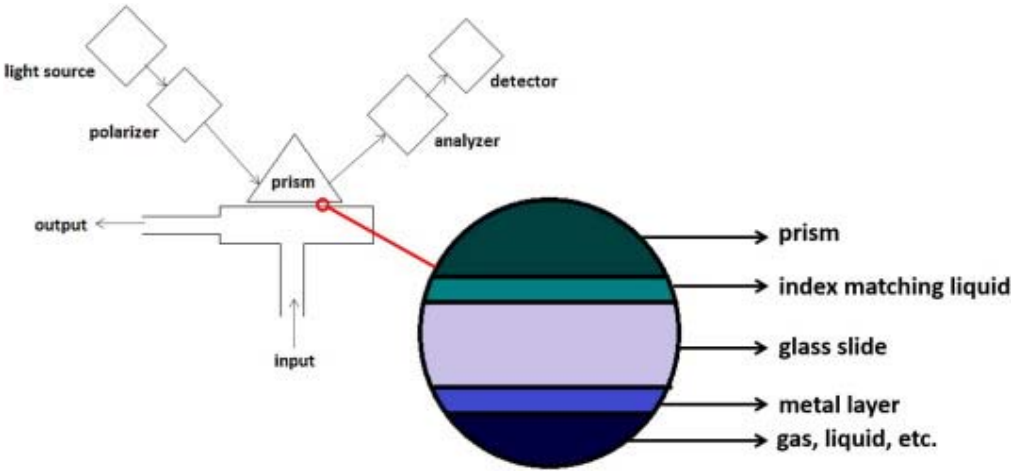

Fig. 13. Schematic view of suitable TIRE system. The magnification shows the index-matching liquid inserted between the prism and glass slide and the metal layer deposited on the other side of the glass slide.

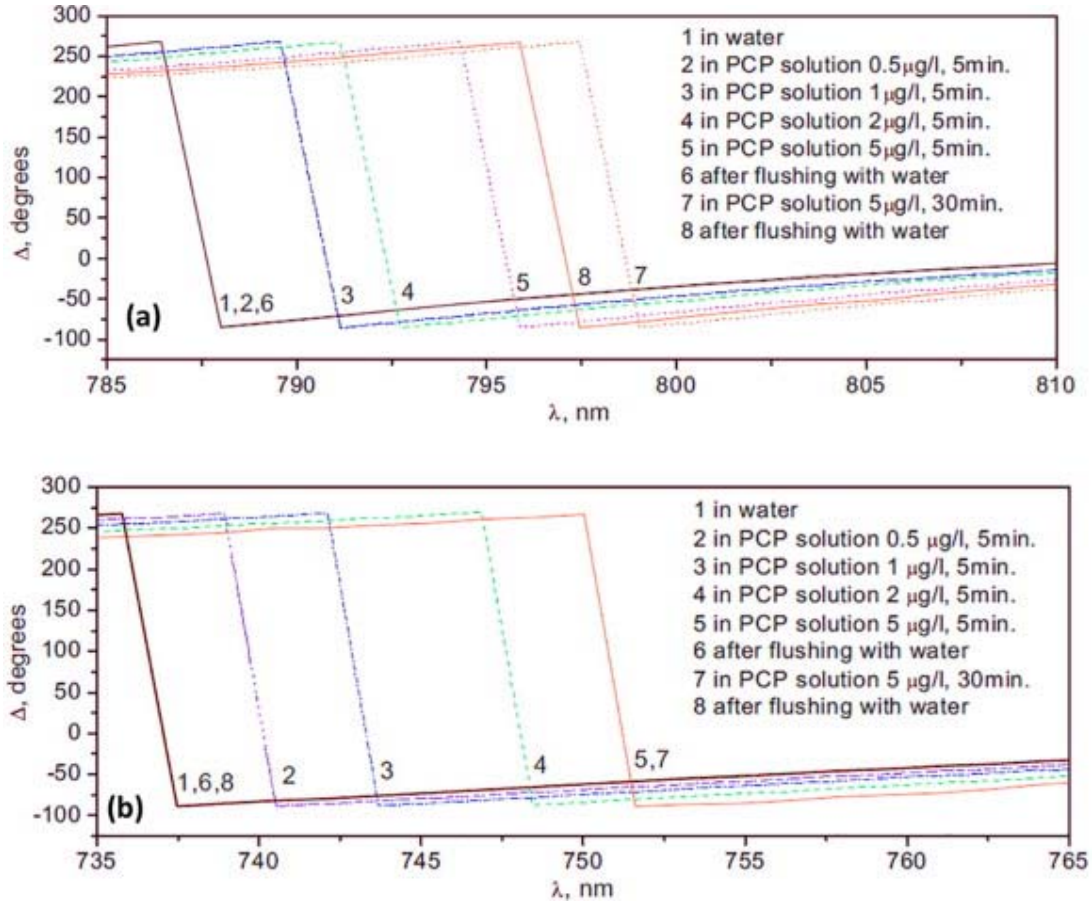

Fig. 14. (a) TIRE spectra of (a) CuPc and (b) SWCNT/CuPc hybrid films in water (1); after injection of pentachlorophenol solution of 0.5 μg L^{-1} (2); 1 μg L^{-1} (3); 2 μg L^{-1} (4); 5 μg L^{-1} (5) for 5 min; after flushing with water (6) and after injecting with pentachlorophenol solution 5 μg L^{-1} for 30 min (7); after flushing with water (8).

The TIRE spectra shown in Fig. 14a-b gives information regarding two ellipsometric parameters, ψ and Δ. The ψ parameter describes an amplitude ratio and Δ represents the phase shift (in nm) between p- and s- components of polarized light [96]. The TIRE response to pentachlorophenol in water were carried out in a range of concentrations (0.5–10.0 μg L^{-1} range as seen in Fig. 14a-b).

There were no shifts in the spectrum after treatment with pure distilled H_2O, but shifts were clearly recorded after introducing pentachlorophenol to the system. When exposed to the varying concentrations of pentachlorophenol (1, 2 and 5 μg L^{-1}), adsorption of the analyte on the hybrid film recorded larger shifts of 6.41, 10.98 and 14.19 nm as compared to the pristine CuPc film, which recorded shifts of 3.05, 4.67 and 7.82 nm. The phase shift spectra (Δ (λ)) was approximately two time larger for the hybrid film than the pristine CuPc film. The enhanced response by the hybrid film was accounted for by the high π-electron density of the SWCNTs which improved adsorption properties, especially towards oxygen containing molecules such as pentachlorophenol [98]. The aromatic system of pentachlorophenol was played a significant role in the adsorption on the SWCNTs surface due to π-π interactions. The LOD for the hybrid film was recorded at 0.50 μg L^{-1} whilst the pristine CuPc recorded a slightly higher LOD of 0.8 μg $L^{-1.}$

Consecutive studies based on the chromogenic identification of phenolic compounds using water-soluble MPcs have been reported [99], [100], [101], [102] and describes the synthesis of two novel water-soluble FePcs, iron(III) tetra-(4-carboxyphenoxy)phthalocyanine (FePc1) and iron(III) tetra-(8-quinolineoxy-5-sulfonicacid)phthalocyanine (FePc2) used in a chromogenic process, involving the formation of a dye that absorbs light within the visible region. The two FePcs were used as catalysts towards the oxidation of phenols whilst their bulky sulfur-based substituents conferred water solubility character to the FePc complexes. During the catalytic oxidation experiments phenol (P), 2-chlorophenol (2-CP), 4-chlorophenol (4-CP), 2,4-dichlorophenol (DCP) and 1-naphthol (1-NP) were oxidised by a combination of *tert*-butyl hydroperoxide (t-BuOOH), 4-aminoantipyrine (4-AAP) and the FePcs in solution. During the catalytic oxidation, the reaction mixtures undergo a chromogenic change from green to dark pink. Fig. 15a shows the time-dependent UV–Vis absorption spectra for the oxidation of phenol using FePc1. The magnitude of the peak at ~ 508 nm increased due to the formation of conjugated dyes whilst a noticeable decrease in the Q-band intensity at 634 nm was observed until its disappearance when the maximum absorbance of the newly formed dyes was reached. Based on the rate of dye absorbance, FePc1 was deemed a better catalyst than FePc2 as the chromogenic process was completed in ~10 mins (Fig. 15b-c). The catalytic oxidation mechanism shown in Fig. 16 reveals that the interaction between t-BuOOH and FePcs were key in forming the oxidised dyes. The proposed mechanism suggests that the FePc-OO^{t}Bu complex follows either a heterolytic or homolytic pathway to produce a highly reactive Fe(IV)═O species that can coordinate to the O atom from the hydroxyl group of the phenol analytes and N atom from the amino group of the 4-AAP. This consequently leads to radical formation that participates in oxidative coupling to form the dyes.

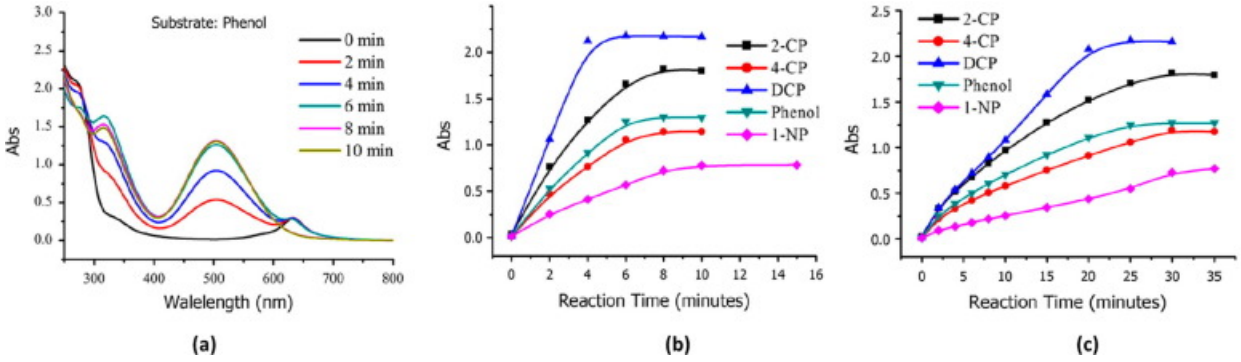

Fig. 15. (a) Time-dependent UV–Vis absorption spectra for dye formation in the presence of FePc1 and t-BuOOH towards phenol, (b) Comparative dye formation for the five phenolic derivatives with FePc1 catalyst and (c) with FePc2 catalyst.

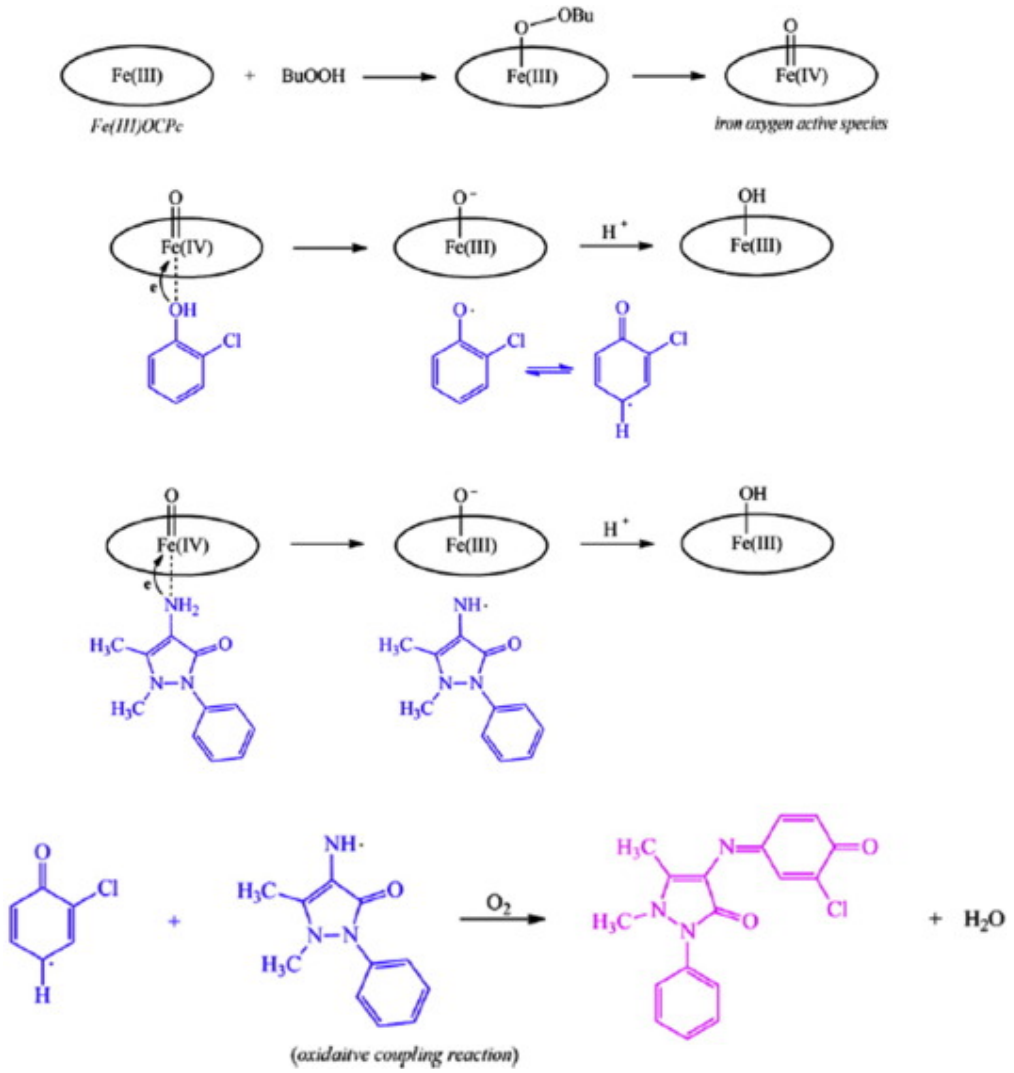

Fig. 16. Proposed mechanisms of the generation of iron(IV)–oxygen active species and the formation of the dyes.

Further progress was made in chromogenic identification of phenols when magnetic Fe_3O_4/Carbon/CuPc composites as catalysts were fabricated [103]. The catalyst was used in conjunction with aminoantipyrine (4-AAP, chromogenic agent) and BuOOH for the oxidation of phenolic compounds without additional heating or light irradiation. Although a similar catalytic oxidation mechanism was proposed as in previously reported work (Fig. 16), the added surface area and adsorption capacity provided by the Fe_3O_4 nanoparticles improved the catalytic oxidation of the phenol analytes. More significantly, the composite was retrieved magnetically from the reaction mixtures due to the inherent magnetic nature of Fe_3O_4 nanoparticles and continued to display high catalytic activity after four consecutive cycles. Other phenolic derivatives have also been detected in aqueous media using MPc/carbon-based hybrid materials to increase the active surface layer and provide additional adsorption sites for analyte attachment [104], [105], [106], [107].

The usefulness and applicability of MPcs have transpired into numerous fields, including water treatment against pharmaceutical drugs such as paracetamol, codeine and ibuprofen [108], [109]. Amongst the diverse and complex range of pharmaceuticals, sulfonamides are recognised as the first modern reagents against bacterial infections in humans including urinary tract infections pneumonia [110], meningococcal meningitis [111]. Their mechanism of treatment involves inhibiting enzymes essential for bacterial growth. Although used for the benefit of the human species for many years, the misuse and improper disposal of sulfonamide-based drugs can severely impact aquatic life, the environment and human health. Heeding the call for detection and removal of these drugs from the environment, Wang et al. proposed improving an FePc oxidative system to degrade a sulfur-containing bacteriostatic called sulfamethoxazole (SMX) using activated carbon fibres (ACFs) [112]. An asymmetric FePc was synthesised by converting a tetra-substituted nitro-FePc into a mono-amino-trinitro-FePc. The amino moiety assisted in the direct binding to the ACFs via a deamination reaction to form an FePc/ACF composite. The catalytic oxidation of the FePc/ACF was tested against SMX using liquid chromatography. As seen in Fig. 17a, the use of (1) H_2O_2 as an oxidizing agent did not decrease the SMX concentration, but the use of (4) FePc/ACF without H_2O_2 resulted in the SMX concentration decreasing by 57% during a 90-minute period until an adsorption equilibrium was reached. The best result was obtained by (6) FePc/ACF in the presence of H_2O_2, as a significant decrease of almost 99% in the SMX concentration was observed over 90 min. A proposed SMX oxidation mechanism can be viewed in Fig. 17b which indicates that this oxidation would not be as efficient without the presence of H_2O_2, FePc and ACF. The decomposition of H_2O_2 produces the active Fe(IV)$=$O species. The ACF behaves like an electron reservoir, pumping electrons into the mechanism and establishing quick electron transfer to the π-system of the FePc. The abundance of electrons promotes the homolysis of H_2O_2 leading to the production of $^{\bullet}$OH and $^{\bullet}$OH radicals that ultimately cause the oxidation of SMX.

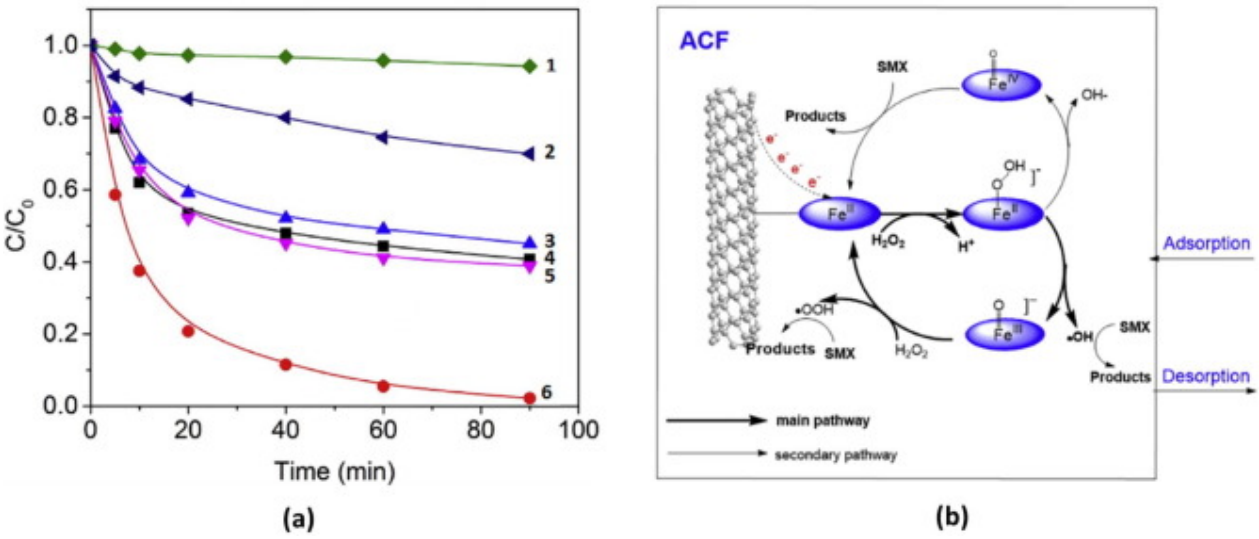

Fig. 17. (a) Concentration changes of SMX under different conditions: (1) H_2O_2; (2) FePc/H_2O_2; (3) ACF; (4) FePc/ACF; (5) ACF/H_2O_2; (6) FePc/ACF/H_2O_2 and (b) Speculative mechanism proposed for SMX decomposition.

Sulfadiazine, another sulfur-containing compound belonging to a class of sulfonamides is an anti-infective prescribed for the treatment of burns against bacterial and yeast infections [113]. Sulfadiazine was studied by Hong et al. as they developed a novel CoPc composite for the electrochemical detection of sulfadiazine [114], [115]. The combination of a tetrasubstituted CoPc with carbon nanotubes (CNTs) and Nafion on a GCE via electropolymerization was described. Nafion, a polymeric ionomer was employed to prevent CNT leakage [116]. The electroactivity of a bare GCE, CNT/Nafion/GCE and CoPc/CNT/Nafion/GCE were studied using CV and the latter displayed better anodic responses towards sulfadiazine than the other electrodes. A negative shift in the peak potential was observed and was attributed to the synergistic and catalytic relationship of the composite material i.e. quicker electron transfer kinetics of the CoPc and the excellent conductivity and redox properties associated with CNTs [117], [118]. Fig. 18a shows the current–time responses of CoPc/CNT/Nafion/GCE when injected with varying concentrations of sulfadiazine. With each injection of sulfadiazine, there is a corresponding increase in the anodic currents in less than three seconds. The inset in Fig. 18b exhibits the proportional relationship between the concentration of sulfadiazine and current response.

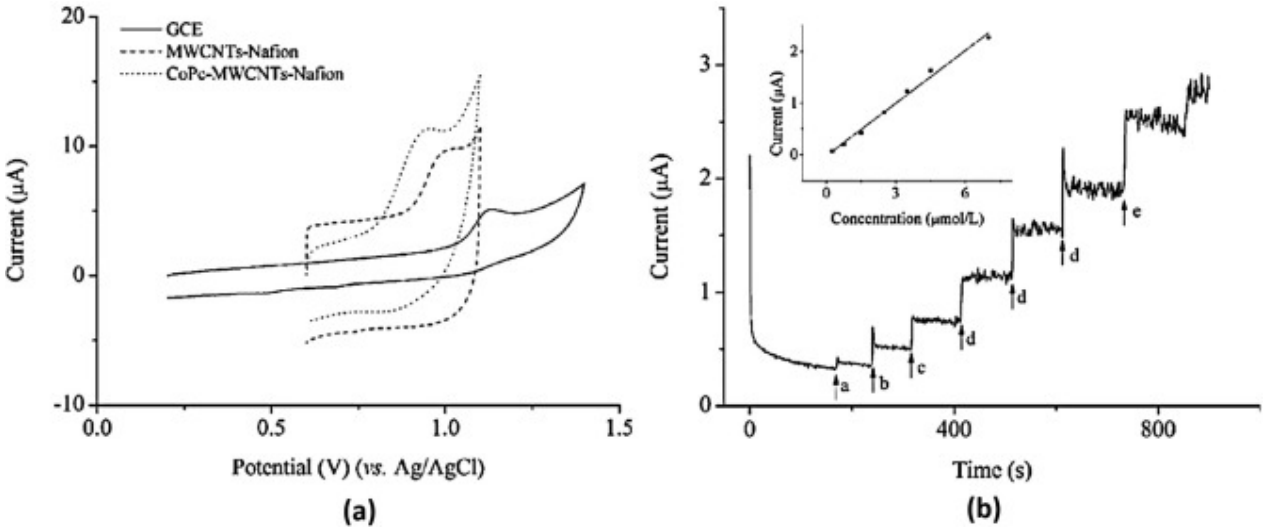

Fig. 18. (a) CVs of 0.1 mmol L^{-1} of sulfadiazine at GCE (solid line), CNT/Nafion/GCE (dashed line) and CoPc/CNT/Nafion/GCE (dotted line) and (b) chronoamperometric response of CoPc/CNT/Nafion/GCE after successive injections of varying concentration of sulfadiazine solution: (1) 5 μL; (2) 10 μL; (3) 15 μL; (4) 20 μL and (5) 50 μL of a 1 mmol L^{-1} sulfadiazine solution.

3. Phthalocyanines in non-linear optics (NLO)

Since the inception of the high-powered laser beam in the 1950s, there has been extensive and specialised use of laser beams in commercial, military, medicinal and scientific fields that require optics with great intensity and coherency. Despite the unrivalled usefulness of the laser, recent studies are directed towards sourcing optical limiters or non-linear materials to protect sensitive optical devices and components such as the human eye from laser damage [119]. An optical limiter is essentially able to attenuate the output energy of an emerging intense beam which is feature useful in a variety of applications requiring alteration of the polarization, frequency and phase of the incident light.

3.1. Principles of NLO

Non-linear optics studies non-linearities of intense light (e.g. laser beam) when interacting with matter. When light of low intensity interacts with the electronic distribution of a material, a linear response or linear polarization occurs whereby the incident light is the same as the transmitted light [120]. Non-linear optical behaviour arises when very intense incident light interacts with the electrons within a material and is powerful enough to pass the "limiting threshold", ultimately changing the properties of the transmitted light [121]. The non-linear behaviour resides in the medium through which the light travels, rather than in the light itself resulting in the modification of certain properties of the incident light. At the molecular level, non-linear behaviour resonates from the presence of delocalised π electrons, therefore the NLO phenomena commonly occur in organic molecules with a network of π-conjugated delocalized electrons [122]. The Jablonski diagram (Fig. 4) is used to explain the photophysical processes that occur when Pcs absorb light of appropriate wavelengths. Excited molecules in the S_1 state are further excited to the higher energy S_n singlet state. The average lifetime of molecules while in the S_n is short and the excited molecules undergo vibration relaxation (VR) to the lower energy S_1 state. During this relaxation, some of the molecules populate the T_1 energy state via intersystem crossing (ISC) with a rate of τ_{ST}.

Consecutively, a molecule from the T_1 state is excited to the T_n state [121]. For materials to be considered efficient optical limiters, they should ideally display [120]: i) high ratio of $T_n \rightarrow T_1$ to $S_0 \rightarrow S_1$ transitions; ii) fast ISC rate ($\tau_{ST} < 10$ ns); iii) long triplet lifetimes (relative to the pulse properties); and iv) high ISC quantum yield.

Both open and closed aperture Z-scan techniques are simple, sensitive and efficient methods to measure NLO properties of materials. A schematic diagram illustrating the working principle of Z-scan is shown in Fig. 19. The sample is held by a movable holder and is moved from one point to another, long the path (Z) of a focused Gaussian beam. During closed aperture measurements, an aperture is used to prevent some of the light from reaching the detector whereas for open aperture measurements, the aperture is removed allowing all the light to reach the detector. The transmitted light is recorded as function of the sample potions relative to the beam [119], [123].

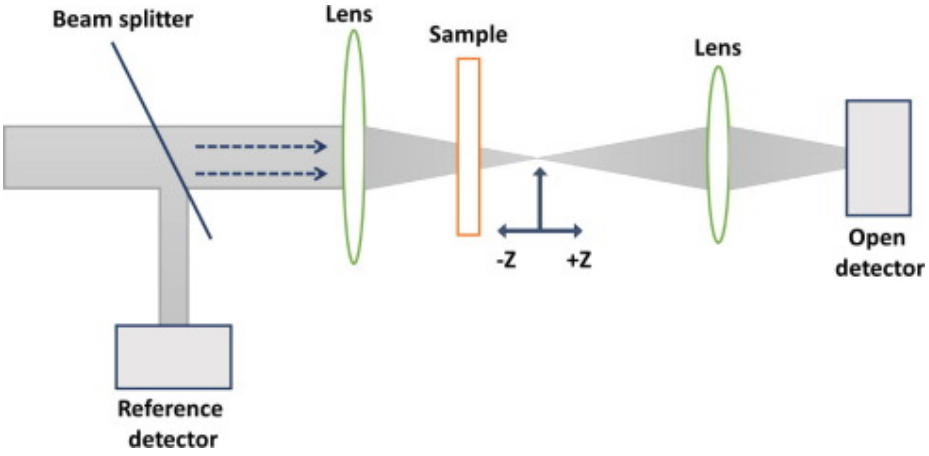

Fig. 19. Schematic diagram of an open aperture Z-scan apparatus.

An optical limiting curve can be constructed from Z-scan measurements as the intensity of the incident laser versus transmittance, Fig. 20. Optical limiting capacities of materials are often reported as absorption coefficients from theoretical derivations such as the third-order susceptibility ($l_m[\chi^3]$) and the two-photon non-linear absorption coefficient (β_{eff}) [124]. The $l_m[\chi^3]$ parameter is an indication of the speed and sensitivity to which the material responds to the laser whereas the β_{eff} parameter is proportional to the optical intensity. These parameters are used to determine the suitability of compounds as optical limiters, i.e. the higher the values, the better the optical limiter [125]. The reduced transmitted beam by the material along the Z-positions is an indication of positive non-linear absorption. This peculiar shape of the Z-scan signal is referred to as reverse saturable absorption (RSA) which is the dominant mechanism responsible for non-linear absorption (NLA) in MPcs. Other mechanisms that might contribute to optical limiting are free-carrier absorption, two-photon absorption, thermal scattering, photo-refraction, non-linear refraction and induced scattering.

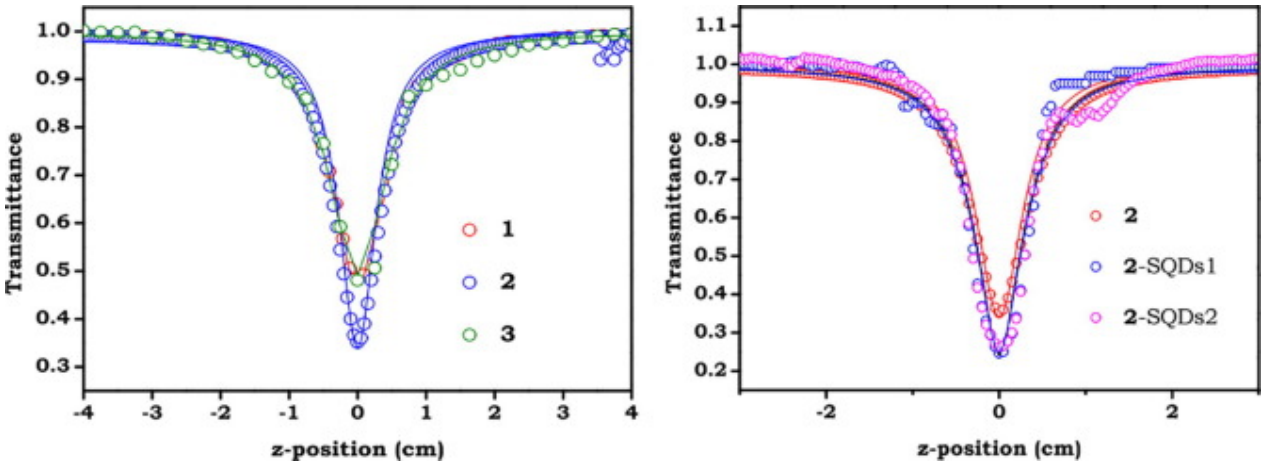

Fig. 20. Examples of open aperture Z-scan plots [123].

3.2. Phthalocyanines as optical limiters

MPcs conform to the structural prerequisites for an optical limiter (OL), have highly polarizable π-systems and produce large non-linear absorption coefficients with quick response times [126]. For Pcs, the spectral window between the Q and B bands consequently give rise to an optical phenomenon known as reverse saturable absorption (RSA) due to multiphoton absorptions [127]. Materials displaying RSA show high transmittance under normal/low light intensity whilst displaying decreased transmissions under high light intensities [121]. Phthalocyanines display RSA because of intersystem crossing from the lowest excited singlet state (S_1) to the lowest triplet state (T_1) [123].

Heavy metals such as lead (Pb), indium (In) and gallium (Ga) are often incorporated into Pcs for optical limiting mechanisms as they display enhanced intersystem crossing through spin–orbit coupling [128]. This desirable property improves the probability of accumulating a larger populated triplet state. Indium and gallium are also able to coordinate axially which assists in decreasing and preventing intermolecular interactions causing Pc aggregation [119], [121]. Nyokong's group have done extensive work on the nonlinear properties of In and Ga Pcs as well their nanocomposite derivatives [129], [130], [131], [132]. Their recent study reported the synthesis and NLO properties of asymmetric Ga(III) and In(III) Pcs bearing two diethylene glycol chains [132]. Using Z-scan at 532 nm, the $l_m[\chi^3]$ and β values were found to be higher for the InPc than the GaPc (Table 2). This result coincided with the calculated triplet state quantum yield as the InPc had a greater triplet state population than the GaPc. The GaPc and InPc were also examined as thin films embedded with poly (bisphenol A carbonate) for their NLO properties. Like the results in solution, the InPc gave a better β response value of 6.0×10^{-9} mW^{-1} compared to the GaPc which had a response of 4.8×10^{-9} mW^{-1}. It was expected that the Pc thin films with poly (bisphenol A carbonate) would present with lower β values than those found in solution due to the centrosymmetric alignment of the dipole moment in bulk material [133]. Table 2 summarises other NLO characteristics including the I_{lim} values. The I_{lim} values are another parameter that can be used to classify materials which are ideal for optical limiting applications. The lower the I_{lim} value the better the optical limiter and affirms that the InPc displays better optical limiting character than the GaPc in solution and as a film.

Table 2. Non-linear optical properties of InPc and GaPc in DMSO and thin films at 532 nm wavelength and 10 ns pulses.

Complex	In solution (DMSO)		Thin film (poly (bisphenol A carbonate)	
	InPc	GaPc	InPc	GaPc
β ($\times 10^{-9}$ mW^{-1})	7.2	6.0	6.0	4.8
$l_m[\chi^3]$ ($\times 10^{-10}$ esu)	2.36	1.97	6.3	4.77
I_{lim} (μJ cm^{-2})	2.51	7.43	–	–

*The I_{lim} values were obtained by using a solution-based calculation and could not be applied to the thin films.

Although the insertion of heavy metal atoms into the central cavity of the Pc ring encourages the population of excited states by ISC, extenuating cases where certain metals hinder the optical limiting abilities of Pc molecules have been reported. This anomaly was observed by Mwanza et al. who synthesised and characterised the NLO properties of tetra-propargyloxyphenoxy substituted H_2Pc and metallated (Co and Mn) Pcs [134]. The open aperture Z-scan study was carried out in DCM using a Nd: YAG laser source (532 nm) and revealed that more than one mechanism contributed to the optical properties of the Pcs complexes. The H_2Pc displayed a single valley Z-scan profile indicating RSA whilst the MPcs displayed "W" shaped Z-scans. In agreement with other studies, the CoPc showed a narrow W shaped plot that suggested that the molecule undergoes transitions from RSA to saturable absorption (SA) [135], [136]. The Z-scan curve of the MnPc at 532 nm displayed a relatively broad 'W' shape suggesting that the complex underwent excited saturable absorption (ESA) when exposed to the laser. The ESA resulted from the laser wavelength at 532 nm, exciting the region of charge transfer bands (LMCT or MLCT) of the MnPc. To prevent this, the experiment was carried out for the MnPc at 560 nm and produced the generic RSA plot. The measured β_{eff} correlated to theoretical DFT results and displayed the following trend: metal-free Pc (23.5×10^{-5} m MW^{-1}) > CoPc (14.3×10^{-5} m MW^{-1}) > MnPc (9.20×10^{-5} m MW^{-1} at 532 nm and 14.4×10^{-5} m MW^{-1} at 560 nm). The lower β_{eff} values were attributed to the paramagnetic nature of Co and Mn as their half-filled d-orbitals quenched the excited state and was unable to reduce the intensity of the incoming light, thus making these complexes poor optical limiters.

Pcs have also been modified using rare earth metals such as dysprosium [137], neodymiym [138] and ytterbium [139] for NLO. A 2017 study described the synthesis of polymeric carboxyl MPcs using rare earth metals, lanthanum (LaPPc-COOH), holmium (HoPPc-COOH) and ytterbium (YbPPc-COOH) as the central atoms [140]. Polymeric Pcs have a larger electron distribution and hence have a greater polarization capacity and so it was expected that the combination of the rare earth heavy metal atoms together with the large polymeric carboxyl groups would result in stronger OL responses with additional stability than monomeric counterparts when subjected to laser radiation [141]. However, these macro-molecules hinder the solubility and dispersibility of MPcs, restricting their use in NLO research. The acetate salts of lanthanum, holmium and ytterbium were refluxed with tetrakis-[(2,3-dicyanophenoxy)methyl and DBU in tetrahydronaphthalene to yield the MPcs. Although UV–vis spectra displayed extensive aggregation for all the MPcs, the NLO plots under open aperture conditions exhibited well defined valleys, indicating RSA with positive coefficients. The Z-scan experiment was also conducted under closed aperture conditions were a valley to peak plot was obtained, suggesting a self-focus effect of non-linear reflection [142]. The $l_m[X^3]$ values for the three MPcs are to the order 10^{-12} esu and follow a decreasing sequence of LaPPc-COOH > HoPPc-COOH > YbPPc-COOH for their NLO properties.

Studies have shown that NLO responses not only originate from extended π-electron delocalization of the Pc ring but also from the asymmetrical electronic structure induced by ring substitution [143]. Britton et al. demonstrated this concept by synthesising a novel octa-substituted 2,3 -bis[2′-(2″-hydroxyethoxy)ethoxy]-9,10,16,17,23,24-*hexa*-n-butoxy ZnPc [125]. The formation of the asymmetric ZnPc formed *via* a cross condensation of two phthalonitriles, i.e. (a) 1,2-dicyano4,5-bis[2′-(2″-hydroxyethoxy)ethoxy]benzene and (b) 4,5-di-n-butoxyphthalonitrile (with an excess of (a)). The asymmetric ZnPc displayed an ($l_m[\chi^3]$) value to the order of 10^{-11} esu.

Tetra-substituted Pcs can form four positional isomers of the following symmetries: C_s, C_{2v}, C_{4h} and D_{2h}. Ngubeni et al. (2015) and Gounden et al. (2017) conducted NLO studies on 4-(4-*tert*-butylphenoxy) H_2Pcs isomers substituted either at the α- and β- positions, respectively [135], [144]. Both studies used theoretical (DFT and TD-DFT) and experimental (Z-scan) approaches to assess the second-order non-polarizability (β) of each isomer. The studies proved all four isomers display strong RSA profiles but the α substituted isomers displayed superior β values with magnitudes to the order 10^{-5} m MW^{-1} whilst the β substituted isomers showed magnitudes to the order of 10^{-10} m MW^{-1}. In both cases, the C_{4h} isomer showed the strongest non-linear behaviour and was attributed to the fact the C_{4h} isomer has higher symmetry than its three counterparts.

The attractive optical limiting abilities of Pcs were combined with other interesting materials such as metal nanoparticles [145], [146], polymers [147], graphene oxide [148], carbon nanotubes [149] and quantum dots [150]. Wang et al. constructed two hybrid composites consisting of ZnPcs namely (a) 1,8,15,22-tetra-(3-(5-hydroxyl)pentyloxy) ZnPc (ZnPc(TD)$_4$) and (b) 1,8,15,22-tetra-(3-[2-(2-hydroxyl)ethoxy]ethoxy) ZnPc (ZnPc(DG)$_4$) combined with graphene oxide (GO) [151]. Similar to Pcs, carbon-based materials have garnered interest for their interesting NLO properties as they are also structured with conjugated organic molecules [152]. The conjugation was achieved via an ester covalent bond between the ZnPcs and GO and this linkage was confirmed by various spectroscopic characterisation techniques including XPS, UV–vis and FT-IR. Referencing the Jablonski diagram (Fig. 4), the T_1 state can arise from the electron transition between the S_1 to T_1 state via ISC. In this hybrid material, fluorescent spectroscopy suggested that the T_1 state could also arise from the S_1 state via charge-separated state (CSS) by photo-induced electron transfer (PET), see Fig. 21.

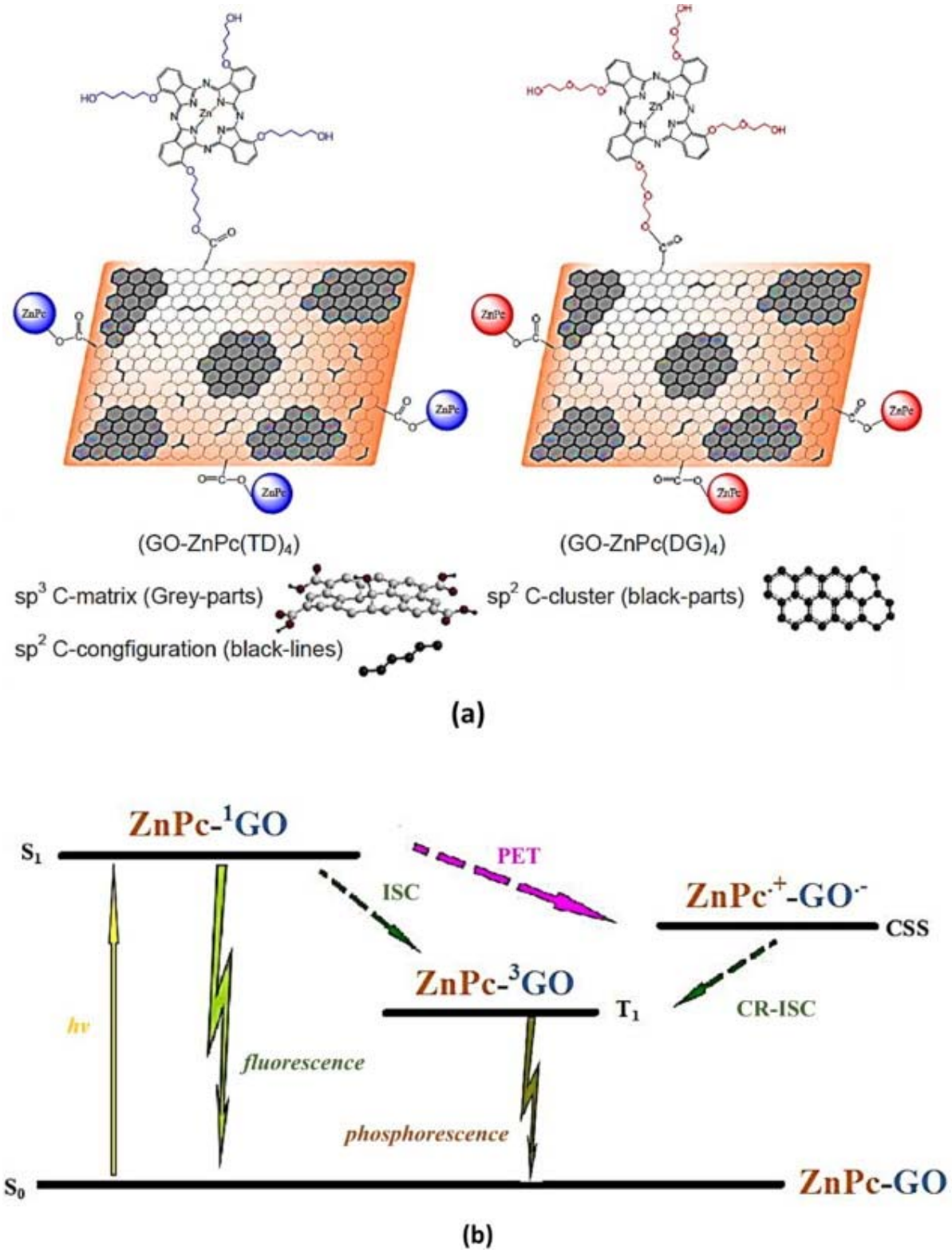

Fig. 21. (a) Hybrid composites GO-ZnPc(TD)$_4$ and GO-ZnPc(DG)$_4$ and (b) energy level model showing the PET process of GO-ZnPc hybrid composites.

Using the Z-scan method, typical RSA profiles were obtained for both composites. The β value of the GO-ZnPc(DG)$_4$ was larger than that of GO-ZnPc(TD)$_4$ which was attributed to the former hybrid possessing a larger electron cloud. Generally, Pcs with peripheral substituents that are tailored with strong electron-donating capabilities increase the electron cloud density and enhance ISC as well the polarizability of the π conjugated systems, thereby improving the overall NLO properties.

Recently, Mgidlana et al. synthesized three novel ZnPcs, (a) Zn(II) mono 3-carboxyphenoxy-tris(pyridin-2-yloxy) phthalocyanine (ZnCPPc), (b) Zn(II) mono aminophenoxy-tris(benzothiazole) phthalocyanine (ZnAPPc) and (c) Zn (II) mono amino-carboxyethylphenoxy phthalocyanine (ZnACPc) and combined them with different semiconductor quantum dots (SQDs) [123]. The ZnPc derivatives were covalently linked *via* amide bonds to appropriately functionalised CdTe/ZnS (core/shell) and CdTe/ZnS/ZnO (core/shell/shell) QDs. These conjugates were expected to display enhanced optical limiting behaviour than Pc complexes alone due to spin–orbit coupling emanating from the heavy metal atoms of the SQDs [153]. Table 3 shows the optical limiting properties of the ZnPc complexes and ZnPc-SQDs conjugates. The conjugates showed better triplet quantum yields as the "heavy metal atom effect" that encouraged a higher populated triplet state that influenced faster ISC. With regards to the core/shell orientations of the conjugate materials, there were no significant variations observed for the triplet quantum yields in the presence of the extra shell. Z-scan was used to measure the NLO characteristics of the conjugates.

Table 3. Experimental NLO for MPcs and the QD-nanoconjugates in DMSO.

Compound	$\lvert\chi^3\rvert$ (esu)	β_{eff} (cm GW^{-1})
ZnCPPc	7.12×10^{-13}	42.2
ZnCPPc – SQDs1	8.83×10^{-13}	52.2
ZnCPPc – SQDs2	1.20×10^{-12}	71.2
ZnAPPc	1.32×10^{-12}	78.1
ZnAPPc – SQDs1	1.35×10^{-12}	80.0
ZnAPPc – SQDs2	1.52×10^{-12}	80.8
ZnACPc	8.12×10^{-13}	48.0
ZnACPc – SQDs1	1.18×10^{-12}	70.0
ZnACPc – SQDs2	1.25×10^{-12}	74.0

4. Phthalocyanines in energy and data storage devices

4.1. Energy storage

Challenges associated with energy production has always been a highly contested global topic but the majority of scientists agree that one of the most devastating and irreversible consequence to our fossil fuel dependence for energy production is climate change. In a time of huge technological advancements, batteries and supercapacitors are being developed to lower the carbon footprint. The flexible Pc electrocatalytic structure can attain superior electron transfer capacities and when incorporated into electrochemical storage devices can improve existing setbacks such as charge and discharge rates [154], intercalation chemistry between electrodes [155], improvement of life cycles [156] etc. In the following studies, Pcs are incorporated in electrochemical capacitors (ECs). ECs are energy storage devices whose storage capacity originates from interactions occurring at the surface of electrode materials

[157]. ECs can be classed as electrical double layer capacitors (EDLC) that stores charge at the interface between the electrode and electrolyte or pseudo-capacitors, that have an inherent charge due to their faradaic/redox properties [158]. MPcs have unfavourable electrical conductivity, thus limiting its applicability unless combined with a highly conductive material such as graphite and graphene-based materials [159]. These carbonaceous materials are popular in ECs for various reasons including ease of preparation, synthesis in large quantities, and has an sp^2 hybridized carbon network that provides fast charge transfer channels necessary for efficient ECs [160]. The combination of MPcs with graphene materials is advantageous. MPcs readily integrate with conjugated systems such as graphene *via* coordinate bonds, hydrogen bonds, van der Waals forces, etc. [161], and form stable composites. Furthermore, these carbonaceous materials prevent Pc stacking thereby enhancing the overall rate capacity of the electrochemical system [162].

4.1.1. Energy storage – MPcs, graphene oxide (GO) and reduced graphene oxide (rGO)

A composite material of nickel(II) tetraaminophthalocyanine (NiTAPc) and modified graphene oxide sheet for its pseudocapacitive properties has been tested [163]. The fabricated NiTAPc/GO were prepared in a 1:1 ratio and were subjected to ultrasonication and overnight drying at 60 °C. Nickel foam was modified with a homogenous paste made of NiTAPc/GO, carbon black (CB, conductive material), polyvinylidene fluoride (PVDF, binder) and a few drops of N-methyl-2-pyrrolidone (NMP). Using a two-electrode system CV, electrochemical impedance spectroscopy (EIS) and galvanostatic charge–discharge (GCD) measurements were carried out, see Fig. 22a–c.

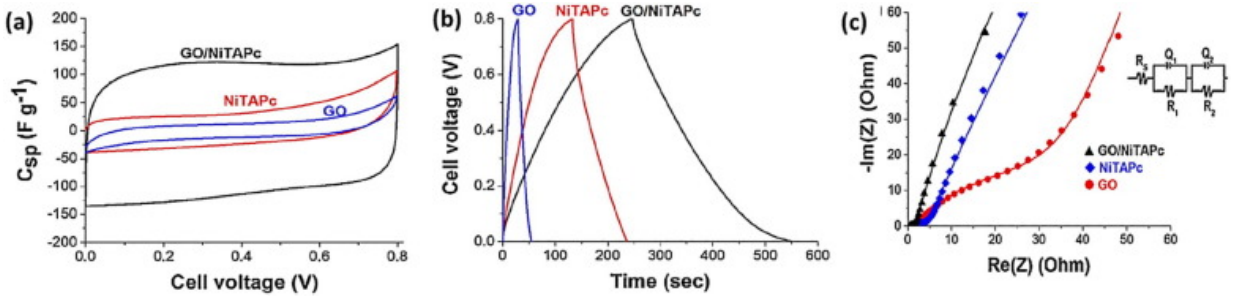

Fig. 22. (a) CVs of the GO, NiTAPc and NiTAPc/GO obtained at 5 Mv s^{-1}, (b) GCD curves for GO, NiTAPc and NiTAPc/GO at 0.5 A g^{-1} and (c) Nyquist plot for GO, NiTAPc and NiTAPc/GO.

The voltammograms indicated that the NiTAPc/GO displayed a larger capacitive behaviour than its precursor counterparts. The quasi-rectangular shape of the voltammogram correlates with the Ni(II)/Ni(III) redox couple, confirming the pseudocapacitive nature of the NiTAPc/GO composite. A similar outcome was observed for the galvanostatic charge–discharge measurements. The EIS results were represented as Nyquist diagrams (Fig. 22c). The curve for the composite shows a slight shift towards the "imaginary axis" at lower frequencies. This identifies with traits of an ideal capacitor and indicates ion diffusion between the electrode and electrolyte interface [164], providing further confirmation that the composite displays the best capacitive behaviour. The composite reported a specific capacitance of 163 F g^{-1}, a power density of 140 kW kg^{-1} and retained it capacitive behaviour after a 50-hour voltage holding test. Similarly, a 2010 study tested a NiTAPc/MWCNT composite for its super capacitive properties [159]. The composite displayed a specific capacitance of 981 F g^{-1} and power density of 700 W kg^{-1}. The superior capacitive behaviour

of the NiTAPc/MWCNT composite is possibly due to a larger surface area that provides both anchorage for the NiTAPcs and a greater conductive carbon network.

A related system whereby a composite material comprising of NiPc nanofibers (NiPcNF) and rGO acts an EC has been described [165]. The NiPcNFs and rGO were prepared *via* simple synthetic routes and were eventually combined and heated for 24 h at 100 °C in a hydrothermal vessel to form the composite material. The UV–vis spectrum of the composite showed the characteristic Q and B bands of the NiPcNFs and an additional peak at 270 nm corresponding the $\pi \rightarrow \pi^*$ transitions of the sp^2 hybridized carbon network of rGO whilst electron micrographs in Fig. 23a-b confirmed the physical interface formed between the NiPcNFs and rGO. The composite dispersed well in DMF and was used to modify a pencil graphite rod (PGE). Using CV, the electrochemical behaviour of NiPcNFs, rGO and the NiPcNF/rGO composite were assessed to provide insight into the faradaic interactions of the modified electrodes. The CV scans show an enhanced capacitive response for NiPcNF-rGO over its individual components. The larger capacitance was as a result of the synergistic relationship created between the NiPcNFs and rGO whereby the rGO acted as the EDLC and the NiPcNFs acted a pseudo-capacitor due to the central Ni metal having a Ni(II)/Ni(III) redox couple and electroactive nitrogen moieties. The NiPcNF-rGO composite also underwent several charge–discharge cycles and proved to be relatively stable. The specific capacitance of the NiPcNF-rGO modified electrode was calculated as 223.28 F g^{-1} with a deliverable efficiency of 88.24% at 1 A g^{-1}.

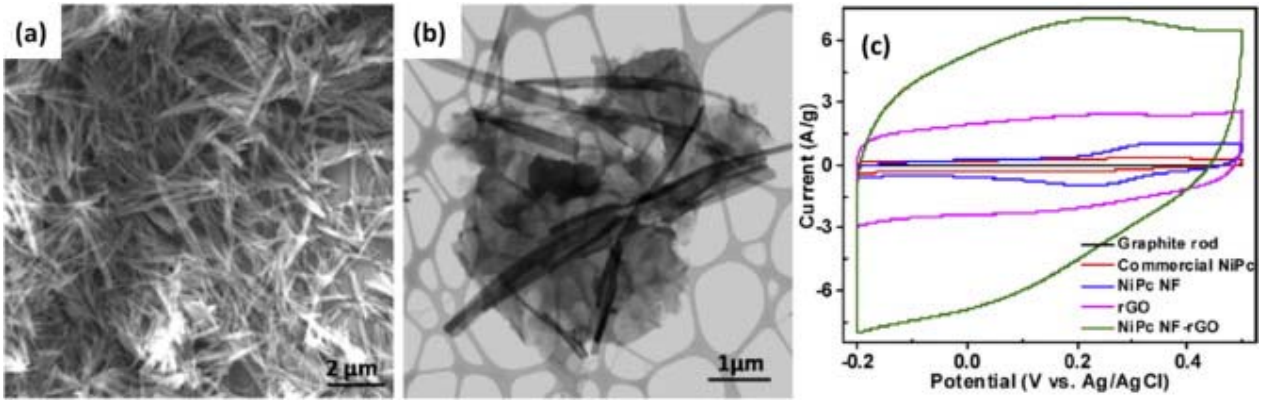

Fig. 23. (a) FEGSEM, (b) STEM micrographs of the NiPcNF-rGO composite and (c) CVs of the different modified electrodes. (Scan rate: 100 mV s^{-1} in 1 M H_2SO_4 electrolyte).

The synthesis of nanosized Pcs was also reported and described the preparation of non-peripheral octa methyl-substituted copper(II) phthalocyanine nanorods (CuPc) with graphene oxide (GO) as a composite material for supercapacitors [162]. The rectangular-shaped CVs of the composite indicated pseudo-capacitance originating from the Cu metal, similar to the faradaic response as the NiPc in the previous study, i.e. Cu(II) $\leftrightarrow$ Cu (III) + e^-. A contributing factor to the pseudo-capacitance could also resonate from redox reactions that take place at the N atoms on the CuPc skeleton which could improve charge mobility of the GO and increase electron transfer processes [166]. The weight ratio of the CuPc:GO composite was optimised at a 2.0 mg: 10 mg and obtained a specific capacitance of 291.6 F g^{-1} which is approximately three times greater than the pure CuPc nanorods (84.3 F g^{-1}) and GO (90.9 F g^{-1}). This optimised ratio possibly offered more sites for redox reactions ensuring higher charge storage behaviour. The charge storage ability of the CuPc/GO electrodes was characterised by EIS and processed into Nyquist plots. The

presence of a semicircle region at higher frequencies confirmed pseudo-capacitance whilst the straight line closer to the imaginary axis at lower frequencies was an indication of capacitive behaviour [167]. The optimised electrode delivered a maximum energy and power density of 3.38 Wh kg^{-1} and 0.138 kW kg^{-1}, respectively. These values were higher than that of previously reported RuS_2 (1.51 Wh kg^{-1}) [167] and FeS (2.56 Wh kg^{-1}) devices [168]. The CuPc/GO electrode displayed superior stability as almost 100% of its initial capacity was retained after 5000 cycles.

4.1.2. Energy storage – MPcs and lithiation

Yang et al. prepared an electrode for secondary lithium-ion (Li-ion) batteries by casting a homogenous slurry of an iron phthalocyanine-graphene nanosheet composite (FePc/GN), PVDF and NMP onto a copper foil and drying at 100 °C for 6 h [169]. The resulting electrode was placed in an electrochemical setup with Li foil as the counter electrode, $LiPF_6$ in diethyl carbonate/ethylene carbonate/dimethyl carbonate electrolyte solution and a micro-porous membrane separator. Cyclic voltammetry was used to interpret the kinetics and reversibility of the FePc/GN composite towards Li interaction and de-intercalation.

Fig. 24a shows the CVs of composite versus the Li/Li+ reference electrode. Lithiation and de-interaction occurred at ~0.17 V and~0.20 V for the graphene component in the composite [170].

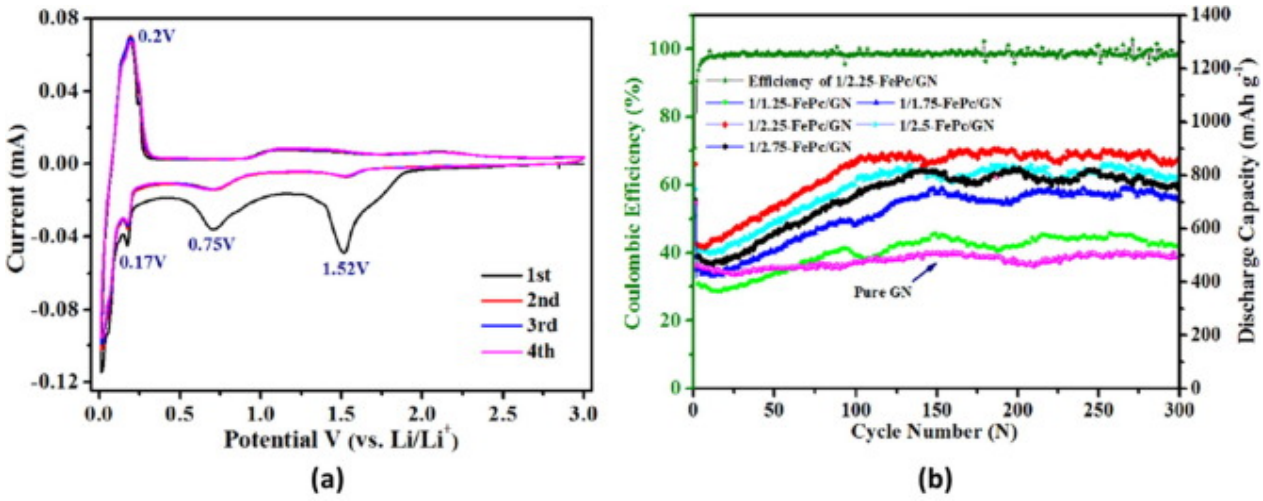

Fig. 24. (a) CVs of the FePc/GN composite (weight ratio 1/2.25) and (b) Cycle performance of FePc/GN at different weight ratios and pure GN at a current density of 300 mA g^{-1}.

From previous studies, it was expected that Li^+ ions intercalate and de-intercalate with the FePc via electrochemical mechanisms [171], [172]. As shown in Scheme 1, there are six C═N bonds, whereby the nitrogen atoms carry a lone pair on which reversible redox reactions can take place (Step 1) [173]. Ideally, an unsubstituted FePc has 19 double bonds that can undergo a reversible addition reaction with a Li^+ ion. Step 2 shows that each C_6 aromatic ring accepts six Li^+ ions to form a Li_6/C_6 complex [174], [175]. Subsequently, each FePc molecule can reversibly accept 38Li^+ ions.

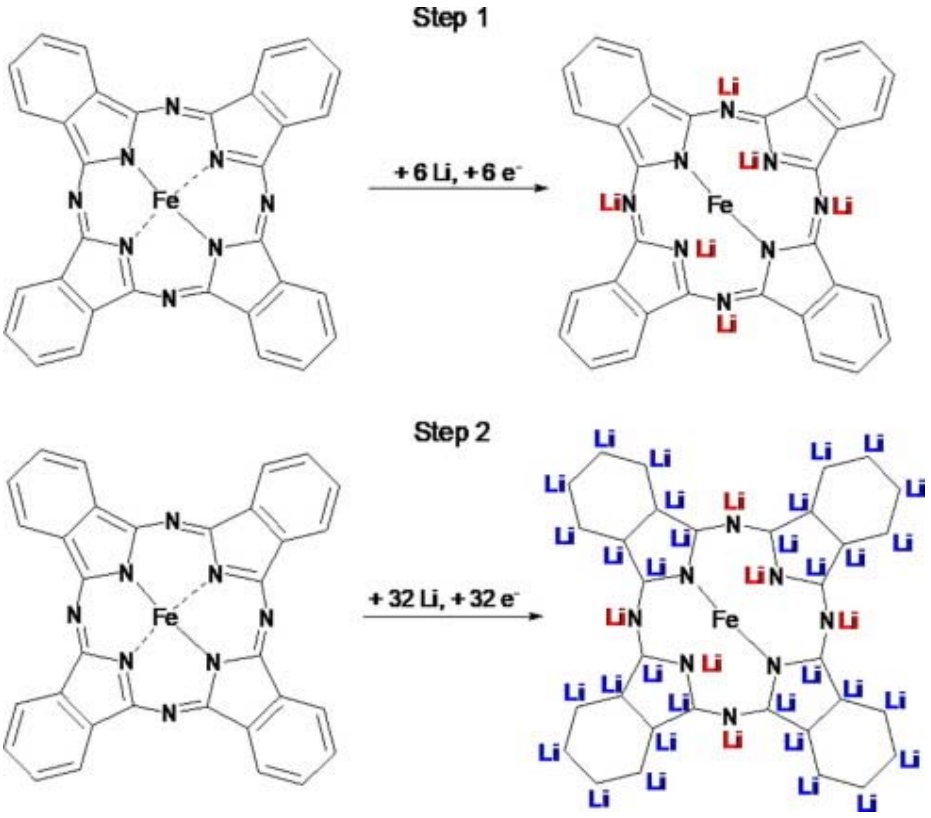

Scheme 1. Lithiation sites on the FePc complex.

Fig. 24b shows that lithiation of the FePc component of the composite at the C_6 of the aromatic rings was observed at ~0.75 V and signalled the formation of a solid electrolyte interphase (SEI) [173]. The much broader peak at 1.52 V was associated to the lithiation of the nitrogen atoms of the FePc complex [173], whilst the oxidation peaks between 1.0 and 1.6 V were attributed to the de-intercalation of the FePcs. There were no major changes to the CV after the second cycle, suggesting that the FePc/GN composite electrode is stable and reversible towards the Li^+ ion intercalation and de-intercalation. The study also optimised the FePc/GN ratio to obtain the highest capacity. Despite the different ratios, the composites all show an increased capacity until the 100th cycle and plateaus thereafter. The 1/2.25 Fe/GN composite displayed the best capacity of 873 mAh g^{-1}. This is twice the theoretical capacity of commercial graphite (372 mAh g^{-1}). The contribution of the FePc towards the capacity was calculated using the following equation:

$$C_N = C_A \times W_A + C_B \times W_B$$

where C_N is the capacity of the FePc/GN composite, C_A is the specific capacity based on the FePc component, C_B is the specific capacity based on GN component, W_A is the weight ratio of FePc, and W_B is the weight ratio of GN, see Table 4.

Table 4. Capacity contribution of FePc and GN at different weight ratios.

Weight ratios of FePc/GN composite	The capacity of FePc/GN (mAh g^{-1}) (C_N)	The capacity of GN (mAh g^{-1}) (C_B)	The capacity of FePc (mAh g^{-1}) (C_A)
1:1.25	539	509	606
1:1.75	706	509	1149
1:2.25	849	509	1614
1:2.50	796	509	1441
1:2.75	766	509	1344

From Table 4, the FePc/GN electrode displays a lower discharge capacity when the graphene content of the composite was lower or higher than a weight ratio of 1:2.25 and was explained as follows: the lower graphene content (ratio < 1:1.25) could not compensate for the poor electronic conductivity of FePcs whilst at higher graphene content (ratio > 1:2.25) the decreased discharge capacity was attributed to lower storage capacity of graphene in caparison to the storage capacity of the FePc.

4.1.3. Energy storage – MPcs and dopants

Nitrogen doping has been employed as a beneficial technique in many graphene EDLC studies as a means to tailor the electronic system of a material to improve device performance [176], [177], [178], [179]. The additional nitrogen atoms can assist in [180]: i) Improving interactions with ions in solution, ii) the lone pair electrons on nitrogen atoms can contribute to pathways for charge transfer in conductive networks (e.g. graphene), iii) pyrrolic nitrogen atoms can participate in reversible faradaic reactions, and iv) doping can induce disordered surface morphology that can improve electrode wettability. He et al. developed a one-pot synthesis to produce three dimensional (3D), honeycomb-shaped nitrogen-doped graphene composite using solid-state pyrolysis [181]. Briefly, the experimental involved stirring metal-free Pc (H_2Pc), GO and H_2SO_4 at room temperature for 24 h to form the precursor GO/H_2Pc composite. Subsequent steps included centrifugation, washing (with dH_2O) and drying at 60 °C. The precursor composite was pyrolyzed in a quartz holder at 800 °C to yield the nitrogen-doped graphene with a honeycomb morphology. Microstructure analysis indicated that the planar orientation of H_2Pcs self-assemble into the GO sheets via π-π interactions. At 800 °C the interlaminated H_2Pc molecules pyrolyze into the nitrogen-graphene and bind to the reduced GO. This conjugation prevents the restacking of graphene and produces graphite powder. The 3D honeycomb network forms as a result of hydrogen released from the pyrolyzed organic molecules. The SEM micrographs in Fig. 25a-b clearly depict the porous network and the edges of the GO multi-layered sheets.

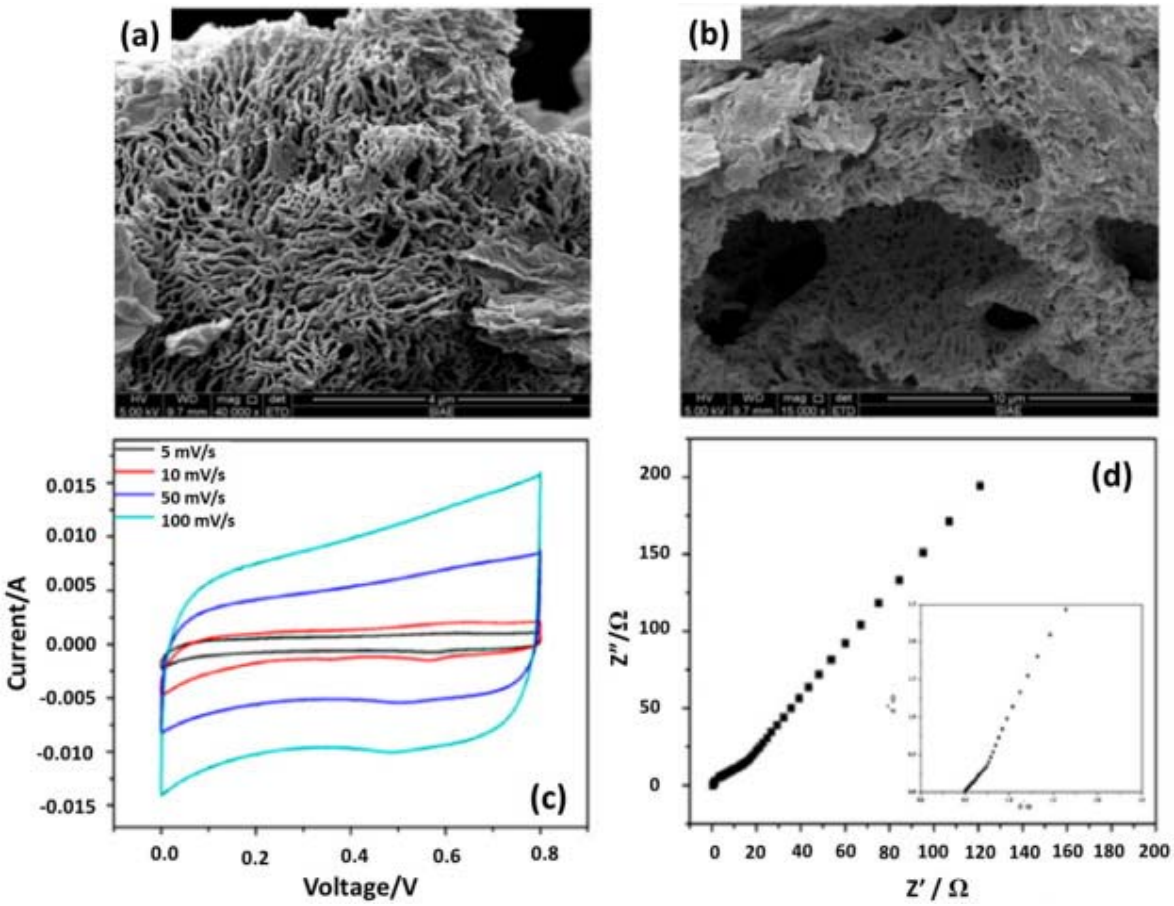

Fig. 25. (a-b) SEM micrographs of the 3D-graphene/H_2Pc, (c) CVS of 3D-graphene/H_2Pc measured at scan rates of 5, 10, 50, and 100 mV s^{-1} and (d) Nyquist plots of the 3D-graphene/H_2Pc.

The capacitive performance of the 3D-graphene/H_2Pc was evaluated by CV and EIS. Fig. 25c shows rectangular-shaped voltammograms of the 3D-graphene/H_2Pc at scan rates up to 100 mV s^{-1}, an indication of good electrochemical capacitance and low resistance. The magnified insert of the Nyquist plot (Fig. 25d) shows a straight line in the low-frequency region and a semicircle in the high-frequency region. The semicircle represents low interfacial charge transfers resistant and is characteristic of materials with high electrical conductivity. The 3D-graphene/H_2Pc material displayed a specific capacitance of 175 F g^{-1} at 0.5 A g^{-1} and exhibited a long-life cycle of 5000 cycles whilst retaining ~100% of its capacitance. The promising results obtained by the 3D-graphene/H_2Pc were attributed to: i) the abundance of macro and mesopores that provided larger surface areas compared to 2D graphene, ii) the macro and mesopores also behaved as ion portals for better ion transfer, and iii) the nitrogen doping contributed to the enhanced capacitance due to favourable and reversible redox reactions in the electrolyte.

Lu et al. reported a study in which a tetrasulfonic acid tetrasodium copper-phthalocyanine salt (CuPcTs) was used as a dopant to improve electrochemical properties and manipulate the nanopores of polypyrrole/multi-walled carbon nanotube (PPy/MWCNTs) composites for energy storage [182]. The measured specific capacitance of the doped-CuPcTs composite (CuPcTs/PPy/MWCNTs) was compared to another doped composite containing phytic acid (PA/PPy/MWCNTs) and the undoped PPy/MWCNTs composite. The specific capacitance at

10 m Vs^{-1} was measured for the doped-CuPcTs composite (CuPcTs/PPy/MWCNTs) that was compared to another doped composite containing phytic acid (PA/PPy/MWCNTs) and the undoped PPy/MWCNTs composite. The CuPcTs/PPy/MWCNTs composite attained the highest specific capacitance of 451 F g^{-1}, the PA/PPy/MWCNTs composite obtained a specific capacitance of 288 F g^{-1} whilst the un-doped PPy/MWCNTs composite displayed the lowest specific capacitance of 267 F g^{-1}. The BET results for the PPy/MWCNTs, CuPcTs/PPy/MWCNT and PA/PPY/MWCNTs electrodes were reported as 32.33, 50.17 and 39.33 m^2 g^{-1}, respectively, and indicated that the CuPcTs/PPy/MWCNTs composite provided a far greater surface area. The greater surface area provided better electron transfer channels and ion diffusion sites and resulted in specific capacitance values that are approximately double that of the PPy/MWCNTs and PA/PPY/MWCNTs electrodes.

4.2. Data storage

The 21st century is widely recognised as the information or digital age, consumed by an abundance of information and has created a need for devices with greater data storage capacity. Researchers look to construct data storage devices that encompass features such as high speeds, stability, reduced energy usage and portability [183], [184]. Within the MPc family, CuPcs has been at the forefront in providing active layers for data storage devices and are highlighted in most of the following reviewed studies [185], [186], [187].

Tripathi et al. performed a comparative study that evaluated the effectiveness of CuPc as an additive to a cadmium sulfate and polystyrene nanocomposite (CdS/PS) active layer for memory storage [188]. Device A was fabricated with the CdS/PS nanocomposite whilst device B included a CuPc layer inserted between the bottom Al electrode and the CdS/PS layer. The configuration of both devices are shown in Fig. 26a. As per the I-V curves in Fig. 26b, both devices show both electrical hysteresis behaviour which is vital for memory storage applications as well as metal to semiconductor contact (M-S contact). The M-S contact in this instance is ohmic as justified by the linear I-V plots. The performance of the semiconductors was judged by the quality of the M-S contact using thermionic field emission theory and the Schottky diode, seen in the equation below:

$$J = J_s\left(e^{\frac{V}{nV_T}} - 1\right)$$

where J is the diode current, J_s is the reverse saturation current density, V is the voltage across the diode, V_T is the thermal voltage: kT/q (Boltzmann constant times temperature divided by electron charge) and n is the ideality factor.

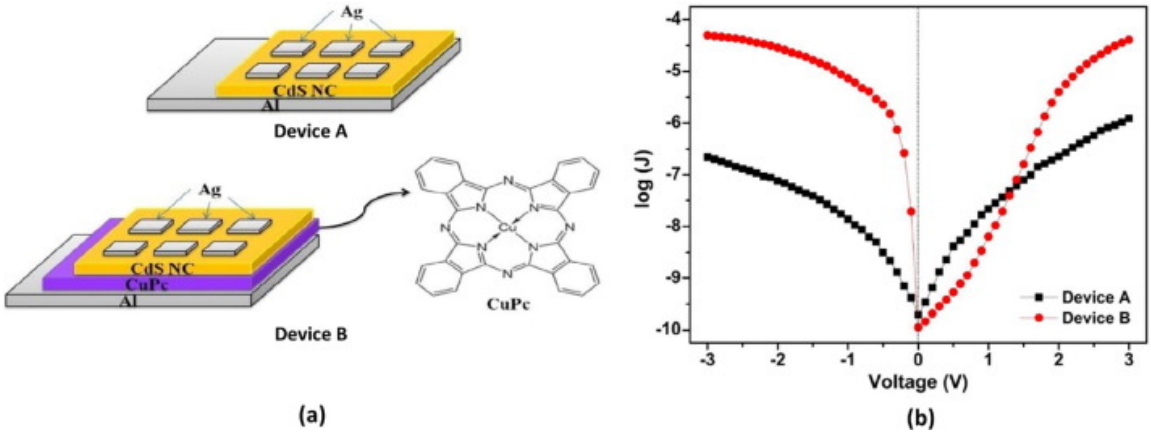

Fig. 26. (a) Configuration of devices A and B and (b) I-V plots of both fabricated devices.

The addition of the CuPc in device B showed a decrease in the J_s value from 3.68×10^{-10} A to 6.32×10^{-11} A. The lower J_s value indicates that device B shows lower power dissipation and better thermal stability compared to device A. CuPc is an established p-type semiconductor and behaves as the hole trapping layer whilst the CdS/NP nanocomposite behaves as the electron trapping layer [189]. The LUMO of the CuPc has a higher energy level compared to the CdS, which facilitates electron transfer to the CdS when a positive voltage is applied to the Ag electrode. Once the electrons are trapped in the CdS layer, the high energy barrier of the CuPc layer prevents tunnelling of trapped electrons back to the Al electrode, as represented in the energy diagram in Fig. 27a.

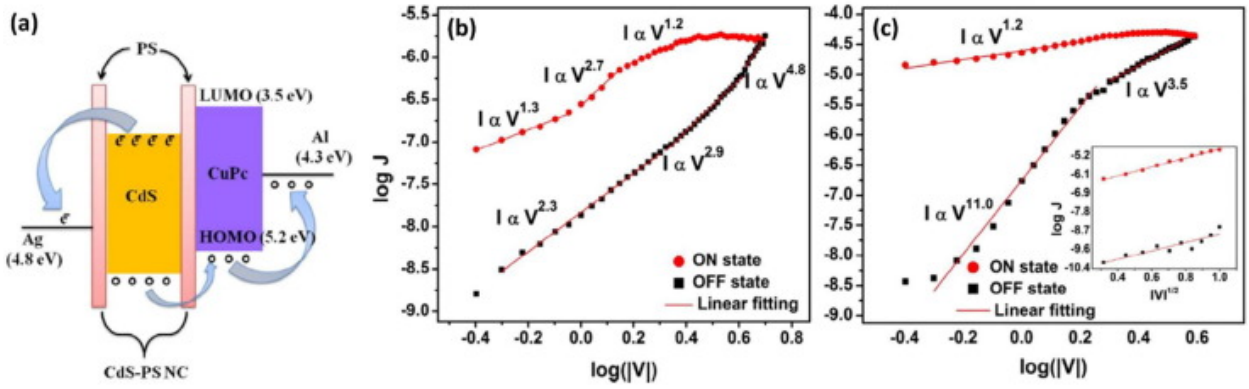

Fig. 27. (a) Energy diagram for device B and I-V plots of (b) Device A and (c) Device B for negative bias. The solid lines represent the fitted curves.

The CuPc acts as a serially connected internal resistor that controls filament formation in the CdS layer, thereby reducing alternative, parasitic current pathways [190]. Fig. 27b-c shows theoretically fitted I-V characteristics for the reverse bias whereby device B shows an increase in current by a magnitude of 3 with an $I_{ON}/I_{OFF} \sim 1.4 \times 10^4$ A.

Lutetium bis-phthalocyanines ($LuPc_2$) are believed to be the first intrinsic molecular semiconductors at room temperature displaying conductance of $6.0 \times 10^{-5}\ \Omega^{-1}\ cm^{-1}$, approximately six magnitudes greater than standard divalent MPcs [191], [192]. These studies found that the conductive behaviour is linked to their radical nature [193]. An OTFT study by Chaure et al. benefitted from the highly conductive nature of $LuPc_2$ [194]. Liquid

crystalline, peripherally substituted hexylthio $LuPc_2$ (SC_6H_{13}-$LuPc_2$) were spun into films and onto n-doped silicon wafers which were annealed under two different temperatures, T_1 = 125 °C and T_2 = 242 °C. Au/Ti layers were constructed as source-drain electrodes. Typical curves were obtained from the current (I_{DS}) - voltage (V_{DS}) plot of the OTFTs (at both T_1 and T_2), showing no hysteresis. The electrical properties of the OTFTs were affected by the molecular orientation of the deposited SC_6H_{13}-$LuPc_2$ as a result of the annealing treatment. The films annealed at T_1 were of a low crystalline order, producing lower conductance. However, the films annealed at T_2 formed well-ordered crystalline structures which contributed to its high conductivity. The high and low conductance of the $LuPc_2$ OTFT was assigned "1″and "0" states for a non-volatile, write-once-read-many (WORM) device. Using the phase-modulated excimer-laser annealing technique, "on" and "off" information was written onto the OFTFs [195]. The on state was read by applying voltage cycles of 10 V with good reproducibility and a read time of 15 s. The OTFT device was able to retain the information during month-long testing. These results indicated that liquid crystalline SC_6H_{13}-$LuPc_2$ are suitable for storage class memory devices. As observed in numerous studies in this review, the morphology of the active layer plays a vital role in the overall performance of any electronic device. Onlaor et al. found that whilst preparing CuPc films *via* thermal evaporation for an electrical memory unit, increasing the deposition rate caused the crystallinity of the CuPc films to decline thereby changing the morphology from a large grain to a fine grain structure [196]. This change in morphology affected the bi-stability of the device. The conduction mechanism of the "on" and "off" states was modelled theoretically and concluded that these structural defects in the CuPc layer altered the trapping and de-trapping processes within the device. Similarly, Chidambara et al. used an alternative deposition technique, vacuum evaporation to form CuPc films as the active layer in an OFET [197]. The study incorporated a fullerene (C_{60}) layer on top of the CuPc layer forming a CuPc-C_{60} interface. The resultant device exhibited electrical bistability as no significant degradation to the device was observed in both the "on" and "off" states.

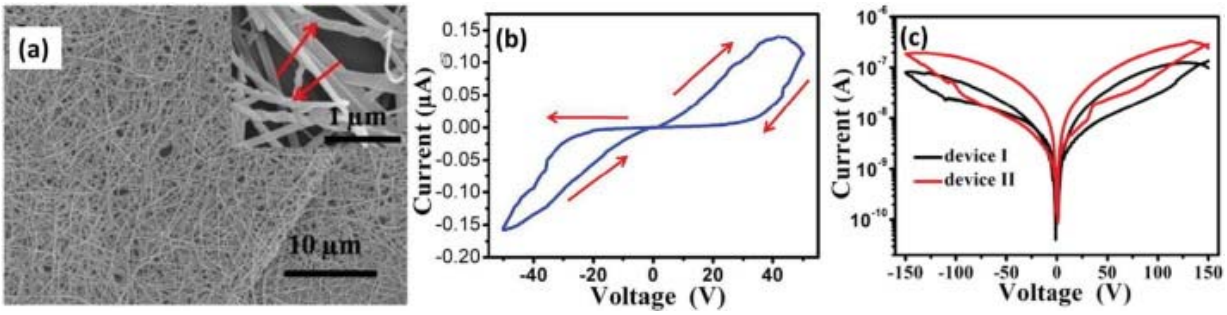

Fig. 28. (a) SEM micrograph the CoPc NW film, (inset: higher magnification of the same film), (b) I–V characteristics of the CoPc NW film device and (c) I–V characteristics of device 1 (CoPc NRs) and device 2 (CoPc NWs) as the active layers.

Xiao et al. successfully incorporated a free-standing CoPc film into a memory storage device using physical vapor deposition (PVD) [198]. Crystalline films are typically difficult to transfer between substrates due to strong interactions between the film and the original substrate thus limiting their applicability in electronic devices [199], [200], [201]. In this study, the CoPc film was constructed in a quartz tube furnace using an ionic liquid, [HEMIM][BF_4] as the growth substrate. After the PVD, a layer of blue CoPc was visible on the surface of the ionic liquid. The higher density of the ionic liquid was key in the formation of a continuous CoPc film and was detached from the ionic liquid by the dissolution of the ionic liquid in water. The SEM micrographs in Fig. 28a shows that a network of CoPc

nanowires (NWs) formed on the surface of the ionic liquid. It was found that increasing the flow rate of the N_2 carrier gas formed nanorods (NRs) rather than NWs, however, XRD analyses indicate that both morphologies had the same β crystalline structure.

Two devices were constructed using the respective morphologies as the active layer, device 1 used NRs and device 2 used NWs. Preliminary I-V testing using device 2 indicated reversible hysteresis where the "on" state shows high conductivity between the −50 V to 50 V sweep whilst the reverse 50 V to −50 V sweep shows low conductance of the "off" state. This hysteresis switching behaviour represents the memory switching and electrical bistability of device 2 (Fig. 28b). Further electrical bi-stability testing was performed on both devices as seen in Fig. 28c. Noticeably smaller current values were obtained for device 1 than for device 2. Although both devices displayed conductive switching behaviour, the current observed for the "on" state was three times greater for device 2 (0.032 μA) than device 1 (0.01 μA). CV measurements explained that the conductive mechanism of the CoPc active layer resonated from charge trap sites of the Co^{II}/Co^{I} redox couple and is consistent with SCLC principles. The PVD in combination with the ionic liquid proved to be a valuable technique to obtain transferable CoPc films suitable for memory storage.

With a similar fabrication approach, Guo et al. used chemical vapor deposition (CVD) to deposit copper polyphthalocyanines (CuPPc) thin films onto Si-based substrates as the active layer for non-volatile memory devices [187]. Using AFM, TEM, XPS and UV–vis studies, the CVD grown CuPPc films displayed a high degree of polymerisation and crystallinity. The memory device was configured in a sandwich structure of Au/CuPPc/ITO and was tested under ambient conditions. The CuPPc thin film memory devices exhibited a non-volatile rewritable characteristic (Fig. 29), with a I_{ON}/I_{OFF} ratio of ~10^3.

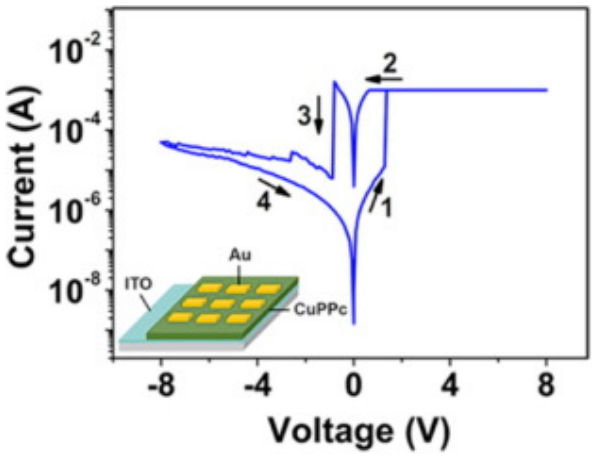

Fig. 29. Typical I-V characteristics of the ITO/CuPPc/Au device.

A positive voltage sweep from 0 V to +8 V (**1**) caused the current to change from 10^{-5} to 10^{-3} A, implying that the device was switched from an OFF state to an ON state (i.e. writing process). The ON state remained unchanged during the sweep from +8 V to 0 V (**2**) and even after the electricity supply turned off, which established that the device possessed non-volatile memory behaviour. An applied negative voltage sweep (**3**) kept the device in the ON state until −0.79 V, followed by an abrupt current decrease from 10^{-3} to 10^{-6} A to return the device to an OFF state with low conductivity (i.e. erasing process). The device further displayed reproducibility of up to 16 consecutive cycles.

Padma et al. modified top contact electrodes with a hybrid a CuPc and Au nanoparticle (CuPc/AuNP) film to investigate the combined effects on the switching characteristic of a low voltage organic memory device [186]. The incorporation of nanoparticles was expected to improve the I_{ON}/I_{OFF} ratio and reduce power consumption by enhancing charge transfer through better trapping mechanisms [202]. The AuNPs were drop cast onto a Si n-type substrate, forming a rough AuNP film. The CuPc was thermally evaporated onto the AuNP film, followed by thermal evaporation of either an Au or Al metal top contact electrode (Fig. 30) or a drop cast Hg drop.

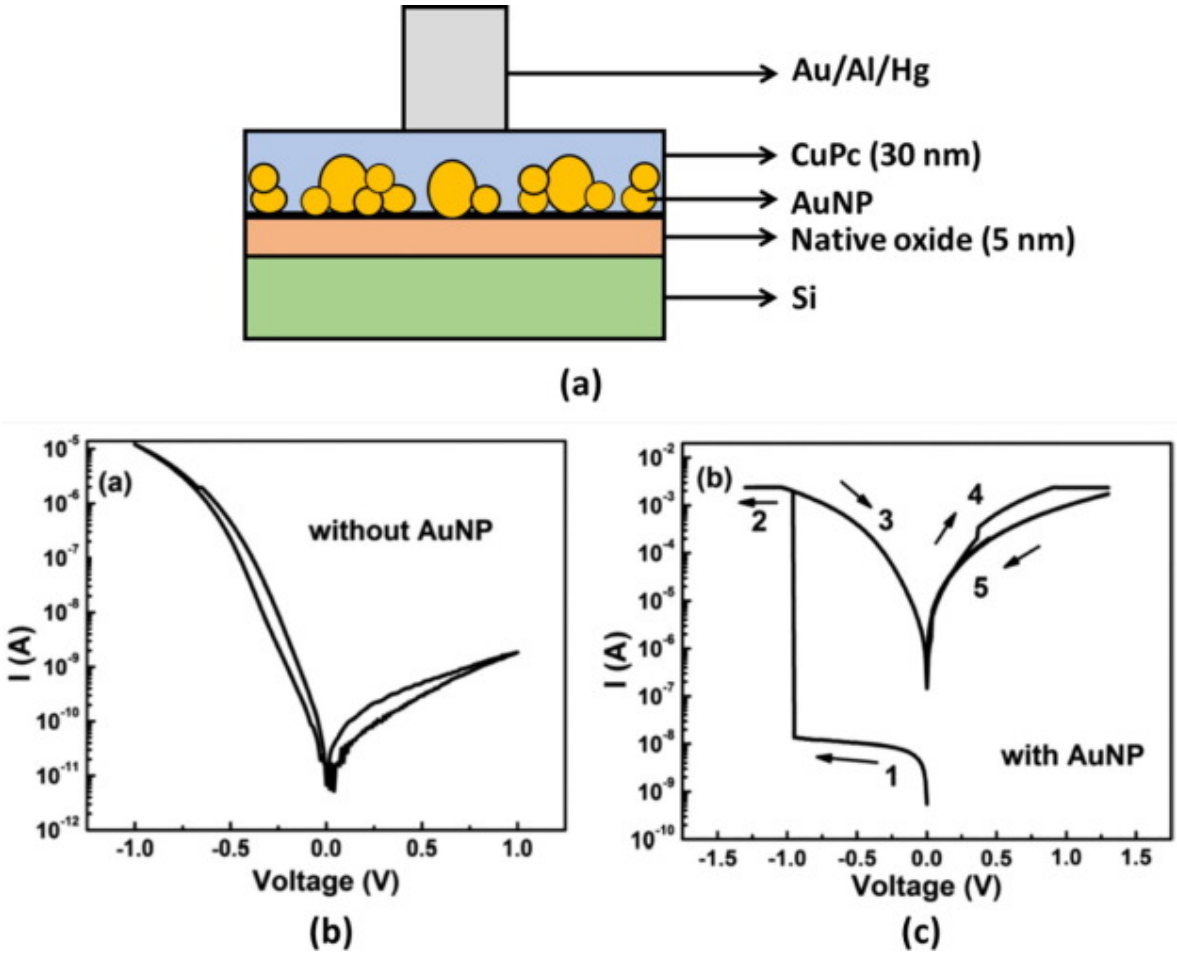

Fig. 30. (a) Configuration of the device with AuNPs, I-V characteristics of devices (b) without AuNP and (c) with AuNP.

Fig. 30 shows the I-V curves of a device with an Au top electrode that is (a) without AuNP and (b) with AuNPs. The figure displays rectification (conversion of alternating current (AC) to direct current (DC)) as a result of the work function difference between the Au (5.1 eV) and Si (4.1 eV) electrodes. A negative voltage causes the Fermi level of the Au electrode to shift closer to the HOMO of the CuPc, allowing the injection of charge carriers to the CuPc. However, when a positive voltage is applied the energy barrier between the Fermi level of Au and the HOMO of the CuPc increases and prevents the injection of charge carriers to the CuPc. This leads to a negligible flow of current and results in the observed rectification. Fig. 30b (inclusion of AuNPs) illustrates a low conducting behaviour between 0 V to −0.95 V (**1**). At −0.95 V, the current exhibits a sharp increase and switches to a high conducting state (i.e.

writing process). At voltages above −0.95 V, an increase in the current is observed and eventually reaches saturation (**2**). The voltage scan in the reverse direction and multiple scans thereafter (**3, 4** and **5**), the device continually exhibits a high conducting behaviour and thus high current flow and establishes the WORM behaviour with an I_{ON}/I_{OFF} ratio greater than 10^5. This WORM behaviour was also observed for the Al device whilst the Hg device showed rewritable behaviour. The switching voltage was influenced by the top electrodes, as the Au and Al devices switched to the ON state at ~1 V and the Hg at ~2 V. Using theoretical modelling, the ON state conduction mechanism was dominated by the Fowler–Nordheim (FN) tunneling through AuNP trap states in all the devices. The rough and porous AuNP layer could have allowed the CuPc molecules to occupy gaps between the AuNPs, thereby extending the AuNPs further into the CuPc layer. Although ohmic contact is expected between the Au and CuPc, an interfacial dipole (Δ) can form between the Au and CuPc and create an energy barrier for hole transport [203]. Additionally, the AuNPs could form trap sites between the HOMO and LUMO of the CuPc, thus creating multiple interfaces and injection barriers between the AuNPs and CuPc, ultimately leading to the trapping of charge carriers and the initially observed low voltages. Therefore, switching characteristics appear to be dependent on the top electrode, as the Au and Al devices displayed sharp switching whilst the Hg electrode displayed a gradual current increase at the onset, before the observed switching. The difference in the switching behaviour between the three electrodes was attributed to the differences in the injection barriers between the top electrode and the CuPc/AgNP active layer interface. The study was able to describe the tuning of the same device structure to exhibit either WORM or rewritable memory behaviors by utilizing a suitable combination of electrode with a nanoparticle containing active layer.

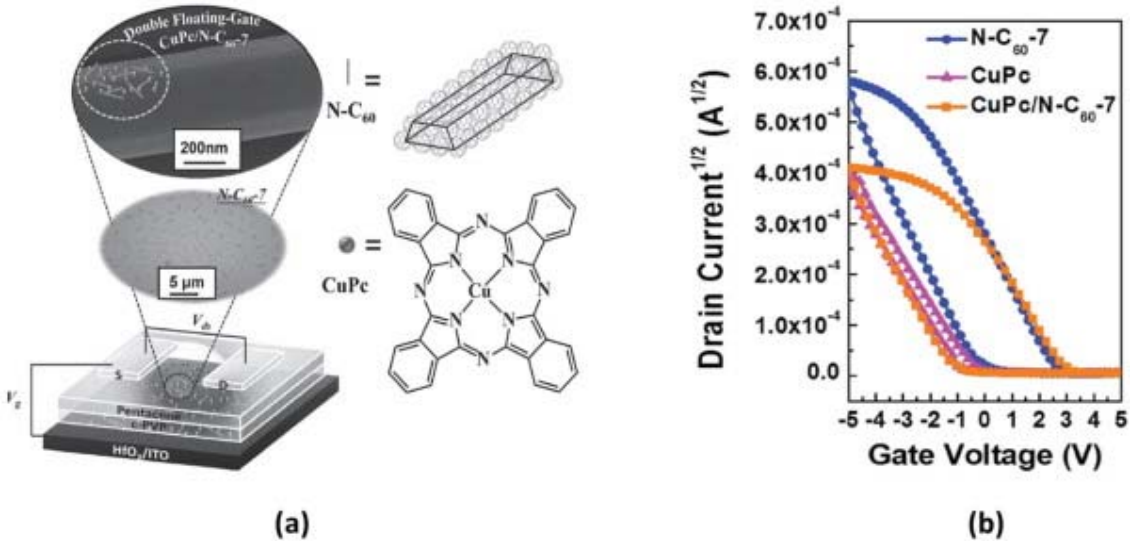

Fig. 31. (a) Schematic cross-sectional diagram of the OFET memory device with the CuPc/N-C_{60} double floating-gate (with TEM images of the N-C_{60} −7) and (b) Transfer characteristics of N-C_{60} −7 and CuPc single floating-gate and CuPc/N-C_{60} −7 double floating-gate memory under dual sweeping scan.

Developing floating gate memory devices based on a basic FET structure that has an electrically isolated conducting gate can be used as a discrete charge storage site for charging or discharging during the writing and erasing processes. This is a valuable feature as the amount of charge stored in the floating gate can be precisely controlled, unlocking the potential for miniaturization, faster programming speeds, lower power consumption and higher density memory devices [204], [205]. In 2015, Chang et al. employed C_{60} single

crystal needles (N-C_{60}) and CuPc nanoparticles (CuPcs) to create a semiconductor (N-C_{60}/CuPcs) layer with ambipolar behaviour (i.e. hole/electron trapping effect) [206]. To create the N-C_{60}/CuPc semiconductor, the CuPc nanoparticles were thermally evaporated onto preformed N-C_{60} trapping sites and then covered by a crosslinked poly(4-vinylphenol) (c-PVP) layer (Fig. 31a).

The aspect ratio of the N-C_{60} crystals were optimised by varying the concentration parameter. An aspect ratio of 7 showed well dispersed needle shaped crystals that could benefit the charge storage properties, i.e. N-C_{60}-7/CuPc. To test the presence of "ambipolar charge trapping" based on the hole trapping ability of the CuPc nanoparticles and electron trapping ability of the N-C_{60}-7, a pulse stimulus with parameters: V_g of −5 V to 5 V with a fixed at V_d of −5 V was applied to the devices. The CuPc and N-C_{60}-7 only devices displayed unipolar character, as the V_{th} only shifted in one direction indicating that the memory behaviour is a result of trapping and releasing holes and electrons in these single floating gate memory devices. In contrast, the N-C_{60}-7/CuPc device showed shifts of the V_{th} in both the positive and negative directions due to the independent trapping of both electrons and holes. This confirmed the formation of a N-C_{60}-7/CuPc floating gate memory device that is capable of ambipolar trapping. Furthermore, hysteresis loops in the transfer curves of the CuPc/N-C_{60} −7 memory device under various gate sweeping voltages reaffirmed the ambipolar charge trapping nature (Fig. 31b). The OFET characterisation was compared to other work performed by the group and can be seen in Table 5.

Table 5. The electrical performances of pentacene-based OFET devices.

Floating gate	**OFET performances**			**Reference**
	Mobility [cm^2 V^{-1} s^{-1}]	**ON/OFF ratio**	**ΔV_{th} [V]**	
N-C_{60}-7	0.0128	10^3	+3.20	[206]
CuPc	0.0628	10^3	+1.40	
N-C_{60}-7/CuPc	0.0125	10^3	+4.40	
PS_4	0.10	10^7	+3.16	[207]
CuPc-PS_4	0.41	10^8	−21.0	
CuPc-SP_1	0.02	10^6	−66.0	[208]
CuPc-SP_2	0.21	10^7	−23.7	
CuPc-SP_3	0.28	10^7	−14.3	
ZnPc-SP_1	0.10	10^7	−51.3	
ZnPc-SP_2	0.29	10^8	−25.0	
ZnPc-SP_3	0.23	10^8	−11.3	

Aimi et al. considered a star-shaped polystyrene with a copper or zinc phthalocyanine core (CuPc-PS_4 or ZnPc-PS_4) for the semiconductor layer [207], [208]. These studies highlighted the applicability of polymer electrets in electrical storage devices. Polymer electrets are polymer based, dielectric materials capable of quasi-permanently storing electric charges [209]. The CuPc and ZnPc were designed with four-star-shaped polystyrene arms with varying chain lengths *via* successive cyclization and radical polymerization reactions (Fig. 32a).

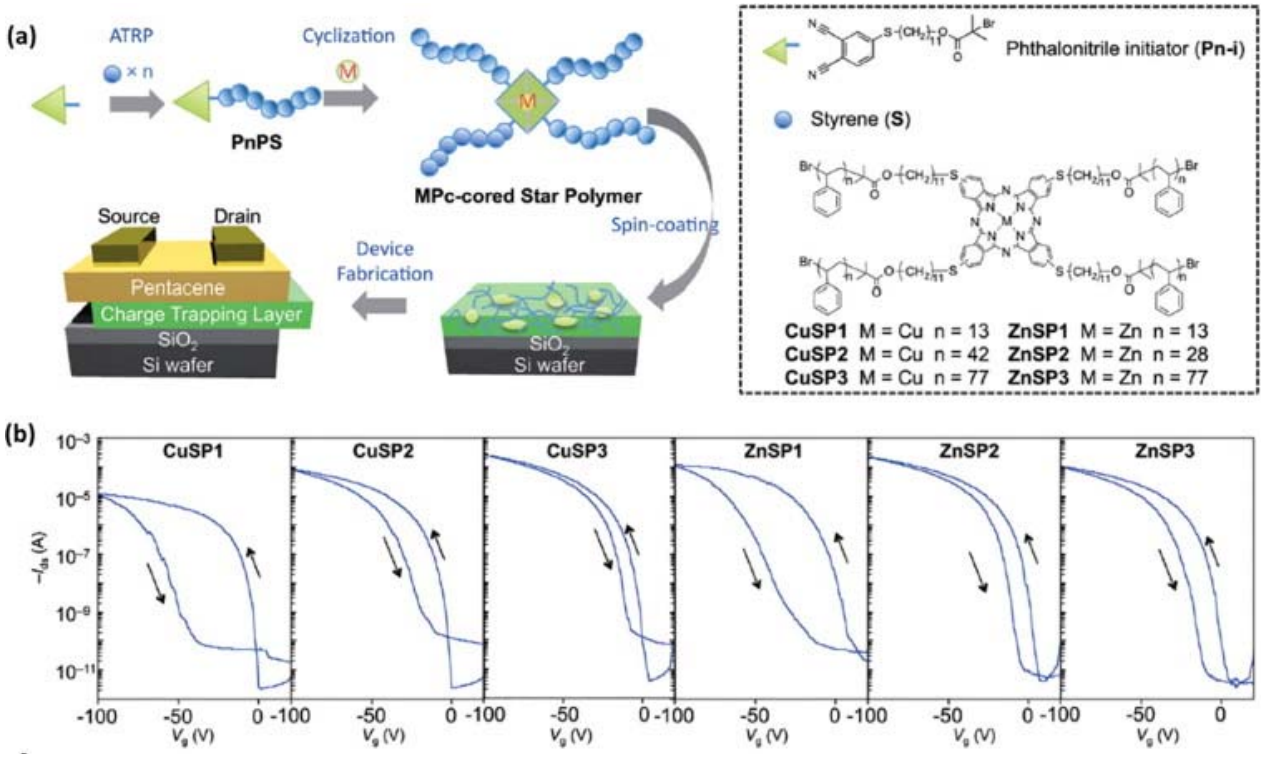

Fig. 32. (a) Schematic representation of the OFET memory devices with an MPc-cored star-shaped polystyrene as a charge storage layer; the polymer design with various arm lengths (n values) and metal ions of the Pc core (M) for controlling device performance and (b) Transfer characteristics of the OFET device with CuSP and ZnSP layers monitored at $V_d = -100$ V.

Upon the application of a negative bias, the CuPc and ZnPc cores displayed hysteresis as seen in Fig. 32b. The $CuSP_1$ device displayed hysteresis approximately three times larger than the $CuSP_3$ device. The same trend was observed between the $ZnSP_1$ and $ZnSP_3$ whereby the $ZnSP_1$ exhibited the biggest V_{th} shift whilst the $ZnSP_3$ exhibited the smallest V_{th} shift. This implied that the CuPc and ZnPc star-shaped polymers with shorter chain lengths had better charge trapping abilities during the application of a negative bias than star-shaped polymers with longer chain lengths, however, the polymer influences that magnitude of the hysteresis and prevented charge leakage. These reversible shifts to the V_{th} and the magnitude of the memory shifts were proportional to the wt% of the MPc cores within the polystyrene matrix. The OFET characteristics can be viewed in Table 5. The OFETs exhibited different charge carrier mobilities that appeared to have varied by either the Pc metal centre or the polymer length. The OFETs memory windows and charge retention times were found to be dependent on the length chain of the polystyrene. In comparison to the N-C_{60}-7/CuPc OFET, these star-shaped MPc core polymer OFETs showed significantly higher I_{ON}/I_{OFF} ratios as a result of the polymer electrets.

5. Conclusions and outlook

The Pc applications described in this review is dependent on specific properties of the relevant material, the properties in turn are the result of their respective molecular- and microstructures (structure–property relationships) and the structure is governed by the chosen synthetic methodology. There is a huge number of both potential and proven topologies and compositions that can still be explored, including different organic derivatives, inter-molecule

connections/bridges, and composites based on polymers and nanoparticle matrices. But the synthetic challenges can only be fully realised once a complete understanding of both the structural and compositional aspects are controlled. This review outlined many examples of innovative synthetic strategies that can be further explored and developed, for example, the highlighted chemical and physical properties need appropriate integration of Pcs into the latest attempts at designing and improving devices. In the area of chemical sensors, new exciting areas of research that will be amplified by work explored here could include development of next generation technologies for wearable chemical sensor systems where Pc systems is yet to make any inroads. This will open the door for new research avenues such as choice of composite materials, type of power sources, digital communication processing, and choice of analytical method etc. against the backdrop of finding appropriate rigidity (and flexibility), size and data collection of the devices. In NLO research, future goals and challenges remain the interplay between “fast” and “slow” light created in a room-temperature solid-state material; such devices have real-world applications in slow/fast light for interferometry, phased- and synchronized-array laser radar, buffers and regenerators for telecom, and construction of quantum memories, to name a few. In the area of energy and data storage focus are directed at systems that can indisputably minimize climate change and studies are directed toward new battery, supercapacitor and improved memory devices, for example replacing resource scarce Li described here with abundant Na.

Pcs offer a number of advantages, including modular composition and facile tuning of electrical and optical properties that place them well within multidisciplinary intersections. The strong and unique absorption of light within the UV–vis and IR regions coupled with redox-active sites promote their incorporation in a variety of materials, and the manipulation of electron acceptor and electron donor moieties influences photophysical features of Pcs, making them invaluable components to charge transfer and energy systems. The ability of these conjugated systems to self-assemble with other conjugated materials to form films as well as 2D and 3D structures for electrical conductivity promotes their applicability towards a variety of futuristic applications. Pcs have always been an active research field, and many of their fundamental and applied properties pervade into other disciplines. In this review, we have introduced and highlighted several exciting yet often underrepresented research avenues that runs parallel with ongoing new synthetic advances. These select applications offer challenges and opportunities that span across both the historic and contemporary aspects of the field that should signal a continued bright future for Pc chemistry.

Declaration of Competing Interest

The authors declare that they have no known competing financial interests or personal relationships that could have appeared to influence the work reported in this paper.

Acknowledgment

D.G. wishes to acknowledge financial support from the National Research Foundation, South Africa (Grant number:108424) and the University of KwaZulu-Natal (UKZN), South Africa.

References

[1] J. Jiang, Functional Phthalocyanine Molecular Materials, Springer, 2010.

[2] N.B. McKeown, Phthalocyanine Materials: Synthesis, Structure and Function, sixth ed., Cambridge University Press, 1998.

[3] N.B. McKeown, Phthalocyanines, Compr. Coord. Chem. II (2003) 507–514, https://doi.org/10.1016/B0-08-043748-6/01071-9.

[4] N. Kobayashi, J. Mack, Low symmetry phthalocyanines and their analogues, Chem. Rev. 111 (2011) 281–321.

[5] F. Dumoulin, M. Durmus, V. Ahsen, T. Nyokong, Synthetic pathways to watersoluble phthalocyanines and close analogs, Coord. Chem. Rev. 254 (2010) 2792–2847, https://doi.org/10.1016/j.ccr.2010.05.002.

[6] K. Kadish, K.M. Smith, R. Guilard, The Porphyrin Handbook: Phthalocyanines: Synthesis, Academic Press, 2000.

[7] M.J. Stillman, T. Nyokong, C.C. Leznoff, A.B.P. Lever, Phthalocyanines: properties and applications, By CC Leznoff ABP Lever, VCH, New York. 1 (1989) 133.

[8] H. Isago, Optical spectra of Phthalocyanines and Related Compounds, Springer, 2015.

[9] M. Gouterman, Optical spectra and electronic structure of porphyrins and related rings, The Porphyrins (1978) 1–165, https://doi.org/10.1016/B978-0- 12-220103-5.50008-8.

[10] I. Okura, Photosensitization of Porphyrins and Phthalocyanines, CRC Press, 2001.

[11] G. de la Torre, M. Nicolau, T. Torres, Phthalocyanines: synthesis, supramolecular organization, and physical properties, Supramol. Photosensit. Electroact. Mater. (2001) 1–111, https://doi.org/10.1016/B978- 012513904-5/50003-X.

[12] P. Gregory, Metal complexes as speciality dyes and pigments, Compr. Coord. Chem. II (2003) 549–579, https://doi.org/10.1016/B0-08-043748-6/09013-7.

[13] C.G. Claessens, U. Hahn, T. Torres, Phthalocyanines: from outstanding electronic properties to emerging applications, Chem. Rec. 8 (2008) 75–97, https://doi.org/10.1002/tcr.20139.

[14] M. Urbani, M.-E. Ragoussi, M.K. Nazeeruddin, T. Torres, Phthalocyanines for dye-sensitized solar cells, Coord. Chem. Rev. 381 (2019) 1–64, https://doi.org/ 10.1016/J.CCR.2018.10.007.

[15] P.-C. Lo, M.S. Rodríguez-Morgade, R.K. Pandey, D.K.P. Ng, T. Torres, F. Dumoulin, The unique features and promises of phthalocyanines as advanced photosensitisers for photodynamic therapy of cancer, Chem. Soc. Rev. 49 (2020) 1041–1056, https://doi.org/10.1039/C9CS00129H.

[16] A.C. Tedesco, F.L. Primo, M. Beltrame, Phthalocyanines: synthesis, characterization and biological applications of photodynamic therapy (PDT), nanobiotechnology, magnetohyperthermia and photodiagnosis (theranostics), Ref. Modul. Mater. Sci. Mater. Eng. (2016), https://doi.org/ 10.1016/B978-0-12-803581-8.02460-7.

[17] J.H. Zagal, S. Griveau, J.F. Silva, T. Nyokong, F. Bedioui, Metallophthalocyanine-based molecular materials as catalysts for electrochemical reactions, Coord. Chem. Rev. 254 (2010) 2755–2791, https://doi.org/10.1016/J.CCR.2010.05.001.

[18] M. Urbani, G. de la Torre, M.K. Nazeeruddin, T. Torres, Phthalocyanines and porphyrinoid analogues as hole- and electron-transporting materials for perovskite solar cells, Chem. Soc. Rev. 48 (2019) 2738–2766, https://doi.org/ 10.1039/C9CS00059C.

[19] D. Wöhrle, S.G. Makarov, G. Schnurpfeil, A. Kazarin, O.N. Suvorova, Practical applications of phthalocyanines – from dyes and pigments to materials for optical electronic and photo-electronic devices, Macroheterocycles 5 (2012) 191–202, https://doi.org/10.6060/mhc2012.120990w.

[20] R. Li, X. Zhang, P. Zhu, D.K. Ng, N. Kobayashi, J. Jiang, Electron-donating orwithdrawing nature of substituents revealed by the electrochemistry of metal-free phthalocyanines, Inorg. Chem. 45 (2006) 2327–2334.

[21] T. Nyokong, Electronic Spectral and Electrochemical Behavior of Near Infrared Absorbing Metallophthalocyanines, in: J. Jiang (Ed.), Funct. Phthalocyanine Mol. Mater., Springer, Berlin, Heidelberg, 2010, pp. 45–87. doi:10.1007/978- 3-642-04752-7_2.

[22] S. Ambily, C.S. Menon, Electrical conductivity studies and optical absorption studies in copper phthalocyanine thin films, Solid State Commun. 94 (1995) 485–487, https://doi.org/10.1016/0038-1098(94)00901-5.

[23] Y. Zhang, X. Cai, Y. Bian, J. Jiang, Organic semiconductors of phthalocyanine compounds for field effect transistors (FETs), in: J. Jiang (Ed.), Funct. Phthalocyanine Mol. Mater., Springer, Berlin, Heidelberg, 2010, pp. 275– 321. doi:10.1007/978-3-642-04752-7_9.

[24] D. Dini, M. Hanack, Physical Properties of Phthalocyanine-based Materials, Academic Press (2003), https://doi.org/10.1016/B978-0-08-092391-8.50007- 8.

[25] M. Pfeiffer, A. Beyer, B. Plönnigs, A. Nollau, T. Fritz, K. Leo, D. Schlettwein, S. Hiller, D. Wöhrle, Controlled p-doping of pigment layers by cosublimation: basic mechanisms and implications for their use in organic photovoltaic cells, Sol. Energy Mater. Sol. Cells 63 (2000) 83–99, https://doi.org/10.1016/S0927- 0248(00)00022-2.

[26] K.M. Smith, R. Guilard, Handbook of porphyrin science with applications to chemistry, physics, materials science, engineering, biology and medicine— Volume 24, Coord. Chem. Mater. (2012).

[27] T. Nyokong, Electrochemistry of some second-row transition-metal phthalocyanine complexes, South African J. Chem. 48 (1995).

[28] A.J. Fry, J.A. Fry, Synthetic Organic Electrochemistry, John Wiley & Sons, 1989.

[29] S.G. and F.I. Adam Hulanicki, Commission on general aspects of analytical chemistry: chemical sensors, Pure Appl. Chem. 63 (1991) 1247–1250.

[30] Z. Sen, D.K. Tarakci, I. Gürol, V. Ahsen, M. Harbeck, Governing the sorption and sensing properties of titanium phthalocyanines by means of axial ligands, Sensors Actuators B Chem. 229 (2016) 581–586, https://doi.org/10.1016/J. SNB.2016.01.145.

[31] Y. Jiang, C. Wang, G. Lu, L. Zhao, L. Gong, T. Wang, D. Qi, Y. Chen, J. Jiang, Compartmentalization within nanofibers of double-decker phthalocyanine induces high-performance sensing in both aqueous solution and the gas phase, Chem. – A Eur. J. 25 (2019) 16207–16213, https://doi.org/10.1002/ chem.201903553.

[32] E.G. Duruk, H.Y. Yenilmez, A. Altındal, Z. Altuntas Bayır, Microwave-assisted synthesis of novel non-peripherally substituted metallophthalocyanines and their sensing behaviour for a broad range of Lewis bases, Dalton Trans. 44 (2015) 10060–10068, https://doi.org/10.1039/C5DT00852B. [

33] L.K. Kumawat, N. Mergu, A.K. Singh, V.K. Gupta, A novel optical sensor for copper ions based on phthalocyanine tetrasulfonic acid, Sensors Actuators B Chem. 212 (2015) 389–394, https://doi.org/10.1016/J.SNB.2015.02.027.

[34] A.G. Gürek, N. Kılınç, Z.Z. Öztürk, V. Ahsen, D. Atilla, Recent studies chemical sensors based on phthalocyanines, J. Porphyr. Phthalocyanines 13 (2009) 1179–1187, https://doi.org/10.1142/s1088424609001522.

[35] H. Wu, Z. Chen, J. Zhang, F. Wu, C. He, B. Wang, Y. Wu, Z. Ren, Stably dispersed carbon nanotubes covalently bonded to phthalocyanine cobalt(II) for ppblevel H2S sensing at room temperature, J. Mater. Chem. A 4 (2016) 1096– 1104, https://doi.org/10.1039/C5TA09213B.

[36] A. Kumar, S. Samanta, N. Ramgir, A. Singh, A.K. Debnath, K.P. Muthe, H.C. Barshilia, Improved H2S sensitivity of cobalt phthalocyanine film fabricated on plasma treated flexible polyethylene terephthalate substrate, Sens. Lett. 15 (2017) 104–110.

[37] P. Jha, M. Sharma, A. Chouksey, P. Chaturvedi, D. Kumar, G. Upadhyaya, J.S.B. Rawat, P.K. Chaudhury, Functionalization of carbon nanotubes with metal phthalocyanine for selective gas sensing application, Synth. React. Inorg. Met. Nano-Metal Chem. 44 (2014) 1551–1557, https://doi.org/10.1080/ 15533174.2013.818021.

[38] Q. Liu, L. Gao, X. Su, F. Zhou, G. Duan, Interfacial self-assembly of CoPc thin films with their high sensing use as NO2 sensors, Mater. Chem. Phys. 234 (2019) 94–101, https://doi.org/10.1016/J.MATCHEMPHYS.2019.05.029.

[39] M. Bouvet, P. Gaudillat, A. Kumar, T. Sauerwald, M. Schüler, A. Schütze, J.-M. Suisse, Revisiting the electronic properties of Molecular Semiconductor – Doped Insulator (MSDI) heterojunctions through impedance and chemosensing studies, Org. Electron. 26 (2015) 345–354, https://doi.org/ 10.1016/J.ORGEL.2015.07.052.

[40] J. Zhao, Z. Qiao, Y. Zhang, T. Zou, L. Yu, L. Luo, X. Wang, Y. Yang, H. Wang, L. Tang, Controllable preparation of copper phthalocyanine single crystal nano column and its chlorine gas sensing properties, AIP Adv. 6 (2016) 95303, https://doi.org/10.1063/1.4962657.

[41] A.K. Sharma, A. Mahajan, R.K. Bedi, S. Kumar, A.K. Debnath, D.K. Aswal, CNTs based improved chlorine sensor from non-covalently anchored multi-walled carbon nanotubes with hexa-decafluorinated cobalt phthalocyanines, RSC Adv. 7 (2017) 49675–49683, https://doi.org/10.1039/C7RA08987B.

[42] S. Kumar, N. Kaur, A.K. Sharma, A. Mahajan, R.K. Bedi, Improved Cl2 sensing characteristics of reduced graphene oxide when decorated with copper phthalocyanine nanoflowers, RSC Adv. 7 (2017) 25229–25236, https://doi. org/10.1039/C7RA02212C.

[43] Q. Sun, W. Feng, P. Yang, G. You, Y. Chen, Highly selective room-temperature NO2sensors based on a fluoroalkoxy-substituted phthalocyanine, New J. Chem. 42 (2018) 6713–6718, https://doi.org/10.1039/c8nj00622a.

[44] Y. Zhu, Q. Xie, Y. Sun, L. Wang, Q. Sun, L. Wang, High-performance NO2 sensors based on ultrathin heterogeneous interface layers, Adv. Mater. Interfaces 7 (2020) 1901579, https://doi.org/10.1002/admi.201901579.

[45] C. Zhang, P. Chen, W. Hu, Organic field-effect transistor-based gas sensors, Chem. Soc. Rev. 44 (2015) 2087–2107, https://doi.org/10.1039/C4CS00326H.

[46] F.I. Bohrer, A. Sharoni, C. Colesniuc, J. Park, I.K. Schuller, A.C. Kummel, W.C. Trogler, Gas sensing mechanism in chemiresistive cobalt and metal-free phthalocyanine thin films, J. Am. Chem. Soc. 129 (2007) 5640–5646.

[47] H. Chang, W. Li, H. Tian, Y. Geng, H. Wang, D. Yan, T. Wang, High performance of rubrene thin film transistor by weak epitaxy growth method, Org. Electron. 20 (2015) 43–48, https://doi.org/10.1016/J.ORGEL.2015.02.003.

[48] C. Lorch, R. Banerjee, C. Frank, J. Dieterle, A. Hinderhofer, A. Gerlach, F. Schreiber, Growth of competing crystal phases of a-sexithiophene studied by real-time in situ X-ray scattering, J. Phys. Chem. C 119 (2015) 819–825, https://doi.org/10.1021/jp510321k.

[49] A. Kumar, S. Samanta, A. Singh, M. Roy, S. Singh, S. Basu, M.M. Chehimi, K. Roy, N. Ramgir, M. Navaneethan, Y. Hayakawa, A.K. Debnath, D.K. Aswal, S.K. Gupta, Fast Response and high sensitivity of ZnO nanowires—cobalt phthalocyanine heterojunction based H2S sensor, ACS Appl. Mater. Interfaces 7 (2015) 17713–17724, https://doi.org/10.1021/acsami.5b03652.

[50] S. Harbeck, D. Atilla, I. Dülger, M. Harbeck, A.G. Gürek, Z.Z. Öztürk, V. Ahsen, The role of hydrogen bonding in the sensitivity of QCM sensors: a spectroscopic study on tosylamido phthalocyanines, Sensors Actuators B Chem. 191 (2014) 750–756, https://doi.org/10.1016/J.SNB.2013.10.021.

[51] S. Harbeck, S. Göçmen, Ö.F. Emirik, Z.Z. Öztürk, V. Ahsen, A.G. Gürek, Synthesis of branched alkoxy side chains containing phthalocyanine derivates and their application in mass sensitive QCM sensors, Sensors Actuators B Chem. 233 (2016) 55–62, https://doi.org/10.1016/J. SNB.2016.04.038.

[52] A. Kumar, J. Brunet, C. Varenne, A. Ndiaye, A. Pauly, M. Penza, M. Alvisi, Tetratert-butyl copper phthalocyanine-based QCM sensor for toluene detection in air at room temperature, Sensors Actuators B Chem. 210 (2015) 398–407, https://doi.org/10.1016/j.snb.2015.01.010.

[53] A. Kumar, J. Brunet, C. Varenne, A. Ndiaye, A. Pauly, Phthalocyanines based QCM sensors for aromatic hydrocarbons monitoring: role of metal atoms and substituents on response to toluene, Sensors Actuators B Chem. 230 (2016) 320–329, https://doi.org/10.1016/J.SNB.2016.02.032.

[54] Y. Çimen, E. Ermis, F. Dumludag˘, A.R. Özkaya, B. Salih, Ö. Bekarog˘lu, Synthesis, characterization, electrochemistry and VOC sensing properties of novel balltype dinuclear metallophthalocyanines, Sensors Actuators B Chem. 202 (2014) 1137–1147, https://doi.org/10.1016/J.SNB.2014.06.066.

[55] B. Mızrak, A. Altındal, S. Abdurrahmanog˘lu, Synthesis, characterization and partition coefficients for VOC vapor adsorption onto novel pyridine derivatives Co(II) phthalocyanines, Prog. Org. Coatings 109 (2017) 92–96, https://doi.org/10.1016/J.PORGCOAT.2017.04.025.

[56] K. Staszek, A. Rydosz, E. Maciak, K. Wincza, S. Gruszczynski, Six-port microwave system for volatile organic compounds detection, Sensors Actuators B Chem. 245 (2017) 882–894, https://doi.org/10.1016/J. SNB.2017.01.194.

[57] B. Wang, X. Wang, X. Li, Z. Guo, X. Zhou, Y. Wu, The effects of amino substituents on the enhanced ammonia sensing performance of PcCo/rGO hybrids, RSC Adv. 8 (2018) 41280–41287, https://doi.org/10.1039/ C8RA07509C.

[58] Z. Guo, B. Wang, X. Wang, Y. Li, S. Gai, Y. Wu, X. Cheng, A high-sensitive room temperature gas sensor based on cobalt phthalocyanines and reduced graphene oxide nanohybrids for the ppb-levels of ammonia detection, RSC Adv. 9 (2019) 37518–37525, https://doi.org/10.1039/C9RA08065A.

[59] R. Saini, A. Mahajan, R.K. Bedi, D.K. Aswal, A.K. Debnath, Solution processed films and nanobelts of substituted zinc phthalocyanine as room temperature ppb level Cl2 sensors, Sensors Actuators B Chem. 198 (2014) 164–172, https://doi.org/10.1016/J.SNB.2014.03.027.

[60] R. Saini, A. Mahajan, R.K. Bedi, D.K. Aswal, A.K. Debnath, Room temperature ppb level Cl2 detection and sensing mechanism of highly selective and sensitive phthalocyanine nanowires, Sensors Actuators B Chem. 203 (2014) 17–24, https://doi.org/10.1016/J.SNB.2014.06.081.

[61] A.K. Sharma, A. Mahajan, R.K. Bedi, S. Kumar, A.K. Debnath, D.K. Aswal, Noncovalently anchored multi-walled carbon nanotubes with hexadecafluorinated zinc phthalocyanine as ppb level chemiresistive chlorine sensor, Appl. Surf. Sci. 427 (2018) 202–209, https://doi.org/10.1016/J. APSUSC.2017.08.040.

[62] A.K. Sharma, A. Mahajan, R. Saini, R.K. Bedi, S. Kumar, A.K. Debnath, D.K. Aswal, Reversible and fast responding ppb level Cl2 sensor based on noncovalent modified carbon nanotubes with Hexadecafluorinated copper phthalocyanine, Sensors Actuators B Chem. 255 (2018) 87–99, https://doi. org/10.1016/J.SNB.2017.08.013.

[63] A.K. Sharma, A. Mahajan, S. Kumar, A.K. Debnath, D.K. Aswal, Tailoring of the chlorine sensing properties of substituted metal phthalocyanines noncovalently anchored on single-walled carbon nanotubes, RSC Adv. 8 (2018) 32719–32730, https://doi.org/10.1039/C8RA05529G.

[64] D. Akyüz, A. Koca, An electrochemical sensor for the detection of pesticides based on the hybrid of manganese phthalocyanine and polyaniline, Sensors Actuators B Chem. 283 (2019) 848–856, https://doi.org/10.1016/J. SNB.2018.11.155.

[65] T. Keles, D. Akyüz, Z. Biyiklioglu, A. Koca, Electropolymerization of metallophthalocyanines carrying redox active metal centers and their electrochemical pesticide sensing application, Electroanalysis 29 (2017) 2125–2137, https://doi.org/10.1002/elan.201700249.

[66] D. Akyüz, T. Keles, Z. Biyiklioglu, A. Koca, Electrochemical pesticide sensors based on electropolymerized metallophthalocyanines, J. Electroanal. Chem. 804 (2017) 53–63, https://doi.org/10.1016/J.JELECHEM.2017.09.044.

[67] M. Tefera, S. Admassie, M. Tessema, S. Mehretie, Electrochemical sensor for determination of fenitrothion at multi-wall carbon nanotubes modified glassy carbon electrode, Anal. Bioanal. Chem. Res. 2 (2015) 139–150, https:// doi.org/10.22036/abcr.2015.11928.

[68] M. de F. Alves, R.A.M. de S. Corrêa, F.S. da Cruz, D.L. Franco, L.F. Ferreira, Electrochemical enzymatic fenitrothion sensor based on a tyrosinase/poly(2- hydroxybenzamide)-modified graphite electrode, Anal. Biochem. 553 (2018) 15–23, https://doi.org/10.1016/J.AB.2018.05.014.

[69] A.A. Ensafi, F. Rezaloo, B. Rezaei, Electrochemical determination of fenitrothion organophosphorus pesticide using polyzincon modified-glassy carbon electrode, Electroanalysis 29 (2017) 2839–2846, https://doi.org/ 10.1002/elan.201700406.

[70] A. Motaharian, F. Motaharian, K. Abnous, M.R.M. Hosseini, M. HassanzadehKhayyat, Molecularly imprinted polymer nanoparticles-based electrochemical sensor for determination of diazinon pesticide in well water and apple fruit samples, Anal. Bioanal. Chem. 408 (2016) 6769–6779, https://doi.org/10.1007/s00216-016-9802-7.

[71] C.W. White, J.G. Martin, Chlorine gas inhalation: human clinical evidence of toxicity and experience in animal models, Proc. Am. Thorac. Soc. 7 (2010) 257–263, https://doi.org/10.1513/pats.201001-008SM.

[72] W.H.O. United Nations Environment Programme, International Labour Organization, Environmental health criteria 21: Chlorine and hydrogen chloride, World Health Organization, Geneva PP – Geneva, 1982.

[73] D.G. de Oteyza, A. El-Sayed, J.M. Garcia-Lastra, E. Goiri, T.N. Krauss, A. Turak, E. Barrena, H. Dosch, J. Zegenhagen, A. Rubio, Y. Wakayama, J.E. Ortega, Copper-phthalocyanine based metal–organic interfaces: the effect of fluorination, the substrate, and its symmetry, J. Chem. Phys. 133 (2010), https://doi.org/10.1063/1.3509394 214703.

[74] Y. Zhao, Y. Guo, Y. Liu, 25th Anniversary article: recent advances in n-type and ambipolar organic field-effect transistors, Adv. Mater. 25 (2013) 5372– 5391, https://doi.org/10.1002/adma.201302315.

[75] Y. Shi, X. Li, Solution-processable ambipolar organic field-effect transistor based on Co-planar bisphthalocyaninato copper, Org. Electron. 15 (2014) 286–293, https://doi.org/10.1016/J.ORGEL.2013.11.017. [

76] G. Lu, K. Wang, X. Kong, H. Pan, J. Zhang, Y. Chen, J. Jiang, Binuclear phthalocyanine dimer-containing yttrium double-decker ambipolar semiconductor with sensitive response toward oxidizing NO2 and reducing NH3, ChemElectroChem 5 (2018) 605–609, https://doi.org/10.1002/celc.201701117.

[77] Y. Chen, M. Bouvet, T. Sizun, Y. Gao, C. Plassard, E. Lesniewska, J. Jiang, Facile approaches to build ordered amphiphilic tris(phthalocyaninato) europium triple-decker complex thin films and their comparative performances in ozone sensing, Phys. Chem. Chem. Phys. 12 (2010) 12851–12861, https://doi. org/10.1039/C0CP00381F.

[78] C. Huang, K. Wang, J. Sun, J. Jiang, Planar binuclear phthalocyanine-containing sandwich-type rare-earth complexes: synthesis, spectroscopy, electrochemistry, and NLO properties, Eur. J. Inorg. Chem. 2014 (2014) 1546–1551, https://doi.org/10.1002/ejic.201301485.

[79] X. Kong, Z. Dong, Y. Wu, X. Li, Y. Chen, J. Jiang, High sensitive ambipolar response towards oxidizing NO2 and reducing NH3 based on bis (phthalocyaninato) europium semiconductors, Chinese J. Chem. 34 (2016) 975–982, https://doi.org/10.1002/cjoc.201600490.

[80] H. Wang, X. Kong, S. Zhao, J. Wu, X. Li, Y. Chen, High-performance ambipolar responses to oxidizing NO2 and reducing NH3 based on the self-assembled film of an amphiphilic tris(phthalocyaninato) europium complex, New J. Chem. 41 (2017) 11955–11961, https://doi.org/10.1039/C7NJ02790G.

[81] K. Abdullah, Y. Wu, S. Zhao, X. Kong, X. Li, Y. Chen, Ambipolar chemical sensors based on the self-assembled film of an amphiphilic (phthalocyaninato) (porphyrinato) europium complex, Inorg. Chem. Commun. 86 (2017) 1–5, https://doi.org/10.1016/J.INOCHE.2017.09.010.

[82] K. Abdullah, Y. Chen, J. Jiang, Synthesis, fabrication of self-assembled film and ambipolar chemical sensing properties of triple-decker (phthalocyaninato) (porphyrinato) europium complex, J. Porphyr. Phthalocyanines. 21 (2017) 893–899, https://doi.org/10.1142/S1088424617500985.

[83] S. Zhao, X. Kong, X. Wang, X. Li, G. Yang, Y. Chen, Fine-tuning intermolecular and intramolecular interactions to build the films of tris(phthalocyaninato) rare earth complexes and their comparative performances in ambipolar gas sensing, IEEE Trans. Electron Devices. 66 (2019) 1930–1936, https://doi.org/ 10.1109/TED.2019.2901007.

[84] A. Moutcine, A. Chtaini, Electrochemical determination of trace mercury in water sample using EDTA-CPE modified electrode, Sens. Bio-Sensing Res. 17 (2018) 30–35, https://doi.org/10.1016/J.SBSR.2018.01.002.

[85] L. Cui, J. Wu, H. Ju, Electrochemical sensing of heavy metal ions with inorganic, organic and bio-materials, Biosens. Bioelectron. 63 (2015) 276– 286, https://doi.org/10.1016/J.BIOS.2014.07.052.

[86] R. Ríos, A. Marín, G. Ramírez, Nitrite electro-oxidation mediated by Co(II)- [tetra(4-aminophenyl)porphyrin]-modified electrodes: behavior as an amperometric sensor, J. Coord. Chem. 63 (2010) 1283–1294, https://doi. org/10.1080/00958971003802091.

[87] M. Ozmen, Z. Ozbek, M. Bayrakci, S. Ertul, M. Ersoz, R. Capan, Preparation and gas sensing properties of Langmuir-Blodgett thin films of calix[n]arenes: Investigation of cavity effect, Sensors Actuators B Chem. 195 (2014) 156–164, https://doi.org/10.1016/j.snb.2014.01.041.

[88] G. Fomo, N. Nwaji, T. Nyokong, Low symmetric metallophthalocyanine modified electrode via click chemistry for simultaneous detection of heavy metals, J. Electroanal. Chem. 813 (2018) 58–66, https://doi.org/10.1016/J. JELECHEM.2018.02.016.

[89] Y. Wei, C. Gao, F.-L. Meng, H.-H. Li, L. Wang, J.-H. Liu, X.-J. Huang, SnO2/ reduced graphene oxide nanocomposite for the simultaneous electrochemical detection of cadmium(II), lead(II), copper(II), and mercury (II): an interesting favorable mutual interference, J. Phys. Chem. C 116 (2012) 1034–1041, https://doi.org/10.1021/jp209805c.

[90] B. Mızrak, M. Agˇar, A. Altindal, S. Abdurrahmanogˇlu, Synthesis, characterization and metal ion sensing properties of novel pyridone derivatives phthalocyanines, J. Porphyr. Phthalocyanines 20 (2016) 1457– 1462, https://doi.org/10.1142/S1088424616501200.

[91] D. Gounden, S. Khene, N. Nombona, Electroanalytical detection of heavy metals using metallophthalocyanine and silica-coated iron oxide composites, Chem. Pap. 72 (2018) 3043–3056, https://doi.org/10.1007/s11696-018-0545- 0.

[92] T.C. Canevari, T.M. Prado, F.H. Cincotto, S.A.S. Machado, Immobilization of ruthenium phthalocyanine on silica-coated multi-wall partially oriented carbon nanotubes: Electrochemical detection of fenitrothion pesticide, Mater. Res. Bull. 76 (2016) 41–47, https://doi.org/10.1016/J. MATERRESBULL.2015.12.007.

[93] J.A. Puhakkad, E.S. Merlin, Bioremediation of chlorinated phenols, in: R.L. Crawford, D.L. Crawford (Eds.), Bioremediation Princ. Appl., Cambridge University Press, 2005, pp. 254–299.

[94] D. Erbahar, G. Gümüs, Ö. Pamir, M.E.V. Ahsen, I. Gürol, M. Harbeck, Polyalkoxy substituted phthalocyanines sensitive to phenolic compounds in water, Sensors Actuators B Chem. 227 (2015) 277–282, https://doi.org/10.1016/j. snb.2015.12.042.

[95] H. Banimuslem, A. Hassan, T. Basova, A.D. Gülmez, S. Tuncel, M. Durmus, A.G. Gürek, V. Ahsen, Copper phthalocyanine/single walled carbon nanotubes hybrid thin films for pentachlorophenol detection, Sensors Actuators B Chem. 190 (2014) 990–998, https://doi.org/10.1016/J.SNB.2013.09.059.

[96] H. Arwin, M. Poksinski, K. Johansen, Total internal reflection ellipsometry: principles and applications, Appl. Opt. 43 (2004) 3028–3036, https://doi.org/ 10.1364/AO.43.003028.

[97] A. Nabok, A. Tsargorodskaya, The method of total internal reflection ellipsometry for thin film characterisation and sensing, Thin Solid Films 516 (2008) 8993–9001, https://doi.org/10.1016/J.TSF.2007.11.077.

[98] M. Abdel Salam, Effect of oxidation treatment of multi-walled carbon nanotubes on the adsorption of pentachlorophenol from aqueous solution: kinetics study, Arab. J. Chem. 5 (2012) 291–296, https://doi.org/10.1016/J. ARABJC.2010.08.021.

[99] D. Li, S. Ge, J. Huang, J. Gong, P. Yan, W. Lu, G. Tiana, L. Ding, Fast chromogenic identification of phenolic pollutants via homogeneous oxidation with tBuOOH in the presence of iron (III) octacarboxyphthalocyanine, Catal. Commun. 45 (2014) 95–99, https://doi.org/10.1016/j.catcom.2013.10.038.

[100] J. Gong, D. Li, J. Huang, L. Ding, Y. Tong, K. Li, C. Zhang, Synthesis of two novel water-soluble iron phthalocyanines and their application in fast chromogenic identification of phenolic pollutants, Catal. Lett. 144 (2014) 487–497, https:// doi.org/10.1007/s10562-013-1178-0.

[101] D. Li, S. Ge, J. Huang, J. Gong, T. Wang, P. Yan, G. Li, L. Ding, Photocatalytic chromogenic identification of chlorophenol pollutants by manganese phthalocyanine under sunlight irradiation, Sep. Purif. Technol. 125 (2014) 216–222, https://doi.org/10.1016/j.seppur.2014.01.052.

[102] Y. Zhong, D. Li, P. Yan, Y. Tong, J. Huang, L. Ding, D. Zeng, First observation of tetranitro iron (II) phthalocyanine catalyzed oxidation of phenolic pollutant assisted with 4-aminoantipyrine using dioxygen as oxidant, J. Mol. Catal. A Chem. 345 (2011) 108–116, https://doi.org/10.1016/j.molcata.2011.06.002.

[103] S. Ge, D. Li, S. Huang, W. Chen, G. Tu, S. Yu, Q. He, J. Gong, Y. Li, C. Hong, C. Wu, Z. Zheng, A magnetically recyclable Fe3O4@C@TNCuPc composite catalyst for chromogenic identification of phenolic pollutants, J. Mol. Catal. A Chem. 410 (2015) 193–201, https://doi.org/10.1016/j.molcata.2015.09.022.

[104] Z.O. Makinde, P. Mashazi, S. Khene, Electrocatalytic behavior of single walled carbon nanotubes with alkylthio-substituted cobalt binuclear phthalocyanines towards oxidation of 4-chlorophenols, J. Porphyr. Phthalocyanines. 23 (2019) 142–153, https://doi.org/10.1142/ S1088424619500172.

[105] H. Karimi-Maleh, M. Moazampour, A.A. Ensafi, S. Mallakpour, M. Hatami, An electrochemical nanocomposite modified carbon paste electrode as a sensor for simultaneous determination of hydrazine and phenol in water and wastewater samples, Environ. Sci. Pollut. Res. 21 (2014) 5879–5888, https:// doi.org/10.1007/s11356-014-2529-0.

[106] M. Govindhan, T. Lafleur, B.-R. Adhikari, A. Chen, Electrochemical sensor based on carbon nanotubes for the simultaneous detection of phenolic pollutants, Electroanalysis 27 (2015) 902–909, https://doi.org/10.1002/ elan.201400608.

[107] M. Norman, S. _ Zółtowska-Aksamitowska, A. Zgoła-Grzes´kowiak, H. Ehrlich, T. Jesionowski, Iron(III) phthalocyanine supported on a spongin scaffold as an advanced photocatalyst in a highly efficient removal process of halophenols and bisphenol A, J. Hazard. Mater. 347 (2018) 78–88, https://doi.org/10.1016/ J.JHAZMAT.2017.12.055.

[108] M.D. França, L.M. Santos, T.A. Silva, K.A. Borges, V.M. Silva, A.O.T. Patrocinio, A.G. Trovó, A.E.H. Machado, Efficient mineralization of paracetamol using the nanocomposite TiO2/Zn(II) phthalocyanine as photocatalyst, J. Braz. Chem. Soc. 27 (2016) 1094–1102.

[109] M. Palanna, I. Mohammed, S. Aralekallu, M. Nemakal, L.K. Sannegowda, Simultaneous detection of paracetamol and 4-aminophenol at nanomolar levels using biocompatible cysteine-substituted phthalocyanine, New J. Chem. 44 (2020) 1294–1306, https://doi.org/10.1039/C9NJ05252F.

[110] S.L. Lewis, L. Bucher, M.M. Heitkemper, M.M. Harding, J. Kwong, D. Roberts, Medical-surgical nursing: assessment and management of clinical problems, single volume, Elsevier Health Sci. (2016).

[111] M. Abramovitz, Meningitis, Lucent Books, a Part of Gale, Cengage Learning, 2014.

[112] Y. Wang, Y. Fang, W. Lu, N. Li, W. Chen, Oxidative removal of sulfa antibiotics by introduction of activated carbon fiber to enhance the catalytic activity of iron phthalocyanine, Microporous Mesoporous Mater. 261 (2018) 98–104, https://doi.org/10.1016/J.MICROMESO.2017.10.055.

[113] T.M. Woo, M.V Robinson, Pharmacotherapeutics for Advanced Practice Nurse Prescribers, F.A. Davis Company, 2015.

[114] X.-P. Hong, J.-Y. Ma, Electrochemical study of sulfadiazine on a novel phthalocyanine-containing chemically modified electrode, Chin. Chem. Lett. 24 (2013) 329–331, https://doi.org/10.1016/J.CCLET.2013.02.010.

[115] X. Hong, Y. Zhu, Y. Zhang, Electrocatalytic response of poly(cobalt tetraaminophthalocyanine)/multi-walled carbon nanotubes-Nafion modified electrode toward sulfadiazine in urine, J. Zhejiang Univ. Sci. B 13 (2012) 503–510, https://doi.org/10.1631/jzus.B1100337.

[116] A. Choi, H. Jeong, S. Kim, S. Jo, S. Jeon, Electrocatalytic reduction of dioxygen by cobalt porphyrin-modified glassy carbon electrode with single-walled carbon nanotubes and nafion in aqueous solutions, Electrochim. Acta 53 (2008) 2579–2584, https://doi.org/10.1016/J.ELECTACTA.2007.10.029.

[117] J. Wang, T. Golden, R. Li, Cobalt phthalocyanine/cellulose acetate chemically modified electrodes for electrochemical detection in flowing streams. Multifunctional operation based upon the coupling of electrocatalysis and permselectivity, Anal. Chem. 60 (1988) 1642–1645, https://doi.org/10.1021/ ac00166a038.

[118] J. Wang, M. Li, Z. Shi, N. Li, Z. Gu, Direct electrochemistry of cytochrome c at a glassy carbon electrode modified with single-wall carbon nanotubes, Anal. Chem. 74 (2002) 1993–1997, https://doi.org/10.1021/ac010978u.

[119] S.M. O'Flaherty, S.V. Hold, M.J. Cook, T. Torres, Y. Chen, M. Hanack, W.J. Blau, Molecular engineering of peripherally and axially modified phthalocyanines for optical limiting and nonlinear optics, Adv. Mater. 15 (2003) 19–32, https://doi.org/10.1002/adma.200390002.

[120] C.-B. Yao, Y.-D. Zhang, J. Li, D.-T. Chen, H.-T. Yin, C.-Q. Yu, P. Yuan, Study of the nonlinear optical properties and behavior in phenoxy-phthalocyanines liquid at nanosecond laser pulses, Opt. Mater. (Amst) 37 (2014) 80–86, https://doi. org/10.1016/J.OPTMAT.2014.05.003.

[121] Y. Chen, M. Hanack, Y. Araki, O. Ito, Axially modified gallium phthalocyanines and naphthalocyanines for optical limiting, Chem. Soc. Rev. 34 (2005) 517– 529, https://doi.org/10.1039/b416368k.

[122] D. Dini, M. Barthel, T. Schneider, M. Ottmar, S. Verma, M. Hanack, Phthalocyanines and related compounds as switchable materials upon strong irradiation: the molecular engineering behind the optical limiting effect, Solid State Ionics 165 (2003) 289–303, https://doi.org/10.1016/J. SSI.2003.08.046.

[123] S. Mgidlana, D.O. Oluwole, T. Nyokong, Fabrication of efficient nonlinear optical absorber using Zn phthalocyanine-semiconductor quantum dots conjugates, Polyhedron 159 (2019) 102–115, https://doi.org/10.1016/j. poly.2018.11.024.

[124] D. Dini, G.Y. Yang, M. Hanack, Perfluorinated phthalocyanines for optical limiting: Evidence for the direct correlation between substituent electron withdrawing character and the nonlinear optical effect, J. Chem. Phys. 119 (2003) 4857–4864, https://doi.org/10.1063/1.1595633.

[125] J. Britton, Y.G. Gorbunova, A.G. Martynov, A.Y. Tsivadze, T. Nyokong, D.O. Oluwole, Improvement of nonlinear optical properties of phthalocyanine bearing diethyleneglycole chains: influence of symmetry lowering vs. heavy atom effect, J. Porphyr. Phthalocyanines 20 (2016) 1296–1305. doi:10.1142/ s1088424616501042.

[126] S. Foley, G. Jones, R. Liuzzi, D.J. McGarvey, M.H. Perry, T. George Truscott, The synthesis and photophysical properties of polyether substituted phthalocyanines of potential use in photodynamic therapy, J. Chem. Soc. Perkin Trans. 2 (1997) 1725–1730, https://doi.org/10.1039/A701079F.

[127] G. de la Torre, P. Vázquez, F. Agulló-López, T. Torres, Role of structural factors in the nonlinear optical properties of phthalocyanines and related compounds, Chem. Rev. 104 (2004) 3723–3750, https://doi.org/10.1021/ cr030206t.

[128] Q. Miao, Q. Liu, E. Sun, T. Ren, Nonlinear dynamics and optical power limiting of nanoseconds pulses in naphthalocyanines and phthalocyanines with central metals gallium and indium, J. Photochem. Photobiol. A Chem. 316 (2016) 19–23, https://doi.org/10.1016/J.JPHOTOCHEM.2015.10.006.

[129] M. Durmus, T. Nyokong, Synthesis, photophysical and photochemical properties of aryloxy tetra-substituted gallium and indium phthalocyanine derivatives, Tetrahedron 63 (2007) 1385–1394, https://doi.org/10.1016/J. TET.2006.11.089.

[130] J. Britton, C. Litwinski, M. Durmus, V. Chauke, T. Nyokong, Optical limiting behavior of ring substituted zinc, indium and gallium phthalocyanines in the presence of quantum dots, J. Porphyr. Phthalocyanines. 15 (2011) 1239– 1249, https://doi.org/10.1142/S1088424611004142.

[131] N. Nwaji, D.O. Oluwole, J. Mack, M. Louzada, S. Khene, J. Britton, T. Nyokong, Improved nonlinear optical behaviour of ball type indium(III) phthalocyanine linked to glutathione capped nanoparticles, Dye. Pigment. 140 (2017) 417– 430, https://doi.org/10.1016/J.DYEPIG.2017.01.066.

[132] N. Nwaji, J. Mack, T. Nyokong, Photophysical and strong optical limiting properties of ball-type phthalocyanines dimers and their monomeric analogues, J. Photochem. Photobiol. A Chem. 352 (2018) 73–85, https://doi. org/10.1016/J.JPHOTOCHEM.2017.10.045.

[133] P.C. Ray, Size and shape dependent second order nonlinear optical properties of nanomaterials and their application in biological and chemical sensing, Chem. Rev. 110 (2010) 5332–5365, https://doi.org/10.1021/cr900335q.

[134] D. Mwanza, M. Louzada, J. Britton, E. Sekhosana, S. Khene, T. Nyokong, P. Mashazi, The effect of the cobalt and manganese central metal ions on the nonlinear optical properties of tetra(4-propargyloxyphenoxy) phthalocyanines, New J. Chem. 42 (2018) 9857–9864, https://doi.org/ 10.1039/C8NJ00748A.

[135] G.N. Ngubeni, J. Britton, J. Mack, E. New, I. Hancox, M. Walker, T. Nyokong, T.S. Jones, S. Khene, Spectroscopic and nonlinear optical properties of the four positional isomers of 4a-(4-tert-butylphenoxy)phthalocyanine, J. Mater. Chem. C. 3 (2015) 10705–10714, https://doi.org/10.1039/C5TC01601K. [

136] S.-J. Ding, F. Nan, D.-J. Yang, X.-L. Liu, Y.-L. Wang, L. Zhou, Z.-H. Hao, Q.-Q. Wang, Largely enhanced saturable absorption of a complex of plasmonic and molecular-like au nanocrystals, Sci. Rep. 5 (2015) 9735, https://doi.org/ 10.1038/srep09735.

[137] A.I. Plekhanov, T.V. Basova, R.G. Parkhomenko, A.G. Gürek, Nonlinear optical properties of lutetium and dysprosium bisphthalocyanines at 1550 nm with femto- and nanosecond pulse excitation, Opt. Mater. (Amst) 64 (2017) 13–17, https://doi.org/10.1016/J.OPTMAT.2016.11.025.

[138] K.E. Sekhosana, T. Nyokong, Nonlinear optical behavior of n-tuple decker phthalocyanines at the nanosecond regime: investigation of change in mechanisms, RSC Adv. 9 (2019) 16223–16234, https://doi.org/10.1039/ C9RA01836K.

[139] K.E. Sekhosana, T. Nyokong, Synthesis of ytterbium bisphthalocyanines: Photophysicochemical properties and nonlinear absorption behavior, Opt. Mater. (Amst) 37 (2014) 139–146, https://doi.org/10.1016/J. OPTMAT.2014.05.013.

[140] P. Zhao, Z. Wang, J. Chen, Y. Zhou, F. Zhang, Nonlinear optical and optical limiting properties of polymeric carboxyl phthalocyanine coordinated with rare earth atom, Opt. Mater. (Amst) 66 (2017) 98–105, https://doi.org/ 10.1016/j.optmat.2017.01.029.

[141] Z. Peng, X. Song, L. Zhong-Yu, Z. Fu-Shi, Nonlinear optical properties of novel polymeric rare earth phthalocyanine studied using picosecond Z-scan technique, Chin. Phys. Lett. 25 (2008) 2058.

[142] Z. Li, S. Xu, Z. Chen, F. Zhang, Photophysical and nonlinear optical properties of an azobenzene substituted zinc phthalocyanine, Optik (Stuttg) 125 (2014) 3833–3836, https://doi.org/10.1016/J.IJLEO.2014.01.176.

[143] D.O. Oluwole, A.V. Yagodin, J. Britton, A.G. Martynov, Y.G. Gorbunova, A.Y. Tsivadze, T. Nyokong, Optical limiters with improved performance based on nanoconjugates of thiol substituted phthalocyanine with CdSe quantum dots and Ag nanoparticles, Dalton Trans. 46 (2017) 16190–16198, https://doi.org/ 10.1039/C7DT03867D.

[144] D. Gounden, G.N. Ngubeni, J. Britton, M.S. Louzada, S. Khene, N. Nombona, Synthesis, spectroscopic and DFT Characterization of 4b-(4-tertButylphenoxy)phthalocyanine positional isomers for non-linear optical absorption, South African J. Chem. (2017) 49–59, https://doi.org/10.17159/0379-4350/2017/v70a8.

[145] N. Nwaji, B. Jones, J. Mack, D.O. Oluwole, T. Nyokong, Nonlinear optical dynamics of benzothiazole derivatized phthalocyanines in solution, thin films and when conjugated to nanoparticles, J. Photochem. Photobiol. A Chem. 346 (2017) 46–59, https://doi.org/10.1016/J.JPHOTOCHEM.2017.05.042.

[146] N. Nwaji, T. Nyokong, Nanosecond optical nonlinearities in low symmetry phthalocyanine nanoconjugates studied using the Z-scan technique, J. Lumin. 192 (2017) 1167–1179, https://doi.org/10.1016/J.JLUMIN.2017.08.053.

[147] W.M. Darwish, A.M. Darwish, E.A. Al-Ashkar, Synthesis and nonlinear optical properties of a novel indium phthalocyanine highly branched polymer, Polym. Adv. Technol. 26 (2015) 1014–1019, https://doi.org/ 10.1002/pat.3520.

[148] W. Song, C. He, W. Zhang, Y. Gao, Y. Yang, Y. Wu, Z. Chen, X. Li, Y. Dong, Synthesis and nonlinear optical properties of reduced graphene oxide hybrid material covalently functionalized with zinc phthalocyanine, Carbon N. Y. 77 (2014) 1020–1030, https://doi.org/10.1016/J.CARBON.2014.06.018.

[149] E. Ramya, N. Momen, D.N. Rao, Preparation of multiwall carbon nanotubes with zinc phthalocyanine hybrid materials and their nonlinear optical (NLO) properties, J. Nanosci. Nanotechnol. 18 (2018) 4764–4770.

[150] K. Sanusi, S. Khene, T. Nyokong, Enhanced optical limiting performance in phthalocyanine-quantum dot nanocomposites by free-carrier absorption mechanism, Opt. Mater. (Amst) 37 (2014) 572–582, https://doi.org/ 10.1016/J.OPTMAT.2014.07.024.

[151] Z.Wang, C. He,W. Song, Y. Gao, Z. Chen, Y. Dong, C. Zhao, Z. Li, Y.Wu, The effect of peripheral substituents attached to phthalocyanines on the third order nonlinear optical properties of graphene oxide–zinc(ii)phthalocyanine hybrids, RSC Adv. 5 (2015) 94144–94154, https://doi.org/10.1039/C5RA18911J.

[152] X.-F. Jiang, L. Polavarapu, H. Zhu, R. Ma, Q.-H. Xu, Flexible, robust and highly efficient broadband nonlinear optical materials based on graphene oxide impregnated polymer sheets, Photonics Res. 3 (2015) A87–A91, https://doi. org/10.1364/PRJ.3.000A87.

[153] K. Hayashi, M. Nakamura, H. Miki, S. Ozaki, M. Abe, T. Matsumoto, T. Kori, K. Ishimura, Photostable iodinated silica/porphyrin hybrid nanoparticles with heavy-atom effect for wide-field photodynamic/photothermal therapy using single light source, Adv. Funct. Mater. 24 (2014) 503–513, https://doi.org/ 10.1002/adfm.201301771.

[154] N.-S. Choi, Z. Chen, S.A. Freunberger, X. Ji, Y.-K. Sun, K. Amine, G. Yushin, L.F. Nazar, J. Cho, P.G. Bruce, Challenges facing lithium batteries and electrical double-layer capacitors, Angew. Chemie Int. Ed. 51 (2012) 9994–10024, https://doi.org/10.1002/anie.201201429.

[155] Y. Zhu, T. Gao, X. Fan, F. Han, C. Wang, Electrochemical techniques for intercalation electrode materials in rechargeable batteries, Acc. Chem. Res. 50 (2017) 1022–1031, https://doi.org/10.1021/acs.accounts.7b00031.

[156] B.K. Kim, S. Sy, A. Yu, J. Zhang, Electrochemical Supercapacitors for Energy Storage and Conversion, Handb. Clean Energy Syst. (2015) 1–25. doi:10.1002/ 9781118991978.hces112.

[157] Y. Wang, Y. Song, Y. Xia, Electrochemical capacitors: mechanism, materials, systems, characterization and applications, Chem. Soc. Rev. 45 (2016) 5925– 5950, https://doi.org/10.1039/C5CS00580A.

[158] B.E. Conway, Energetics and Elements of the Kinetics of Electrode Processes BT – Electrochemical Supercapacitors: Scientific Fundamentals and Technological Applications, in: B.E. Conway (Ed.), Springer US, Boston, MA, 1999, pp. 33–65. doi:10.1007/978-1-4757-3058-6_3.

[159] A.T. Chidembo, K.I. Ozoemena, B.O. Agboola, V. Gupta, G.G. Wildgoose, R.G. Compton, Nickel(ii) tetra-aminophthalocyanine modified MWCNTs as potential nanocomposite materials for the development of supercapacitors, Energy Environ. Sci. 3 (2010) 228–236, https://doi.org/10.1039/B915920G.

[160] J. Zhang, P. Liu, Y. Zhang, G. Xu, Z. Lu, X. Wang, Y. Wang, L. Yang, X. Tao, H. Wang, E. Zhang, J. Xi, Z. Ji, Enhanced performance of nano-Bi2WO6-graphene as pseudocapacitor electrodes by charge transfer channel, Sci. Rep. 5 (2015) 8624.

[161] A.B.P. Lever, The Phthalocyanines — Molecules of Enduring Value; a Twodimensional Analysis of Redox Potentials, J. Porphyr. Phthalocyanines 03 (1999) 488–499. doi:10.1002/(SICI)1099-1409(199908/10)3:6/73.0.CO;2-K.

[162] R. Ramachandran, Q. Hu, F. Wang, Z.-X. Xu, Synthesis of N-CuMe2Pc nanorods/graphene oxide nanocomposite for symmetric supercapacitor electrode with excellent cyclic stability, Electrochim. Acta 298 (2019) 770– 777, https://doi.org/10.1016/J.ELECTACTA.2018.12.163.

[163] K. Makgopa, P.M. Ejikeme, K.I. Ozoemena, Graphene oxide-modified nickel (II) tetra-aminophthalocyanine nanocomposites for high-power symmetric pseudocapacitor, Electrochim. Acta 212 (2016) 876–882, https://doi.org/ 10.1016/J.ELECTACTA.2016.07.027.

[164] W. Wang, I. Ruiz, I. Lee, F. Zaera, M. Ozkan, C.S. Ozkan, Improved functionality of graphene and carbon nanotube hybrid foam architecture by UV-ozone treatment, Nanoscale 7 (2015) 7045–7050, https://doi.org/10.1039/ C4NR06795A. [165] K.P. Madhuri, N.S. John, Supercapacitor application of nickel phthalocyanine nanofibres and its composite with reduced graphene oxide, Appl. Surf. Sci. 449 (2018) 528–536, https://doi.org/10.1016/J.APSUSC.2017.12.021. [166] D. Hulicova-Jurcakova, M. Kodama, S. Shiraishi, H. Hatori, Z.H. Zhu, G.Q. Lu, Nitrogen-enriched nonporous carbon electrodes with extraordinary supercapacitance, Adv. Funct. Mater. 19 (2009) 1800–1809, https://doi.org/ 10.1002/adfm.200801100.

[167] K. Krishnamoorthy, P. Pazhamalai, S.J. Kim, Ruthenium sulfide nanoparticles as a new pseudocapacitive material for supercapacitor, Electrochim. Acta 227 (2017) 85–94, https://doi.org/10.1016/J.ELECTACTA.2016.12.171.

[168] S.S. Karade, P. Dwivedi, S. Majumder, B. Pandit, B.R. Sankapal, First report on a FeS-based 2 V operating flexible solid-state symmetric supercapacitor device, Sustain. Energy Fuels 1 (2017) 1366–1375, https://doi.org/10.1039/ C7SE00165G.

[169] H. Yang, P. Fan, S. Liu, J. Wei, S. Tan, Q. Wang, H. Hou, Electrode characteristics and lithiation mechanism of FePc/GN composites, Int. J. Electrochem. Sci. 13 (2018) 2606–2616.

[170] K. Rana, S.D. Kim, J.-H. Ahn, Additive-free thick graphene film as an anode material for flexible lithium-ion batteries, Nanoscale 7 (2015) 7065–7071, https://doi.org/10.1039/C4NR06082B.

[171] G. Ramos-Sanchez, A. Callejas-Tovar, L.G. Scanlon, P.B. Balbuena, DFT analysis of Li intercalation mechanisms in the Fe-phthalocyanine cathode of Li-ion batteries, Phys. Chem. Chem. Phys. 16 (2014) 743–752, https://doi.org/ 10.1039/C3CP53161A.

[172] O. Crowther, L.-S. Du, D.M. Moureau, I. Bicaku, M. Salomon, J.W. Lawson, L.R. Lucente, K. Mock, J.P. Fellner, L.G. Scanlon, Effect of conductive carbon on capacity of iron phthalocyanine cathodes in primary lithium batteries, J. Power Sources 217 (2012) 92–97, https://doi.org/10.1016/J. JPOWSOUR.2012.06.003.

[173] J. Wu, X. Rui, C. Wang, W.-B. Pei, R. Lau, Q. Yan, Q. Zhang, Nanostructured conjugated ladder polymers for stable and fast lithium storage anodes with high-capacity, Adv. Energy Mater. 5 (2015) 1402189, https://doi.org/10.1002/ aenm.201402189.

[174] X. Han, G. Qing, J. Sun, T. Sun, How many lithium ions can be inserted onto fused C6 aromatic ring systems?, Angew. Chemie Int. Ed. 51 (2012) 5147– 5151, https://doi.org/10.1002/anie.201109187.

[175] A.S. Milev, N. Tran, G.S. Kamali Kannangara, M.A. Wilson, I. Avramov, Polymorphic transformation of iron-phthalocyanine and the effect on carbon nanotube synthesis, J. Phys. Chem. C 112 (2008) 5339–5347, https://doi.org/ 10.1021/jp710923f.

[176] B. You, L. Wang, L. Yao, J. Yang, Three dimensional N-doped graphene–CNT networks for supercapacitor, Chem. Commun. 49 (2013) 5016–5018, https:// doi.org/10.1039/C3CC41949E.

[177] T. Lin, I.-W. Chen, F. Liu, C. Yang, H. Bi, F. Xu, F. Huang, Nitrogen-doped mesoporous carbon of extraordinary capacitance for electrochemical energy storage, Science (80-.). 350 (2015) 1508 LP – 1513. doi:10.1126/science. aab3798.

[178] J. Han, G. Xu, B. Ding, J. Pan, H. Dou, D.R. MacFarlane, Porous nitrogen-doped hollow carbon spheres derived from polyaniline for high performance supercapacitors, J. Mater. Chem. A 2 (2014) 5352–5357, https://doi.org/ 10.1039/C3TA15271E.

[179] Y. Wen, T.E. Rufford, X. Chen, N. Li, M. Lyu, L. Dai, L. Wang, Nitrogendoped Ti3C2Tx MXene electrodes for high-performance supercapacitors, Nano Energy 38 (2017) 368–376, https://doi.org/10.1016/J. NANOEN.2017.06.009.

[180] H. Wang, T. Maiyalagan, X. Wang, Review on recent progress in nitrogendoped graphene: synthesis, characterization, and its potential applications, ACS Catal. 2 (2012) 781–794, https://doi.org/10.1021/cs200652y.

[181] D. He, W. Wang, Y. Fu, R. Zhao, W. Xue, W. Hu, Formation of threedimensional honeycomb-like nitrogen-doped graphene for use in energystorage devices, Compos. Part A Appl. Sci. Manuf. 91 (2016) 140–144, https:// doi.org/10.1016/J.COMPOSITESA.2016.08.032.

[182] Y. Lu, Q. Zheng, J. Wu, Y. Yu, Enhanced electrochemical charge storage performance by doping of copper phthalocyanine-3,40 ,400,4000-tetrasulfonic acid tetrasodium salt into

polypyrrole/multi-walled carbon nanotubes 3Dnanostructured electrodes, Electrochim. Acta (2018), https://doi.org/10.1016/ j.electacta.2018.01.173.

[183] A. Makarov, V. Sverdlov, S. Selberherr, Modeling emerging non-volatile memories: current trends and challenges, Phys. Procedia 25 (2012) 99–104, https://doi.org/10.1016/J.PHPRO.2012.03.056.

[184] F. Pan, S. Gao, C. Chen, C. Song, F. Zeng, Recent progress in resistive random access memories: Materials, switching mechanisms, and performance, Mater. Sci. Eng. R Reports 83 (2014) 1–59, https://doi.org/10.1016/J. MSER.2014.06.002.

[185] N. Padma, V. Saxena, V. Sudarsan, H. Raval, S. Sen, Disordered self assembled monolayer dielectric induced hysteresis in organic field effect transistors, J. Nanosci. Nanotechnol. 14 (2014) 4418–4423.

[186] N. Padma, C.A. Betty, S. Samanta, A. Nigam, Tunable switching characteristics of low operating voltage organic bistable memory devices based on gold nanoparticles and copper phthalocyanine thin films, J. Phys. Chem. C 121 (2017) 5768–5778, https://doi.org/10.1021/acs.jpcc.6b09404.

[187] X. Guo, J. Liu, L. Cao, Q. Liang, S. Lei, Nonvolatile memory device based on copper polyphthalocyanine thin films, ACS Omega 4 (2019) 10419–10423, https://doi.org/10.1021/acsomega.9b01224.

[188] S.K. Tripathi, R. Kaur, Jyoti, Effect of CuPc layer insertion on the memory performance of CdS nanocomposite diodes, Mater. Sci. Eng. B 211 (2016) 7– 12, https://doi.org/10.1016/J.MSEB.2016.05.011.

[189] G. Nenna, S. Masala, V. Bizzarro, M. Re, E. Pesce, C. Minarini, T. Di Luccio, Particle size dependence of resonant-tunneling effect induced by CdS nanoparticles in a poly(N-vinylcarbazole) polymer matrix, J. Appl. Phys. 112 (2012) 44508, https://doi.org/10.1063/1.4746783.

[190] S. Choi, S.-H. Hong, S.H. Cho, S. Park, S.-M. Park, O. Kim, M. Ree, Highperformance programmable memory devices based on hyperbranched copper phthalocyanine polymer thin films, Adv. Mater. 20 (2008) 1766– 1771, https://doi.org/10.1002/adma.200702147.

[191] J. Simon, J.-J. Andre, M. Maitrot, Lutetium Bisphthalocyanine: The First Molecular semiconductor BT – molecules in physics, chemistry, and biology: physical aspects of molecular systems, in: J. Maruani (Ed.), Springer Netherlands, Dordrecht, 1988, pp. 599–614. doi:10.1007/978-94-009-2851- 0_20.

[192] P. Turek, P. Petit, J.-J. Andre, J. Simon, R. Even, B. Boudjema, G. Guillaud, M. Maitrot, Two examples of molecular semiconductors: phthalocyanine complexes of lithium and lutetium, Mol. Cryst. Liq. Cryst. Inc., Nonlinear Opt. 161 (1988) 323–327, https://doi.org/10.1080/00268948808070256.

[193] P. Turek, P. Petit, J.J. Andre, J. Simon, R. Even, B. Boudjema, G. Guillaud, M. Maitrot, A new series of molecular semiconductors: phthalocyanine radicals, J. Am. Chem. Soc. 109 (1987) 5119–5122, https://doi.org/ 10.1021/ja00251a012.

[194] N.B. Chaure, T. Basova, A.K. Ray, A.G. Gürek, V. Ahsen, Memory effects in thin film organic transistor characteristics, J. Phys. D. Appl. Phys. 42 (2009), https://doi.org/10.1088/0022-3727/42/12/125103 125103.

[195] S. Shi, J. Peng, J. Lin, D. Ma, Write-once read-many-times memory based on a single layer of pentacene, IEEE Electron Device Lett. 30 (2009) 343–345, https://doi.org/10.1109/LED.2009.2013976.

[196] K. Onlaor, B. Tunhoo, P. Keeratithiwakorn, T. Thiwawong, J. Nukeaw, Electrical bistable properties of copper phthalocyanine at different deposition rates, Solid State Electron. 72 (2012) 60–66, https://doi.org/ 10.1016/J.SSE.2012.01.003.

[197] V. Chidambara, C.M. Joseph, Electrical bistability studies on vacuum evaporated copper phthalocyanine (CuPc)/fullerene (C60) bilayers, Dye Pigment. 117 (2015) 24–27, https://doi.org/10.1016/J.DYEPIG.2015.01.024.

[198] Y. Xiao, L. Zhang, F. Peng, G.-B. Pan, Fabrication of a cobalt phthalocyanine free-standing film on an ionic liquid surface for memory device applications, RSC Adv. 8 (2018) 5344–5349, https://doi.org/10.1039/C7RA12953J.

[199] G. Roelkens, J. Van Campenhout, J. Brouckaert, D. Van Thourhout, R. Baets, P. R. Romeo, P. Regreny, A. Kazmierczak, C. Seassal, X. Letartre, G. Hollinger, J.M. Fedeli, L. Di Cioccio, C. Lagahe-Blanchard, III-V/Si photonics by die-to-wafer bonding, Mater. Today. 10 (2007) 36–43, https://doi.org/10.1016/S1369- 7021(07)70178-5.

[200] J. Yin, Y. Zhou, T. Lei, J. Pei, A butterfly-shaped amphiphilic molecule: solution-transferable and free-standing bilayer films for organic transistors, Angew. Chemie Int. Ed. 50 (2011) 6320–6323, https://doi.org/10.1002/ anie.201100712.

[201] Y. Ito, A.A. Virkar, S. Mannsfeld, J.H. Oh, M. Toney, J. Locklin, Z. Bao, Crystalline ultrasmooth self-assembled monolayers of alkylsilanes for organic fieldeffect transistors, J. Am. Chem. Soc. 131 (2009) 9396–9404, https://doi.org/ 10.1021/ja9029957.

[202] H. Lin, Z. Pei, Y. Chan, Carrier transport mechanism in a nanoparticleincorporated organic bistable memory device, IEEE Electron Device Lett. 28 (2007) 569–571, https://doi.org/10.1109/LED.2007.899668.

[203] S. Lindner, U. Treske, M. Knupfer, The complex nature of phthalocyanine/gold interfaces, Appl. Surf. Sci. 267 (2013) 62–65, https://doi.org/10.1016/J. APSUSC.2012.06.104.

[204] J.S. Meena, S.M. Sze, U. Chand, T.-Y. Tseng, Overview of emerging nonvolatile memory technologies, Nanoscale Res. Lett. 9 (2014) 526, https://doi.org/ 10.1186/1556-276X-9-526.

[205] L. Zhou, J. Mao, Y. Ren, S.-T. Han, V.A.L. Roy, Y. Zhou, Recent advances of flexible data storage devices based on organic nanoscaled materials, Small 14 (2018) 1703126, https://doi.org/10.1002/smll.201703126.

[206] H.-C. Chang, C. Lu, C.-L. Liu, W.-C. Chen, Single-crystal C60 needle/CuPc nanoparticle double floating-gate for low-voltage organic transistors based non-volatile memory devices, Adv. Mater. 27 (2015) 27–33, https://doi.org/ 10.1002/adma.201403771.

[207] J. Aimi, C.-T. Lo, H.-C. Wu, C.-F. Huang, T. Nakanishi, M. Takeuchi, W.-C. Chen, Phthalocyanine-cored star-shaped polystyrene for nano floating gate in nonvolatile organic transistor memory device, Adv. Electron. Mater. 2 (2016) 1500300, https://doi.org/10.1002/aelm.201500300.

[208] J. Aimi, P.-H. Wang, C.-C. Shih, C.-F. Huang, T. Nakanishi, M. Takeuchi, H.-Y. Hsueh, W.-C. Chen, A star polymer with a metallo-phthalocyanine core as a tunable charge storage material for

nonvolatile transistor memory devices, J. Mater. Chem. C 6 (2018) 2724–2732, https://doi.org/10.1039/C7TC05790C.

[209] I. Graz, A. Mellinger, Polymer Electrets and Ferroelectrets as EAPs: Fundamentals BT - Electromechanically Active Polymers: A Concise Reference, in: F. Carpi (Ed.), Springer International Publishing, Cham, 2016, pp. 1–10. doi:10.1007/978-3-319-31767-0_24-1.